

NASA CR-72288
GDC-DBG67-002



GPO PRICE \$ _____

CFSTI PRICE(S) \$ _____

Hard copy (HC) 3.00

Microfiche (MF) .65

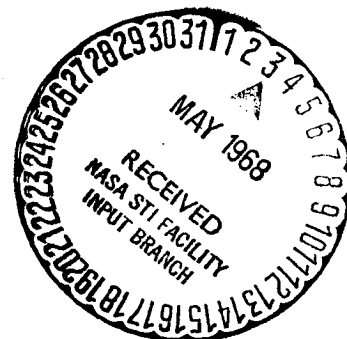
ff 653 July 65

WELDMENT FLAW GROWTH CHARACTERISTICS OF 2219-T81 ALUMINUM ALLOY

by
W. E. Witzell and C. J. Kropp

Prepared for
NATIONAL AERONAUTICS AND SPACE ADMINISTRATION

CONTRACT NAS 3-7951



GENERAL DYNAMICS
Convair Division

N 68-20923

(ACCESSION NUMBER) 158 (THRU) _____

(PAGES) CK 72288 (CODE) _____

(NASA CR OR TAX OR AD NUMBER) _____ (CATEGORY) _____

NOTICE

This report was prepared as an account of Government sponsored work. Neither the United States, nor the National Aeronautics and Space Administration (NASA), nor any person acting on behalf of NASA:

- A.) Makes any warranty or representation, expressed or implied, with respect to the accuracy, completeness, or usefulness of the information contained in this report, or that the use of any information, apparatus, method, or process disclosed in this report may not infringe privately owned rights; or
- B.) Assumes any liabilities with respect to the use of, or for damages resulting from the use of any information, apparatus, method or process disclosed in this report.

As used above, "person acting on behalf of NASA" includes any employee or contractor of NASA, or employee of such contractor, to the extent that such employee or contractor of NASA, or employee of such contractor prepares, disseminates, or provides access to, any information pursuant to his employment or contract with NASA, or his employment with such contract.

Requests for copies of this report should be referred to

National Aeronautics and Space Administration
Office of Scientific and Technical Information
Attention: AFSS-A
Washington, D.C. 20546

Security Classification Approved
per Requirements of Paragraph 10, DOD 5220.22-M



D. J. Hallman,

Supervisor, Technical Reports

FINAL REPORT

WELDMENT FLAW GROWTH CHARACTERISTICS
OF 2219-T81 ALUMINUM ALLOY

by
W. E. Witzell and C. J. Kropp

Prepared for
NATIONAL AERONAUTICS AND SPACE ADMINISTRATION

September 1967

CONTRACT NAS 3-7951

Technical Management
NASA Lewis Research Center
Liquid Rocket Technology Branch
R. N. Johnson

GENERAL DYNAMICS
Convair Division

PRECEDING PAGE BLANK NOT FILMED.

FOREWORD

This final report summarizes all work performed under NASA Lewis Research Center Contract NAS3-7951, except for the literature search and industry survey that were reported in NASA CR-72097, January 1967.

Mr. Richard N. Johnson of the NASA-LeRC was project manager. Mr. W. E. Witzell was the Convair program manager.

Other Convair personnel involved in this task were:

C. J. Kropp (Testing and Metallurgical analysis)

R. T. Anderson (Nondestructive testing)

M. S. Hersh (Welding)

ACKNOWLEDGEMENTS

A number of personnel were involved in the successful completion of this project. However, a key man who deserves particular credit was Mr. Max Spencer, who performed all the laboratory tests at three test temperatures, as well as preparation of specimens and coordination of tests.

Other personnel who contributed to this project were:

Jerry Hill

Glenn Lindeneau

Bob Bauman

Hal Brittain

Charles Johnson

Bob Maderazo

Ken Perun

TABLE OF CONTENTS

Section	Page
	SUMMARY · · · · · xiii
1	INTRODUCTION AND BACKGROUND · · · · · 1
	Inspection and Nondestructive Testing · · · · · 2
2	GENERAL TEST PROGRAM · · · · · 3
3	MATERIALS · · · · · 5
4	WELDING · · · · · 7
	Weld Procedures · · · · · 7
	Repair Welding · · · · · 9
5	TEST SPECIMENS · · · · · 13
	Tensile Tests · · · · · 13
	Center-Notched Specimens · · · · · 19
	1.0-Inch Plate Fracture Specimens · · · · · 20
	Notches · · · · · 20
	Location of Notches · · · · · 22
	Notch Sharpening · · · · · 22
	Surface Notch Configuration · · · · · 24
6	EXPERIMENTAL PROGRAM · · · · · 27
	Mechanical Properties Tests · · · · · 27
	Uniaxial Fracture Tests — Sheet · · · · · 29
	Flaw Enlargement of Sheets · · · · · 30
	Uniaxial Fracture Tests — Plate · · · · · 31
7	TEST RESULTS · · · · · 33
	Mechanical Properties · · · · · 33
	Static Fracture Toughness · · · · · 33
	Static Fracture — Plate Material · · · · · 44
	Fracture Appearance · · · · · 49
	Cyclic Flaw Growth Tests — Sheet · · · · · 52
	Cyclic Flaw Growth Tests — Plate · · · · · 63
8	DISCUSSION OF RESULTS · · · · · 73
	Mechanical Properties — Sheet · · · · · 73
	Mechanical Properties — Plate · · · · · 75
	Plane Stress Fracture Toughness (K_C) · · · · · 75
	Variation of Plane Strain Fracture Toughness with
	Location of Crack · · · · · 75
	Plane Strain Fracture Toughness of 1.0-Inch Plates · · · · · 79
	Net Fracture Stress · · · · · 79
	Cyclic Crack Growth — Sheet · · · · · 84
	Cyclic Crack Growth — Plate · · · · · 85
	Stress Intensity Ratio · · · · · 87
9	CONCLUSIONS · · · · · 91

Section		Page
10	REFERENCES	93
11	BIBLIOGRAPHY.	95

Appendix

I	NONDESTRUCTIVE TESTING	I-1
I-1	TEST METHODS	I-1
	Penetrant Testing	I-1
	Ultrasonic Testing	I-1
	Radiographic Testing	I-2
	Eddy Current Testing	I-2
I-2	FLAW GROWTH TESTS	I-5
	Ultrasonic Tests on 0.063-Inch Sheet Flaws.	I-5
	Ultrasonic Testing of Artificial Flaws in One-Inch- Thick Specimens	I-6
	Eddy Current Monitor for Flaw Growth in 0.063-Inch Sheet.	I-9
	Radiographic Testing for Flaw Enlargement Studies	I-10
	DISTRIBUTION	D-1

LIST OF FIGURES

Figure		Page
1	Welded 1.0-Inch Thick Plate Sections of 2219-T81 Aluminum Alloy	9
2	One-Inch Plate Weldment Showing Milled-Out Section Prior to Repair Welding	9
3	Manual Repair Welding of 2219-T81 Aluminum Sheet	11
4	Repair Welding of 1.0-Inch Plate Material	12
5	General Configuration of Unnotched Tensile Specimens Machined From 0.063-Inch Sheet and 1.0-Inch Plate	14
6	Weld Tensile Specimen of 0.063-Inch Thick 2219-T81	15
7	Weld Tensile Specimen of 1.0-Inch Thick 2219-T81	15
8	Specimen Configuration for Plane Strain Fracture Toughness and Cyclic Flaw Enlargement Tests in 1.0-Inch Thick Plate	16
9	Plane Stress Fracture Toughness Specimen (13 Inches Wide).	17
10	Welded 1.0-Inch Plate Round Tensile Specimens. Upper Specimen Has Been Polished and Etched	18
11	Strain Gage Installation on Welded Sheet Tensile Specimen	18
12	Parent Metal Tensile Specimen with Remote Reading Cryogenic Extensometer Attached	19
13	Center-Notched Crack Propagation Sheet Specimens Showing Notches in (Left to Right) Parent Material, Weld Zone, Fusion Line	20
14	Radiographs of Intentional Tungsten Inclusions in 1.0-Inch Plate Weldment	21
15	Shape of Surface Flaw in 1.0-Inch Plate Material	22
16	Location of Notches in Welded Specimens	23
17	Variation of Hardness With Weld Zones For 2219-T81 Plate	25
18	Liquid Hydrogen Cryostat for Small Test Specimens Installed in Tensile Test Machine	28
19	Strain Gage Installation on Sheet Tensile Specimens.	29
20	Strain Gaged Sheet Tensile Test Specimen in Quick-Release Clevis	30

LIST OF FIGURES, Contd

Figure		Page
21	Test Setup for Bending Fatigue Crack Extension of 1.0-Inch Plate Material	32
22	Variation of Strength With Temperature for 2219-T81 Sheet	38
23	Variation of Strength with Temperature of 2219-T81 Aluminum Alloy 1-Inch Plate	39
24	Center-Notched Fracture Toughness Specimen Test at -320° F. Note Transits Used for Determination of Crack Growth	43
25	Variation of Plane Stress Fracture Toughness With Temperature for 2219-T81 Sheet	44
26	Variation of K_{IC} With Temperature for Repair Welded 2219-T81 Sheet	45
27	Variation of Q for Various Values of $\frac{\sigma}{\sigma_{ys}}$	48
28	Fracture Surfaces of 1.0-Inch 2219-T81 Tested in Static Fracture at Various Temperatures	50
29	Fracture Surfaces of Repair Welds in 1.0-Inch 2219-T81 Tested in Static Fracture at Various Temperatures	51
30	Cyclic Crack Growth, Base Metal Sheet	55
31	Cyclic Flaw Growth, Welded Sheet, 75° F	56
32	Cyclic Crack Growth, Welded Sheet (HAZ), 75° F	57
33	Cyclic Crack Growth, Welded Sheet, -320° F	58
34	Cyclic Crack Growth, 2219-T81 Sheet, -423° F	59
35	Cyclic Crack Growth, Repair Welded Sheet, -423° F	60
36	Crack Growth for Welded 2219-T81 Sheet at -320° F ($\sigma_m = 2.5$ ksi)	61
37	Crack Growth for Repair Welded 2219-T81 Sheet at -320° F ($\sigma_m = 20.5$ ksi)	62
38	Fracture Surfaces of 1.0-Inch 2219-T81 Tested in Cyclic Fracture at Various Temperatures	70
39	Fracture Surfaces of Repair Welds in 1.0-Inch 2219-T81 Tested in Cyclic Fracture at Various Temperatures	71

LIST OF FIGURES, Contd

Figure		Page
40	Fracture Surfaces of Repair Welds in 1.0-Inch 2219-T81 Tested in Cyclic Fracture at Various Temperatures	72
41	Stress-Strain Curve, 2219-T81 Aluminum Weldment at Room Temperature	74
42	Distribution of K_{IC} With Weld Zones	76
43	Variation of Plane Strain Fracture Toughness With Temperature for 2219-T81 Plate	80
44	Variation of K_{IC} With Temperature for Repair Welded 2219-T81 Plate	81
45	Fracture Surface of Welded 2219-T81 Aluminum Plate (Crack in Fusion Line, 75° F)	86
46	Fracture Surface of Welded 2219-T81 Aluminum Plate (Crack in Weld Metal, 75° F)	86
47	Schematic of Cycle Life Variation	88
48	Variation of Stress Intensity Ratio With Cycles to Failure for 2219-T81 Plate	89
I-1	Ultrasonic C-Scan, Sheet 2-6 (0.063-Inch), Showing 0.012- and 0.018-Inch-Diameter Wires	I-3
I-2	Shear Wedge Block (70 Degrees) Fabricated to Provide Lateral Transducer Adjustment.	I-5
I-3	Schematic of Shear Wave Test Setup	I-6
I-4	Ultrasonic Transducers for Through-Transmission Test In-Situ on the Fatigue Test Machine	I-7
I-5	Ultrasonic Test Instrumentation Used During Cyclic Flaw Enlargement on the One-Inch-Thick Plate Specimens	I-8
I-6	Eddy Current Probe Holder	I-9
I-7	Measurements From Radiograph of Specimen CF2 (Looking Down on the Specimen)	I-11
I-8	Microdensitometric Scans of Cracks in Specimen 3-4-2	I-13
I-9	Microdensitometric Scan of Starter Notch in Specimen 20	I-14

LIST OF FIGURES, Contd

Figure		Page
I-10	Microdensitometric Scan	I-15
I-11	Microdensitometric Scan of Specimen R12	I-16
I-12	Microdensitometric Scans of Cut-Outs From Specimens B2, B3, and B6. The 0.04 Density Gradient is an Indication of Copper Migration in 2219-T81 Aluminum Alloy	I-17

LIST OF TABLES

Table		Page
1	Major Welding Parameters Used in This Program	8
2	Mechanical Properties of 0.063-Inch 2219-T81 Aluminum Alloy	34
3	Mechanical Properties of 1.00-Inch 2219-T81 Aluminum Alloy	36
4	Static Fracture Tests of 2219-T81 Sheet Stock (t = 0.063 Inch)	40
5	Static Fracture Toughness Test Results - 1.00-Inch 2219-T81 Aluminum Alloy	46
6	Cyclic Flaw Enlargement of 2219-T81 Sheet, Center Notched Tests	53
7	Results of Surface-Notched 2219-T81 Sheet Cyclic Tests (t = 0.062 in., W = 13.00 in.)	54
8	Fracture Tests of 2219-T81 Plate	64
9	Cyclic Flaw Growth Data for 1.0-Inch 2219-T81 Aluminum Alloy	67

SUMMARY

The objectives of this program were to: 1) perform a literature search on the welding and inspection of 2219-T81 aluminum alloy, 2) weld, by the industry standard methods, the 0.063-inch sheet and 1.0-inch plate material, and 3) perform mechanical properties static fracture, and cyclic flaw growth tests on the base material, welded, and repair welded sheets and plates.

A literature search and industry survey were performed and reported in the Interim Report (NASA CR-72097 of January 1967). The plate and sheet were welded using automatic GTA (gas-tungsten-arc, sometimes called TIG) weld techniques and manual repair weld techniques. The fracture characteristics were studied at room temperature, -320 and -423° F by locating notches and cracks in the parent material, heat-affected zone, fusion line, and the center of the weld metal. Mechanical properties of the various zones were obtained by tensile tests utilizing small strain gages.

Welding causes a large reduction in yield strength for 2219-T81 sheet and plate but only a modest reduction in ultimate strength. In general, the static toughness properties of the base material sheet and plate increase with a reduction in temperature. However, the toughness in the center of the weld shows a significant decrease between -320° and -423° F in both plate and sheet.

The cyclic crack or flaw growth for 2219-T81 is somewhat erratic for automatic welded material and is very erratic for repair welded material.

PRECEDING PAGE BLANK NOT FILMED.

1/INTRODUCTION AND BACKGROUND

Although a substantial amount of data has been generated in the area of fracture mechanics in recent years, most of this information has been restricted to parent metal investigations at room temperature. The American Society for Testing and Materials (ASTM) has made recommendations for the specimen configuration of fracture screening specimens (References 1 and 2) at room temperature. These recommendations were primarily concerned with center-notched plane stress specimens and single-edge-notched tensile specimens that made no attempt to simulate flaws found in actual structures. At the same time, Tiffany, Lorenz, and Hall at the Boeing Company had determined that the flaw most observed in aerospace applications is a surface crack resembling a thumb nail. (Reference 3). Such a crack, in a rather thick material, can be quite serious since the crack depth is difficult to determine and is likely to cause catastrophic failure prior to propagating through the thickness. (Even worse is the totally imbedded crack that escapes detection completely). Tiffany evaluated surface flaws in 2219 aluminum alloy plate under static and cyclic conditions. However, since all structures must be joined in some manner, it is probable that the most critical regions are not in the undisturbed parent metal. In the case of aerospace vehicles, the most prominent joining technique is welding. It follows that a most useful program is to evaluate the toughness of a potential aerospace material in a welded plate condition utilizing the part-through crack technique. At the same time, the same material could be evaluated in the welded sheet form by using the center-cracked specimen for comparison.

The 2219-T87 alloy sheet parent metal has been evaluated by various investigators at room and cryogenic temperature (References 4 and 5).

Although, the evaluation of the flaw growth in weldments is undisputedly an excellent idea, the results from such a program are subject to many possible variations due to variables both known and unknown. Not the least of these is the effect of welding. Despite the fact that 2219 is a very weldable alloy (Reference 6), it is possible that loose controls on weld specifications could cause wide variations in fracture properties.

With this in mind, the present program was designed to determine the state-of-the-art in welding and inspection of 2219 aluminum alloy before proceeding. An attempt was to be made to simulate standard production welding techniques rather than closely controlled laboratory techniques. A brief review of recent literature indicates that although 2219 is readily weldable, the repair welding of this material (or any material) could possibly lead to the creation of an embrittled joint. Consequently, the degradation of the welded joint due to repair welding was examined in this program.

INSPECTION AND NONDESTRUCTIVE TESTING

A continuous effort is being made to improve nondestructive testing of welds and weldments in aluminum alloys. Problems are evident both in the areas of defect detection and, after detection, characterization of the defect. The distinction between detection and characterization must be clearly understood in order to fully realize the benefits which can accrue from properly applied nondestructive testing.

An integrated program of flaw enlargement analysis correlated with nondestructive testing is certain to improve the nondestructive testing techniques. On the other hand, if the nondestructive testing can be sufficiently refined during an integrated test program, it may eventually serve to drastically reduce the amount of destructive analysis required.

If the physical limitations of a particular nondestructive testing method are not understood, the test may be of little value. When a defect goes undetected after a nondestructive test has been applied, criticism is often leveled against the test method. In most cases, the legitimate target of the criticism should be the misapplication of the test through lack of understanding of the basic principles.

A particular nondestructive test may also be misapplied if erroneous assumptions have been made regarding the characteristics of anticipated defects. The sensitivity, or detection ability, of a nondestructive test is highly directional with respect to the major plane(s) of a defect, for example. Naturally occurring defects can assume an almost infinite variety of characteristics in combinations and permutations of discrete variables. Allowing that directional sensitivity is one of several critical factors, certain assumptions are usually necessary to reduce expected defect shape and alignment to a specified number of most probable conditions.

Artificial defects, purposely created to be predictably unidirectional and specifically shaped, provide an excellent basis for refinement of nondestructive testing techniques. Since, at least to some extent, shape and size of flaws can be controlled and predicted, many of the variables resulting from misapplication of nondestructive tests will be eliminated. Effort can then be concentrated on the aspect of nondestructive testing that requires the most refinement - that is, characterization of defects.

Refer to Appendix I for a complete description of the nondestructive testing as applied in this program.

2/GENERAL TEST PROGRAM

The scope of this program, although quite broad, was not designed to provide statistical accuracy of data but was to examine various facets of the fracture area in a promising aerospace alloy, 2219-T81 aluminum. The studies of weld and nondestructive testing techniques were designed to determine the production state-of-the-art in U.S. aerospace companies as well as to point out possible deficiencies. Primarily, the test program intended to obtain various fracture mechanics data for 2219-T81 weldments.

To study the effect of thickness, both 1.0-inch plate and 0.063-inch sheet were studied. For each data point, parent metal tests were performed for comparison purposes. Test specimens for sheets necessarily differed from those for plates, but an attempt was made to duplicate test conditions. In general, the program was divided as follows:

- Task I. Welding and Nondestructive Testing Literature Search

- Task II. Testing of Parent Material and Weldments
 - a. Mechanical Properties Tests
 - b. Static Fracture Tests
 - c. Cyclic Flaw Enlargement Tests

- Task III. Repair Weld Tests
 - a. Mechanical Properties Tests
 - b. Static Fracture Tests
 - c. Cyclic Flaw Enlargement Tests

After testing, all fractures were examined visually. In cases where it was felt that meaningful information could be obtained, light or electron fractographs were obtained. Crack depth and flaw shape measurements were made on all 1.0-inch plate fracture specimens.

3/MATERIALS

The material used throughout this program was 2219-T81 aluminum alloy in two thicknesses, 0.063-inch sheet and 1.0-inch plate. Similar work on parent material was conducted by Boeing on 2219 aluminum in the T87 temper (Reference 3). Companion projects originated by NASA LeRC at Douglas and Frankford Arsenal also utilized the T87 material.

Previous work (References 3 and 5) has indicated that the T81 material is somewhat tougher than the T87. The differences in processing are:

- a. T81 is heat-treated and stretched by the manufacturer while T87 is heat-treated and cold worked approximately 9% by the manufacturer.
- b. T81 is aged 18 hours at 350° F while T87 is aged 24 hours at 325° F (Reference 6).

The 1.0-inch plate obtained from Alcoa was designated as follows:

Alcoa Aluminum Sawed Plate

Mill Finish

Spec. MIL-A-8920, Oiled

Chemical Analysis (percent by weight)

Silicon	0.20 max
Iron	0.30 max
Copper	5.8 to 6.8
Manganese	0.20 to 0.40
Magnesium	0.02 max
Zinc	0.10 max
Titanium	0.02 to 0.10
Others, each	0.05
Others, total	0.15
Aluminum - Remainder	

The 0.063-inch sheet was obtained in 4 × 8 foot sheets under the same specifications from the same supplier.

4/WELDING

The current practices for welding 2219 aluminum alloys were reviewed and the results were reported in Reference 7. An industry survey summarized in that report showed that a wide variation of techniques was being used in this country. It appeared that each of the methods was acceptable because of the fact that 2219 aluminum is so readily weldable. The procedures used by Convair division are summarized in Table 1.

Inasmuch as all welded specimens planned for this program were to be welded perpendicular to the grain direction, all welds were made in 4-foot wide sections, corresponding to the width of the sheet or plate (Figure 1).

Materials were examined by ultrasonic inspection prior to welding. All welded sections were radiographed after each welding process or weld repair. Standard weld specifications were used to accept or reject individual welds. In some cases, unacceptable portions of welds were found outside of the areas that were to be used for test specimens. In one case of repair welding of the 0.063-inch sheet, a tensile test specimen was cut from an area containing marginal porosity and tested. Since the performance of that test was erratic, a replacement specimen was cut from the same sheet and tested satisfactorily.

Information obtained from the industry survey described in Reference 7 indicated that most companies would permit three weld repairs before rejection of the part. Some permitted more than three repairs in the welding of the 2219 aluminum alloy due to its remarkable forgiveness.

WELD PROCEDURES

All welding surfaces were hand-scraped, draw-filed, and cleaned with MEK (methyl ethyl ketone) just prior to welding. Although no backup bars were used for the 1.0-inch plate material, mild steel backup bars with 1/8-inch deep by 3/8-inch wide grooves were used with the sheet. All welds were automatic gas tungsten arc (GTA, frequently called TIG) welds using direct current straight polarity (DCSP). The sheet material was butt-welded in a single pass using 2319 filler wire while the plate was joined in two passes (one from each side) without the use of filler. It was anticipated that there would be no mismatch problems with the 1.0-inch plate because of its rigidity. However, a great deal of difficulty was experienced because of severe warpage of the as-received material.

Table 1. Major Welding Parameters Used in This Program

PARAMETER	0.063-INCH SHEET		1.0-INCH PLATE	
	Automatic GTA-DCSP	Manual Repair GTA-AC	Automatic GTA-DCSP/2 Pass	Manual Repair GTA-AC/Mult. Pass
Voltage	14.5 ± 0.5 volts	11 - 12 volts	11.0 ± 0.5 volts	16 - 22 volts
Current	40.0 ± 2.0 amperes	70 - 120 amperes	475 ± 5 amperes	140 - 200 amperes
Travel Speed	12 ± 1 in./min	Approx. 3-3 1/2 in./min	3.5 ± 0.5 in./min	Not applicable*
Filler Wire	3/64 in. dia - 2319	3/32 in. dia - 2319	None	3/32 in. dia - 2319
Wire Feed Rate	20 ± 2 in./min	Approx. 6-7 in./min	None	Not applicable
Cover Gas	60 cfh of helium	25 cfh of argon	85 cfh of helium	16 cfh of argon
Backup Gas	12 cfh of argon	10 cfh of argon	None	None*
Electrode	3/32 in. dia 2% thoriated W 45° angle tip	1/8 in. dia 2% thoriated W ball tip	5/32 in. dia 2% thoriated W blunt tip	1/8 in. dia 2% thoriated W ball tip
Backup Bar	Mild steel, 1/8 in. deep by 3/8 in. wide groove	Mild steel deep groove	None	None

*Not applicable when filling a cavity.

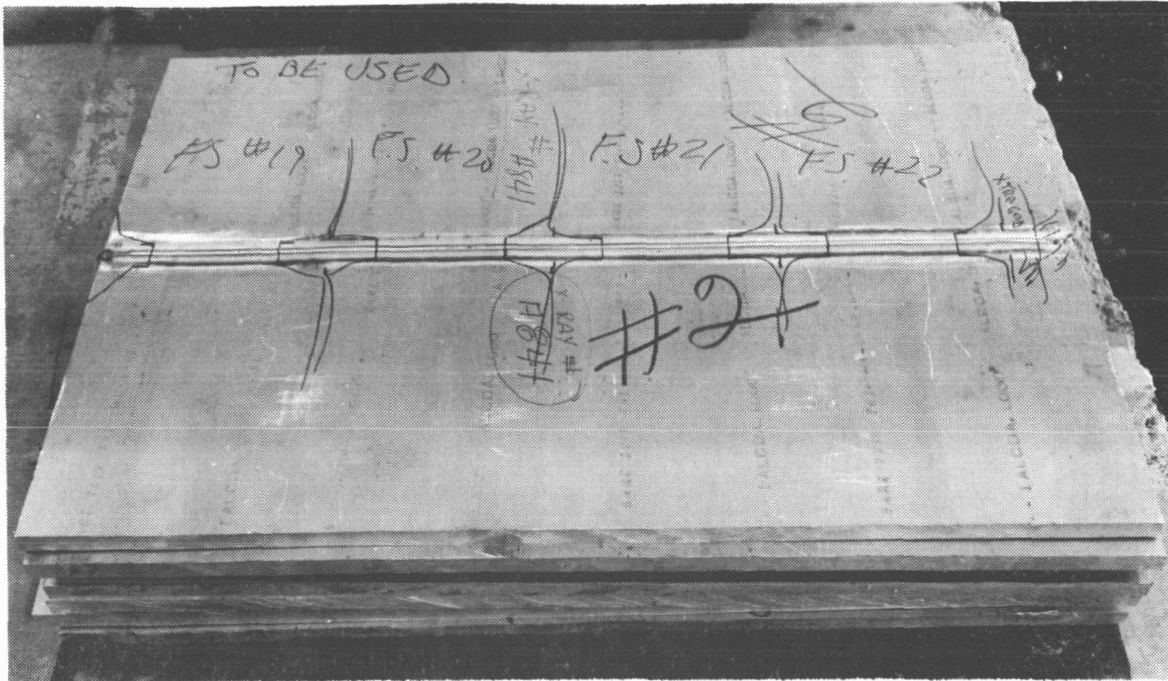


Figure 1. Welded 1.0-Inch Thick Plate Sections of 2219-T81 Aluminum Alloy

REPAIR WELDING

Repair welds were made on the original welds using the parameters shown in Table 1. After the original sheet welds were made, inspected and accepted, the welds were milled out to a depth of 0.040 inch. The repair was made with a single pass over the milled-out portion. This procedure was repeated until three repairs were made.

For the 1.0-inch plate material, the original weld was milled out in the center of the welded specimen to a depth of 0.5 inch. (See Figure 2.)

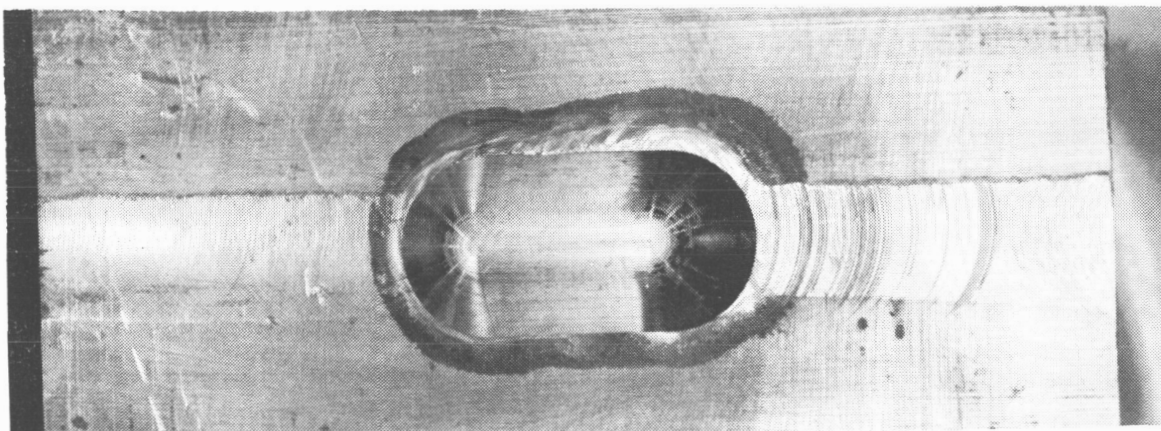


Figure 2. One-Inch Plate Weldment Showing Milled-Out Section Prior to Repair Welding

Repair welds were made manually using GTA-AC techniques for both 0.063-inch sheet and the 1.0-inch plate materials (Figures 3 and 4). The repair on the 0.063-inch sheet was made in a single pass, while multiple passes were made on the 1.0-inch plate.

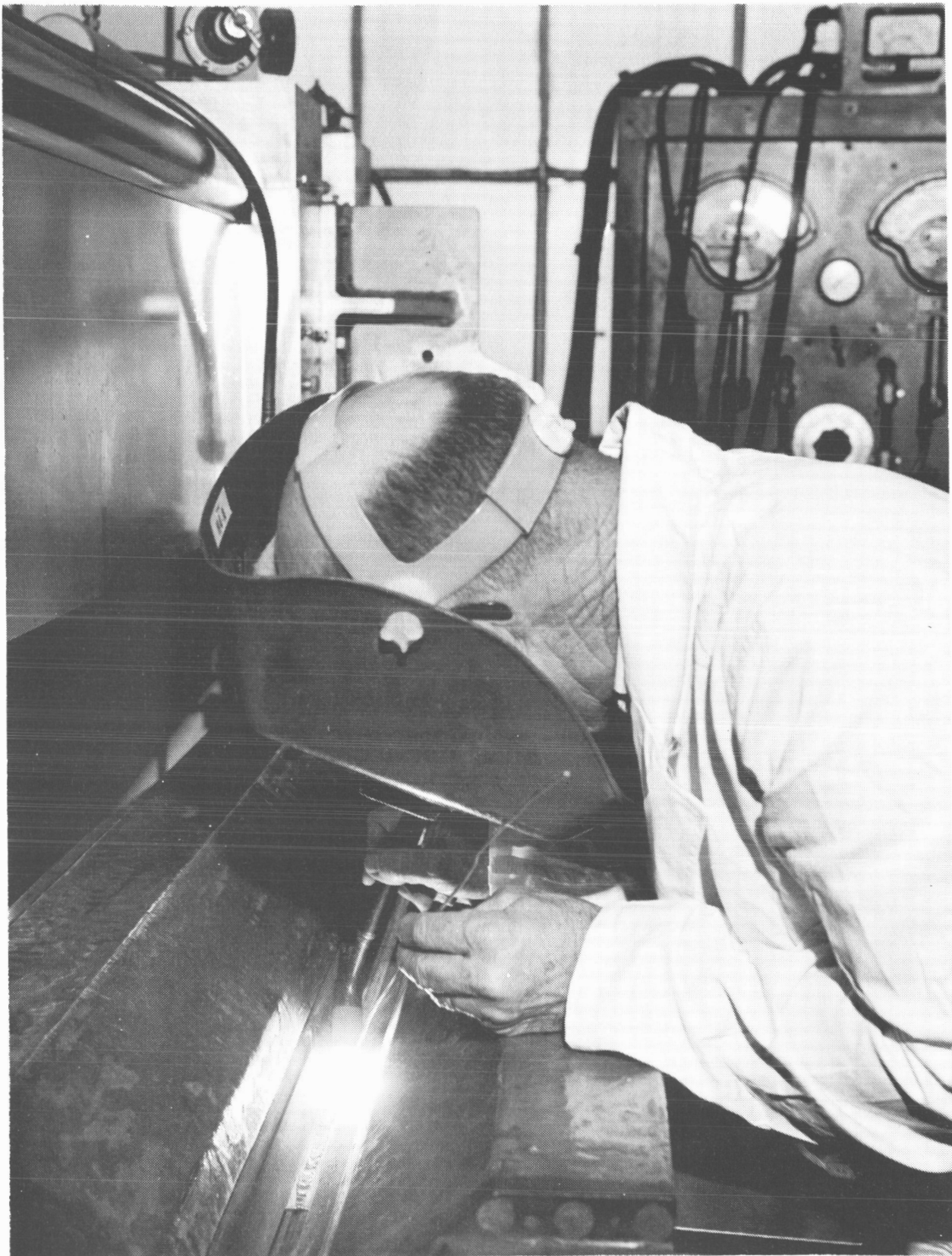


Figure 3. Manual Repair Welding of 2219-T81 Aluminum Sheet

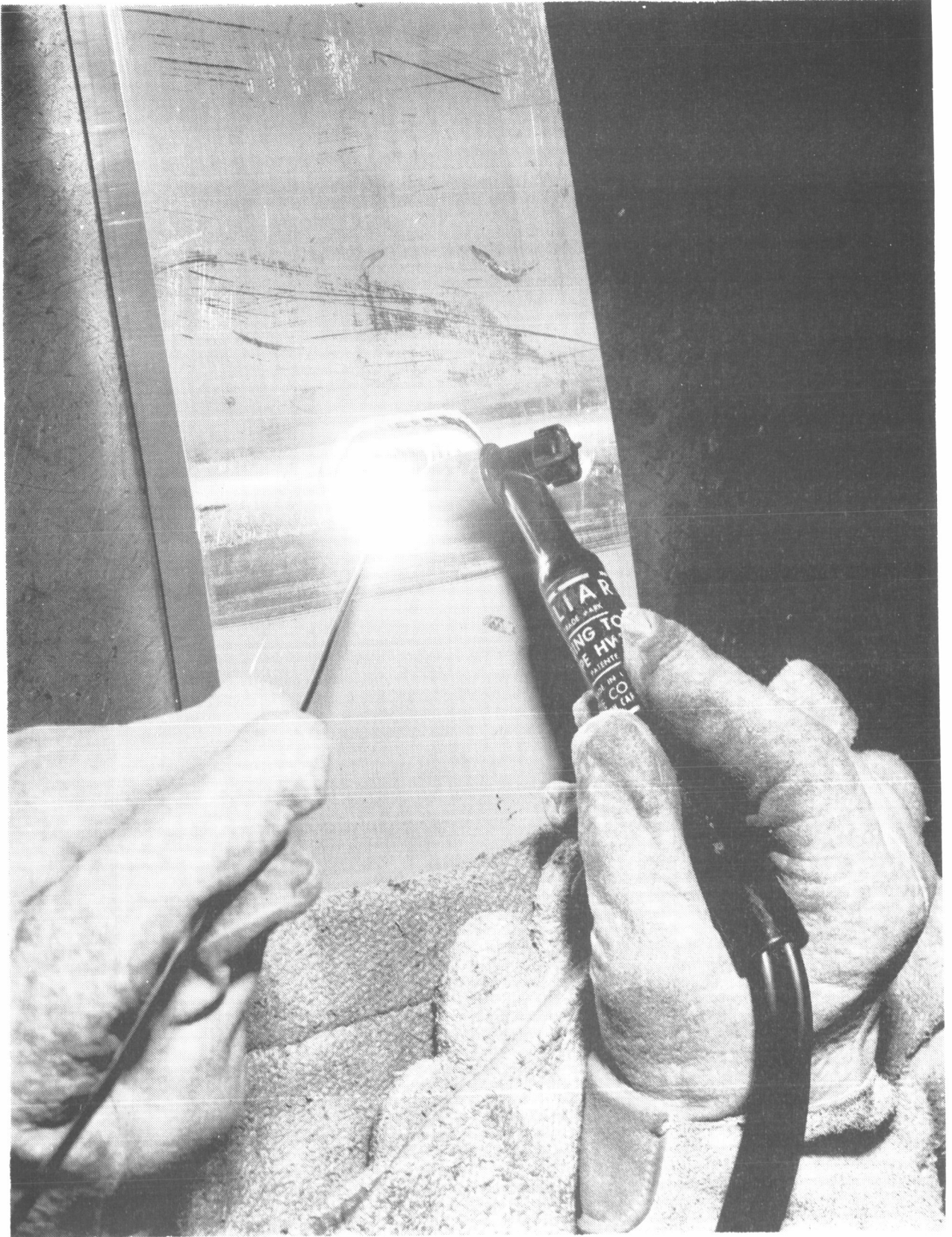


Figure 4. Repair Welding of 1.0-Inch Plate Material

5/TEST SPECIMENS

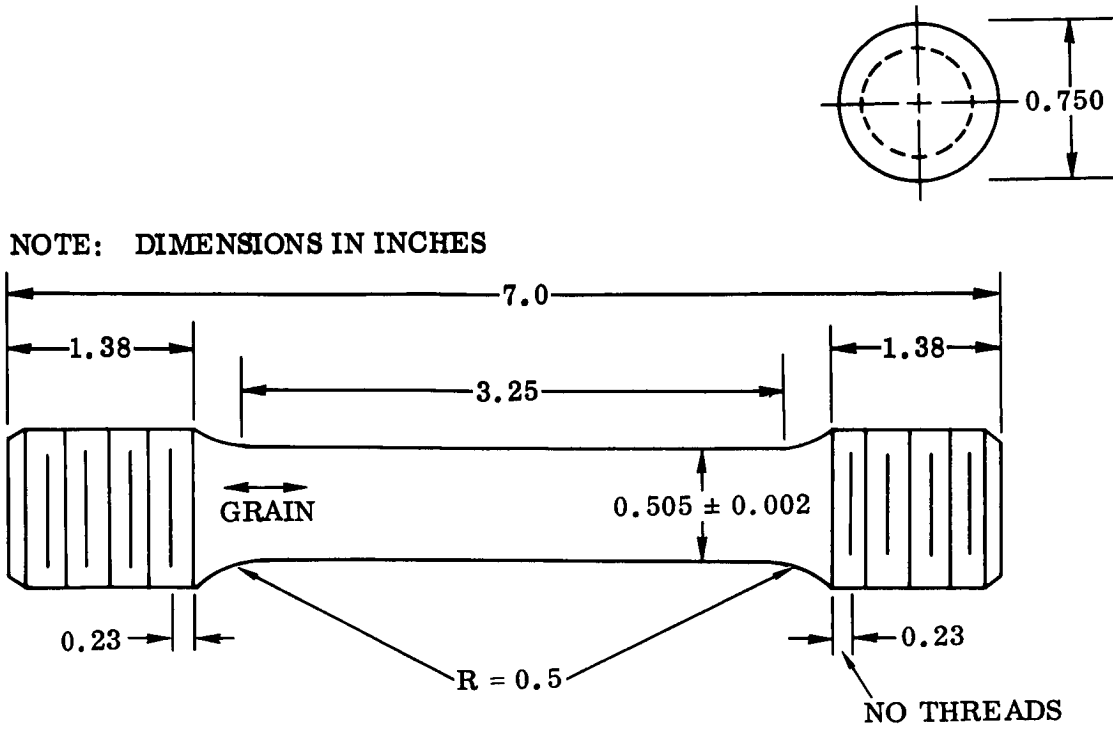
Various test specimen configurations were used to obtain mechanical properties and fracture characteristics, including flat and round tensile specimens, center-notched crack propagation specimens, and surface-notched plane strain fracture specimens. (See Figures 5 through 9 for specimen configurations.) In general, welded test specimens had the same configuration as did the parent metal specimens with the exception of the location of the notches.

TENSILE TESTS

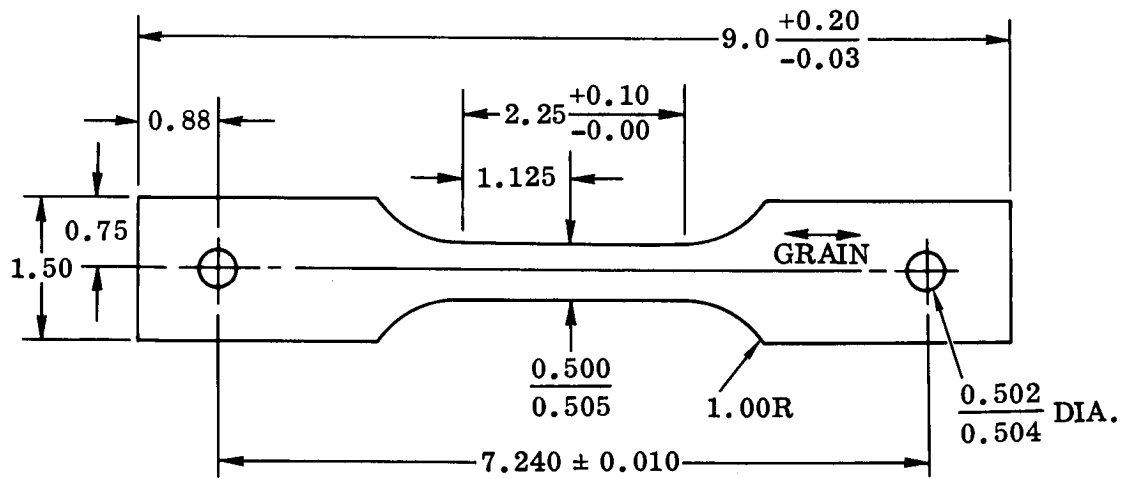
All tensile tests were conducted on two general specimen configurations. (Figures 6 and 7.) Weld specimens were taken from the same pieces as were the fracture specimens. In case of the 1.0-inch plate, round tensile specimens were taken from the section of the plate between the large surface-notched specimens. All welded specimens were determined to be radiographically acceptable according to current specifications.

Welded tensile specimens were polished and etched in order to locate the various weld zones prior to installation of strain gages (Figure 10). Originally, it was planned to use separate tensile specimens for determination of the yield strength of the heat-affected zones (HAZ). However, since the etching process was so effective in locating the HAZ, and since the Convair strain gage laboratory was able to apply small strain gages, it was possible to obtain stress-strain curves in the HAZ on the same specimen used for determination of the properties of the welds. In several cases, the strain at three locations (parent metal, weld zone, heated-affected zone) was obtained on a single test specimen (Figure 11) with back-to-back gages. In some cases, the parent metal tensile specimens were tested without strain gages by using a remote reading cryogenic extensometer (Figure 12).

When the round tensile specimens were fabricated from welded 1.0-inch plate aluminum and etched, the location of the HAZ was somewhat variable. The center of the specimen corresponded to the center (of the thickness) or middle portion of the welded plate. As a consequence, the intersecting planes of weld metal and specimen surface caused a rather undulating fusion line. It was observed that the HAZ was actually divided into two distinct zones, one of which was darker in color than the other. An attempt was made to determine the stress-strain characteristics of both zones. However, it was prudent to locate strain gages 180 degrees apart (back-to-back) around the perimeter in order to eliminate eccentric bending effects. In most cases, the HAZ was not exactly repeatable at 180-degree intervals. Nevertheless, gages were applied and the outputs were recorded with reasonable results.



Round Specimen Machined from Center of 1.0-Inch Thick Plate



Flat Specimen Machined from 0.063-Inch Thick Sheet

Figure 5. General Configuration of Unnotched Tensile Specimens Machined From 0.063-Inch Sheet and 1.0-Inch Plate

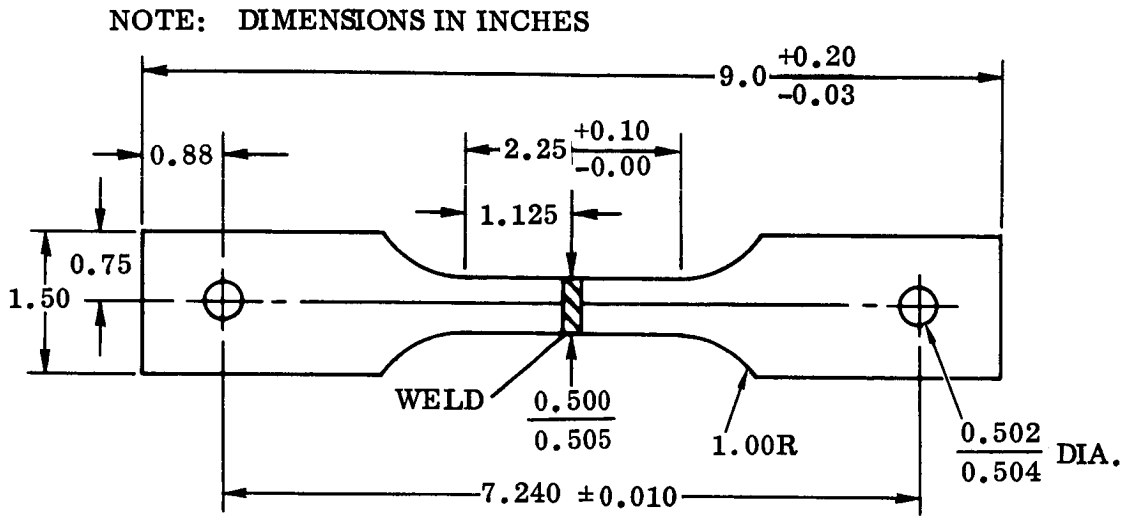


Figure 6. Weld Tensile Specimen of 0.063-Inch Thick 2219-T81

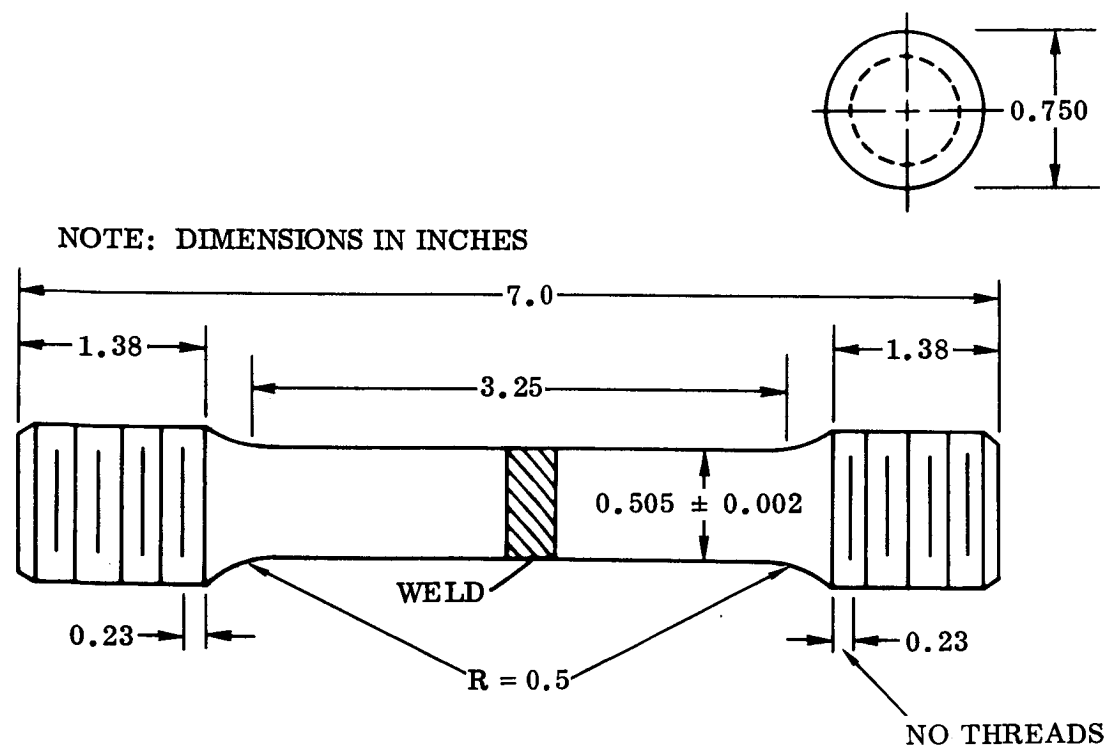


Figure 7. Weld Tensile Specimen of 1.0-Inch Thick 2219-T81

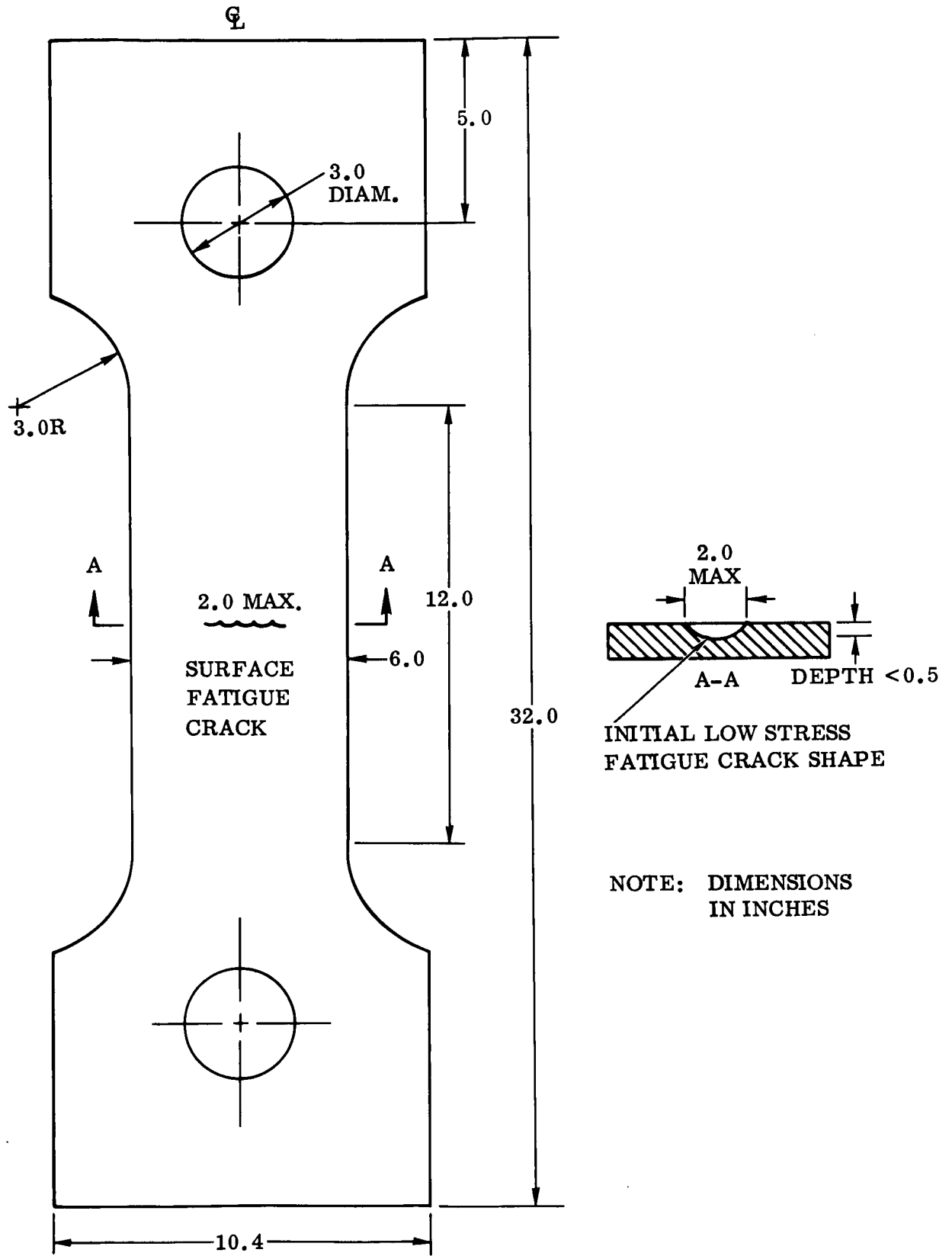
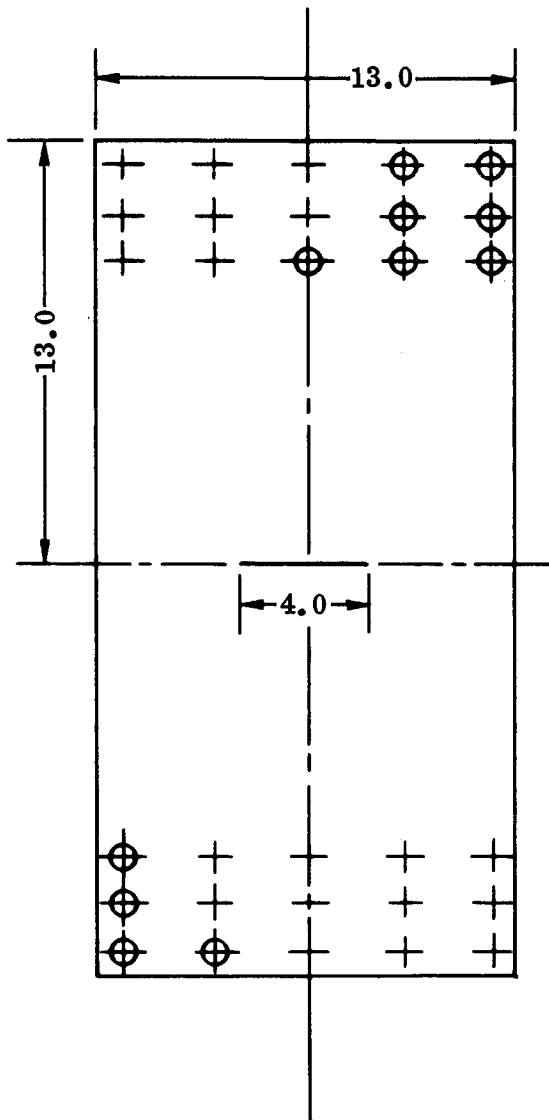
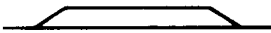


Figure 8. Specimen Configuration for Plane Strain Fracture Toughness and Cyclic Flaw Enlargement Tests in 1.0-Inch Thick Plate



HOLES DRILLED TO
MATCH CLEVIS.



NOTCH DETAIL
TIP RADIUS < 0.005 INCH

NOTE: DIMENSIONS IN INCHES

Figure 9. Plane Stress Fracture Toughness Specimen (13 Inches Wide)

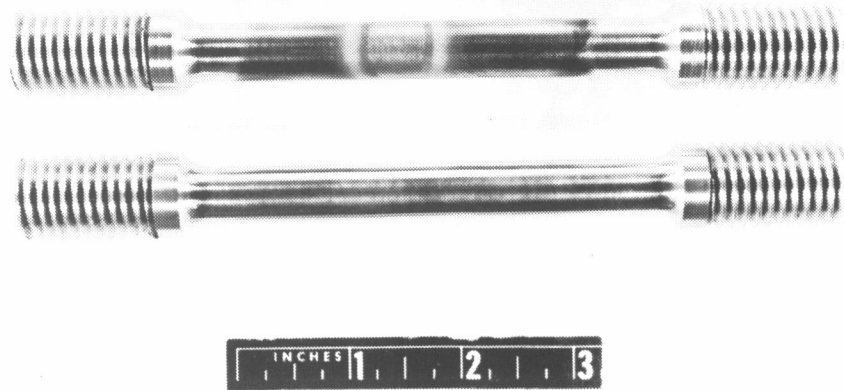


Figure 10. Welded 1.0-Inch Plate Round Tensile Specimens. Upper Specimen Has Been Polished and Etched

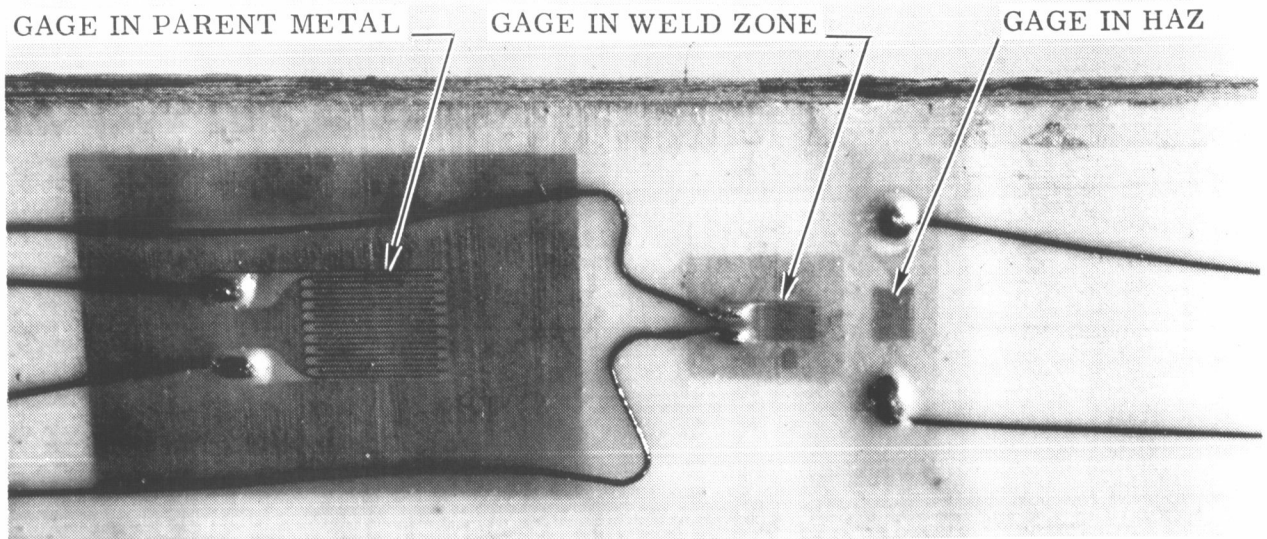


Figure 11. Strain Gage Installation on Welded Sheet Tensile Specimen

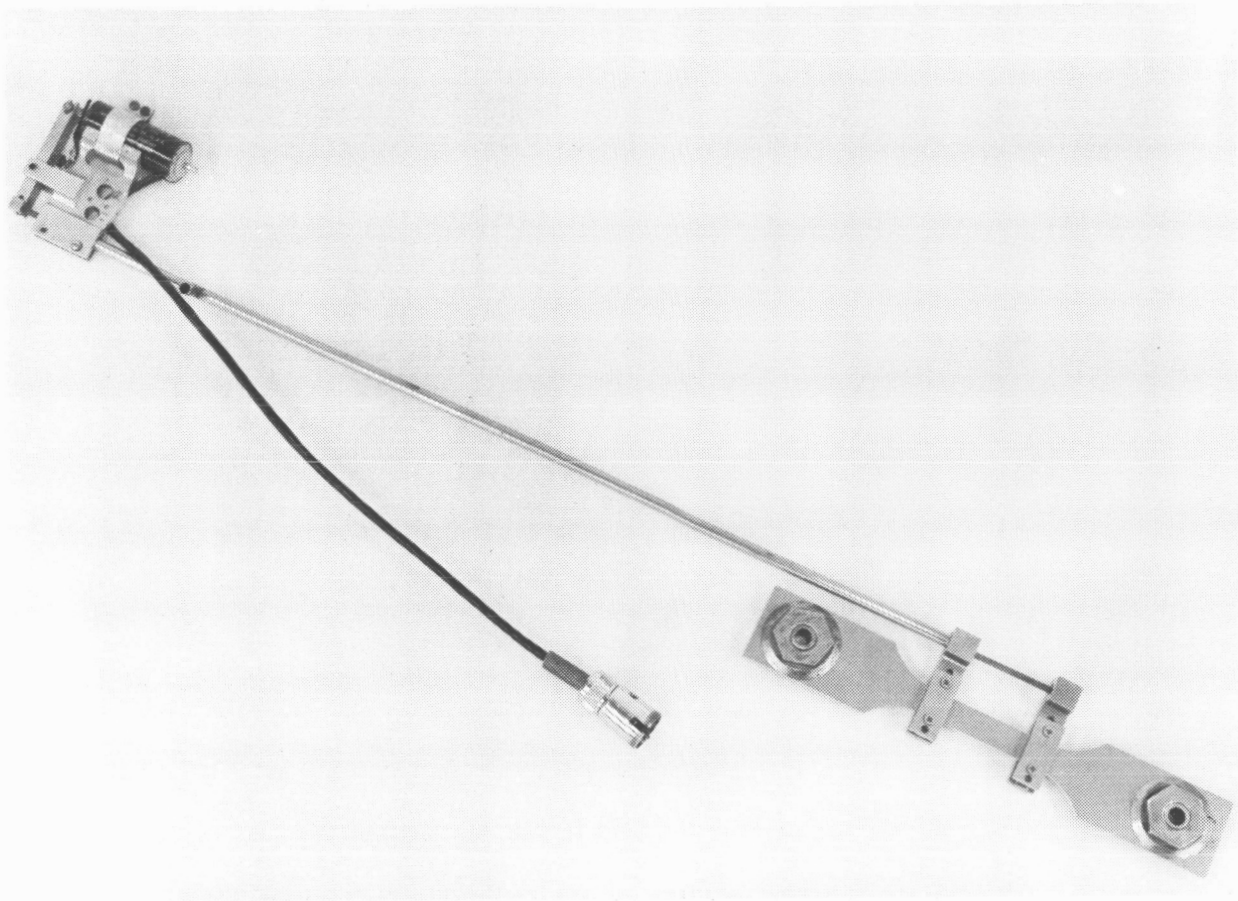


Figure 12. Parent Metal Tensile Specimen with Remote Reading Cryogenic Extensometer Attached

All tensile tests performed on weld specimens were repeated on similar weld repair specimens.

CENTER-NOTCHED SPECIMENS

Center-notched crack propagation specimens were used for sheet base metal, welded, and repair welded static and cyclic fracture tests. Notches were machined in the center of the specimens (Figure 13) and extended by low-stress fatigue cycling. (See Page 20, "Notches" for a more detailed explanation.) For welded specimens, the weld bead was machined off and polished prior to slotting. Lateral stability was provided for these 13-inch wide specimens through heavy clevises that bolted to the ends of the specimens.

Several sheet specimens (13-inch wide) were surface-slotted in order to try to study the flaw growth characteristics of the sheet materials under conditions that approximated plane strain. Control of the machine slot and subsequent fatigue crack extension was extremely difficult because of the thin gauge of material that required extremely small dimensions of the surface slot.

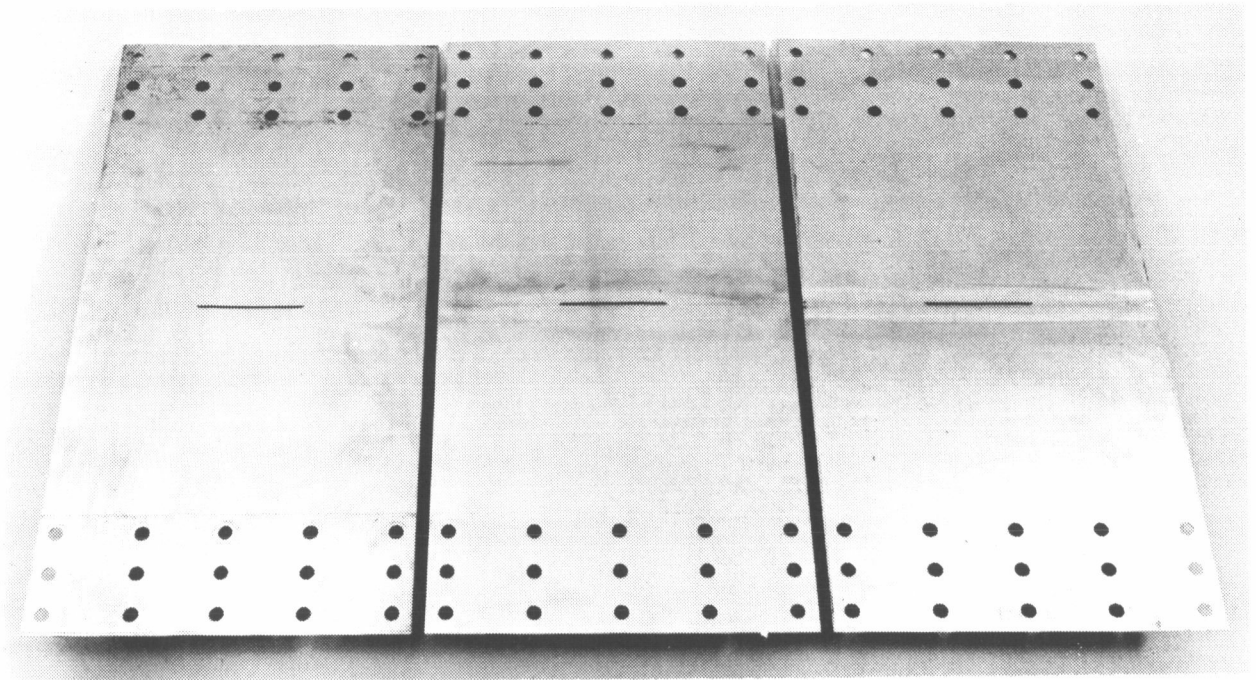


Figure 13. Center-Notched Crack Propagation Sheet Specimens Showing Notches in (Left to Right) Parent Material, Weld Zone, Fusion Line

1.0-INCH PLATE FRACTURE SPECIMENS

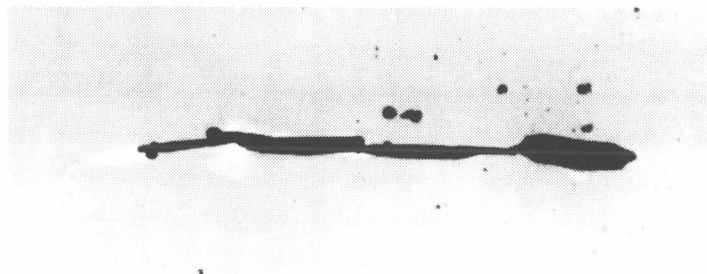
All parent metal, welded, and repair welded static and flaw growth fracture tests utilized the same specimen configuration (Figure 8). The only variation in specimens concerned the depth and shape of the surface notch itself. For flaw growth tests, the notch was shallower than for the static tests. In addition, several repair welded specimens contained internal flaws. These flaws were inserted in the repair weld area by either machining or by depositing tungsten flakes (Figure 14) in the bottom of the repair cavity during welding.

NOTCHES

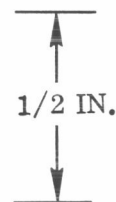
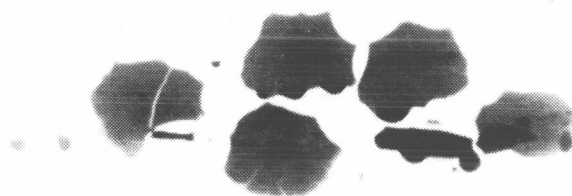
A somewhat critical portion of the program concerned the insertion and location of the notches in the various fracture specimens. Initially, all notch starters were machined by the electrical discharge method. However, this process became exceedingly time consuming for the part-through notches in the 1.0-inch plate material. Consequently, a tool was designed and manufactured that permitted milling the surface notch much more economically.

The through crack specimens using the 0.063-inch sheet material were notched with a Cincinnati ELEKTRO-JET* machine. The shape and size of the notch is

*Trademark.



Top View



Side View

Figure 14. Radiographs of Intentional Tungsten Inclusions in 1.0-Inch Plate Weldment

shown in Figure 9. The chisel-shaped notch tips were selected in order to simplify dressing of the electrode and to minimize the possibility of the notch extremities being in different planes.

The starter notches for the 1.0-inch thick specimens were semicircular discs with beveled edges (See Figure 15).

An attempt was made to provide a tip radius as small as possible in order to facilitate fatigue notch crack extension. To a certain point, the machining of a very sharp notch reduces the cost of testing by reducing the time required for fatigue cracking. However, as the notch tip radius approaches 0.001 inch or less, the time

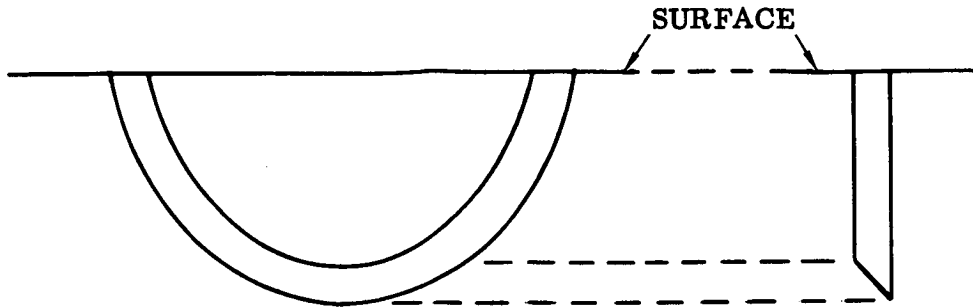


Figure 15. Shape of Surface Flaw in 1.0-Inch Plate Material

required for machining increases exponentially. For this reason, the specimens machined under this program were restricted to a maximum tip radius of 0.005 inch.

In all cases, the notches were machined in such a way as to permit fatigue crack extension of about 1/10 inch before the test initial crack length was attained.

As has been mentioned, the shape of the notching tool was semicircular for the surface-cracked specimens. Since the specimens were fatigue cracked in bending, the surface stresses were somewhat higher than the stresses at the tip of the notch causing the final crack shape to be semielliptical (desirable).

LOCATION OF NOTCHES

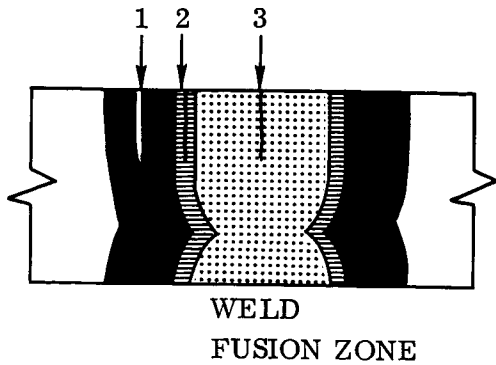
For the parent material specimens, notches were located at the midpoint of the specimen length and symmetric about the transverse center line.

The notches were located in three different areas for the welded specimens as shown in Figure 16.

In order to locate the proper zones, the weld metal was machined off until it was approximately flush with the parent metal. The remainder of the excess weld material was hand polished until an even surface and constant thickness was obtained. The surface was lightly etched with Tucker's etchant to reveal the weld metal, fusion lines, and heat-affected zones.

NOTCH SHARPENING

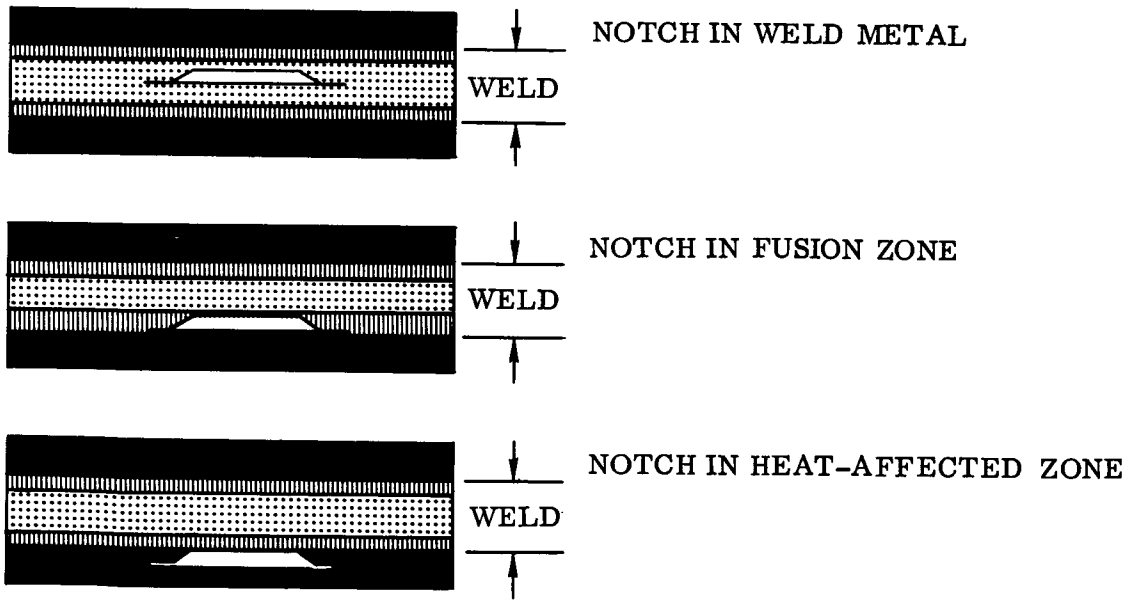
Prior to testing, the notches were sharpened by fatigue cycling at room temperature using a maximum tensile strength of about 20 percent of yield strength of the material. For the welded plate material, it was necessary to increase the surface stress (bending) beyond 20 percent of the yield strength of the weld metal in order to



NOTE: EACH SPECIMEN CONTAINED ONE FATIGUE CRACK.

1. NOTCH IN HEAT-AFFECTED ZONE
2. NOTCH IN FUSION ZONE
3. NOTCH IN WELD METAL

1.0 INCH PLATE MATERIAL



SHEET MATERIAL

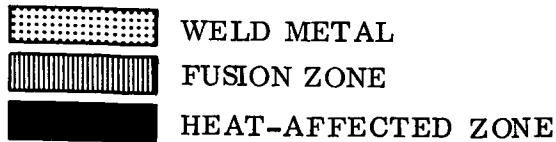


Figure 16. Location of Notches in Welded Specimens

extend the cracks within a reasonable amount of time. Since the bending stress at the tip of the notch at the maximum depth was significantly closer to the neutral axis than the outer fiber, the stress at this area was substantially less than the surface stress.

SURFACE NOTCH CONFIGURATION

The actual dimensions for the plate surface machine notches were obtained by assuming the expected critical crack shape and working back from there. For static test specimens, an $a/2c$ of 0.25 was used. Assuming that the critical crack depth would be between 40 and 50 percent of the thickness, the final machine notch depth of 0.40 inch was selected. Since it was anticipated that fatigue crack extension in bending would cause greater growth at the surface than at the greatest depth of the notch, it followed that a circular cross section for the machined notch would propagate into a semielliptical flaw. Therefore all machined surface notches were shaped like segments of circles.

The shape of the machine notch for flaw enlargement specimens was selected in the same manner, except that the $a/2c$ was 0.10 and the machined notch depth was 0.150 inch.

Fatigue crack extension was obtained by cyclic bending until the surface crack had propagated approximately 0.1 inch at each tip.

VARIATION OF HARDNESS IN WELD AREAS

In addition to visual identification of weld zones, hardness readings were taken of various specimens. In several cases, sections were cut from weld areas, polished, and hardness readings obtained. Typical variations of hardness in a welded plate are shown in Figure 17.

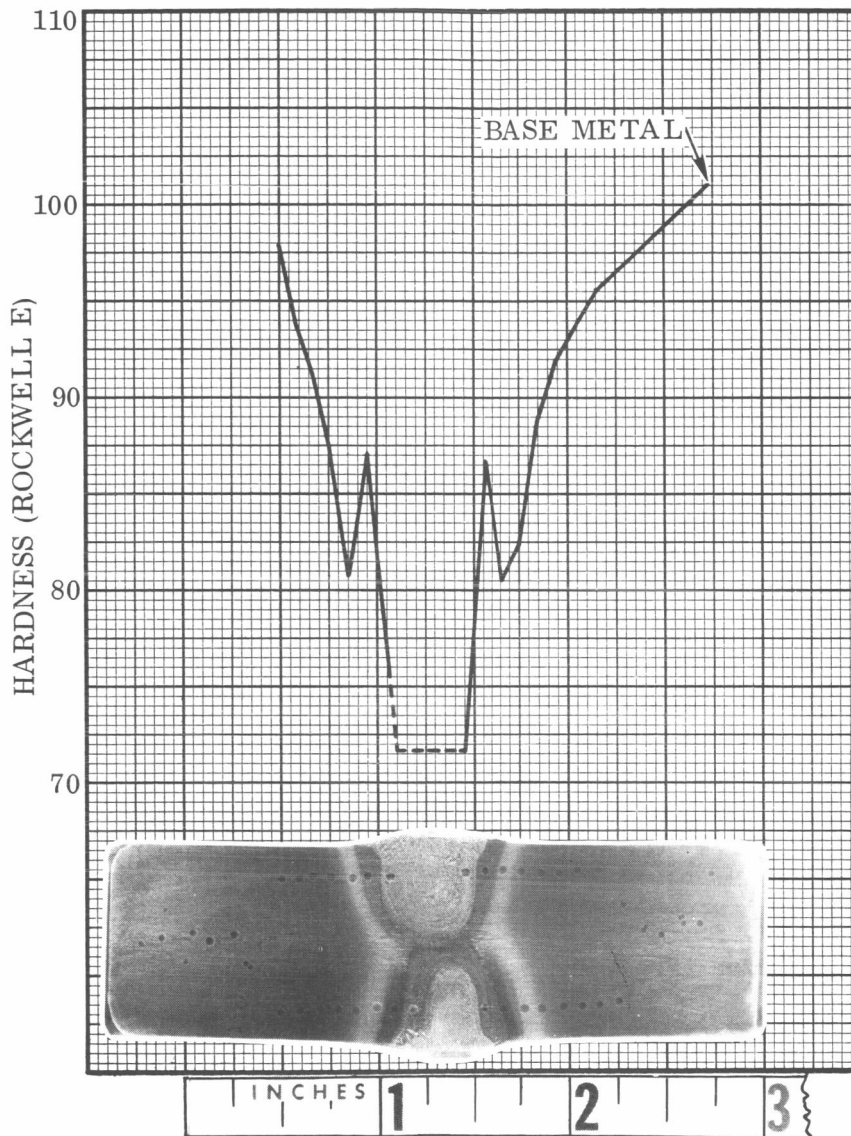


Figure 17. Variation of Hardness With Weld Zones For 2219-T81 Plate

6/EXPERIMENTAL PROGRAM

The experimental program was divided into testing of base metal and welded specimens (Task II) and testing of repair welded specimens (Task III). For each task, tensile tests were performed to determine basic mechanical properties of the parent metal and weldments. In addition, static fracture tests and cyclic flaw growth (fatigue) tests were performed under the required conditions. Due to cost and time limitations, only one specimen was tested for any particular condition. (There was one exception; additional center-notched welded specimens were cycled at -320°F to increase the statistical accuracy of the data for this condition.)

Room temperature tests were performed in one of three laboratories where the temperature range was from 70° to 80°F . Tests at -320°F were performed in several different cryostats containing unpressurized liquid nitrogen. Spot checks of the actual temperature, using thermocouples attached to various test specimens, indicated temperature variations no greater than $\pm 1^{\circ}\text{F}$.

For tests at -423°F , specimens were immersed in liquid hydrogen contained in special closed cryostats (Figure 18).

For fracture tests, the cryostats contained viewing ports that permitted observation of the notched areas of the specimens during testing.

MECHANICAL PROPERTIES TESTS

Tests performed in this category included standard sheet tensile tests on base material and welded sheets, and round tensile tests on base metal and welded 1.0-inch plate.

In all cases stress-strain curves were obtained by either cryogenic extensometers or strain gages and associated recording equipment. Ultimate strength, yield strength, modulus of elasticity, and elongation were obtained for all test specimens. Originally, individual specimens were to be tested to obtain the yield strength of the heat-affected zone and of the weld metal. However, since it was possible to obtain both values with a single specimen (Figure 19), the total number of tests performed was reduced correspondingly.

Strain gages were installed on both sides of sheet specimens and every 90 degrees around the periphery of round plate specimens in order to minimize bending effects. Data were obtained during testing by manual readout on an SR-4 Strain Recorder. Readings were obtained until failure of gages or test specimens occurred.

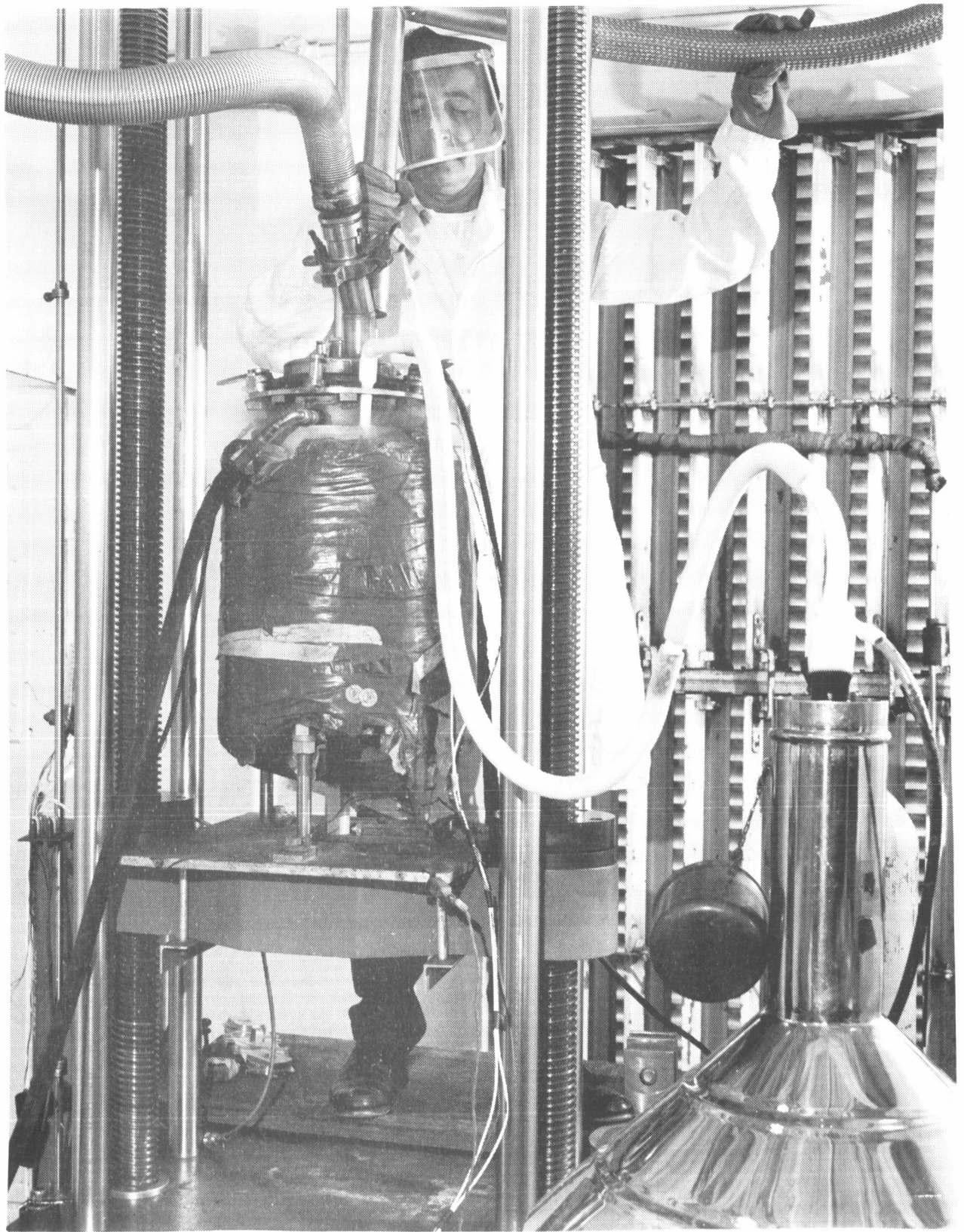


Figure 18. Liquid Hydrogen Cryostat for Small Test Specimens Installed in Tensile Test Machine

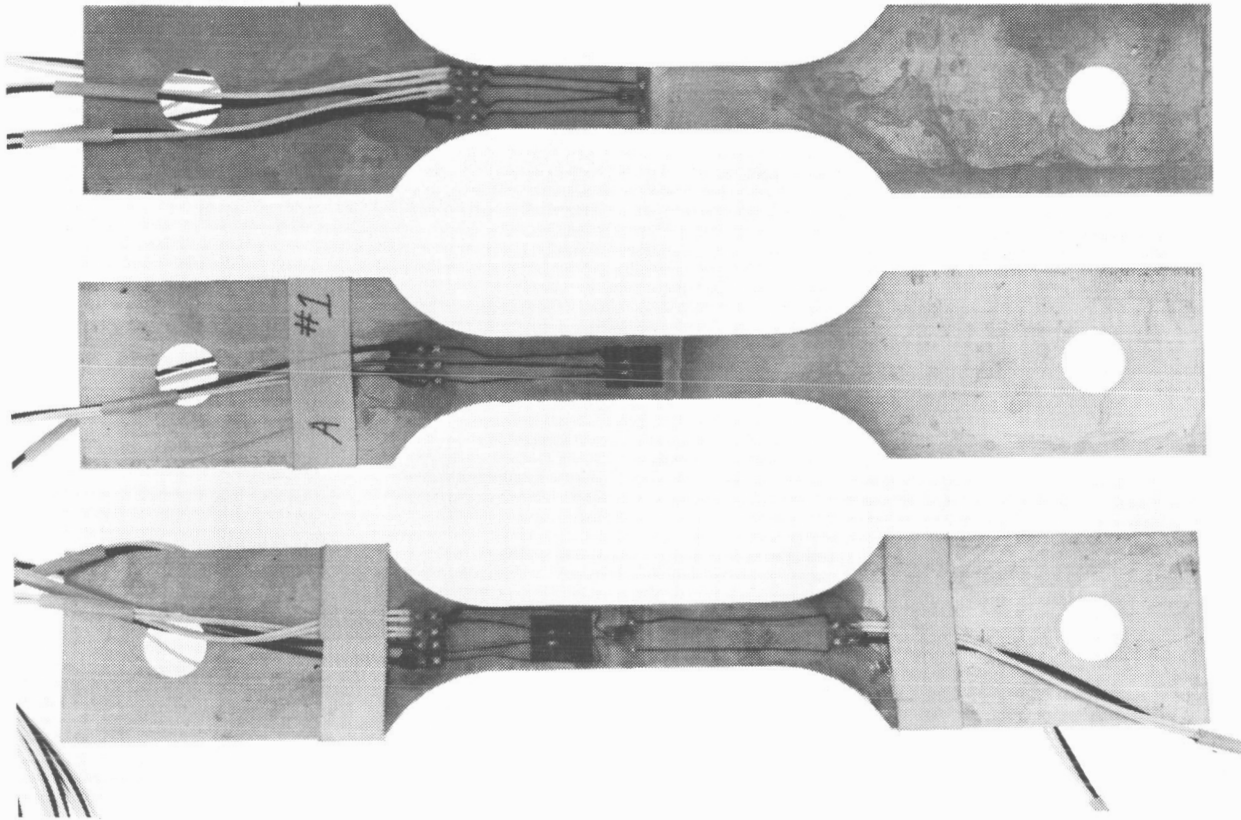


Figure 19. Strain Gage Installation on Sheet Tensile Specimens

A strain rate of 0.005 inch/inch/minute was used until yield strength was reached. After that point, a head travel rate of 0.015 inch/minute was used.

For cryogenic tests, special quick-release clevises were used for all mechanical properties tests (Figure 20).

UNIAXIAL FRACTURE TESTS — SHEET

Static fracture tests were performed on the 0.063-inch sheet parent metal and welded materials utilizing a plane stress, center-notched fracture mechanics test specimen. Crack growth was observed continuously by use of telescopes directed to the crack front areas. Critical crack length was defined as the last reading detected by visual observation. After failure, the fractured surface was examined to verify crack growth. Loading rates were adjusted to provide sufficient time to obtain accurate data in less than five minutes to ultimate fracture of the specimens.

Initial notch sharpening (crack extension) was accomplished by cycling at room temperature at a stress level of about 20 percent of the room temperature yield



Figure 20. Strain Gaged Sheet Tensile Test Specimen in Quick-Release Clevis

strength of the material. Because of the rather large size of the sheet specimens (13 inches wide), cycling was performed in tension in a standard laboratory (Tinius-Olsen) tensile test machine equipped with an automatic cycling programmer.

FLAW ENLARGEMENT OF SHEETS

Specimens used for fatigue testing were identical to those used for static testing except for the initial length of the center cracks.

The maximum cyclic stress was designated to be 90 percent F_{ty} or 71.5 percent of F_{tu} , whichever was smaller. This requirement was relaxed during the program due to difficulty in extending cracks in the weld material. Cyclic loading rate was a minimum of 40,000 psi per minute. The crack length was monitored and recorded at frequent intervals during testing and the load was adjusted correspondingly.

In general, for each test condition and temperature, four specimens were tested as follows: 1) slot in base metal, 2) slot in heat-affected zone, 3) slot in fusion line, and 4) slot in center of weld.

For repair welded specimens, the procedures were repeated except that no additional base metal tests were performed.

One series of tests was performed on 13-inch wide sheet specimens containing only surface notches. These specimens were cycled at various temperatures to determine if the surface crack would grow through the thickness before fracture occurred.

UNIAXIAL FRACTURE TESTS — PLATE

All static, fatigue, base metal, weld metal, and repair welded plate tests were performed on a plane strain fracture toughness specimen containing a semielliptical surface flaw. Static tests were performed at room temperature, -320°F , and -423°F with notches located in the base metal, heat-affected zone, fusion line, or weld metal. Flaw enlargement tests were performed on similar specimens containing shallower notches. In several cases of repair welded tests, flaws were imbedded in the center of the weld material prior to fatigue crack extension.

Notches were cut in the surface of the specimens by electrical discharge or milling machine. The initial machine notch shapes were segments of circles approximately 1/10 inch shallower than the anticipated notch depth. The notches were fatigue cycled in bending (Figure 21) at a surface stress of approximately 20 percent of the yield strength of the material surrounding the notch. However, due to the excessive number of cycles required to extend the notch, the surface stress level was increased to more than 30 percent of yield strength for part of the crack extension.

Originally it was anticipated that stress levels could be selected that would permit failure of the specimens in from 300-500 cycles. However, the toughness of the weld material and the rather low yield strength of the weld metal caused many of the specimens to survive 500 cycles. As a consequence, fatigue cycling of welded specimens was performed at 50 percent (approximately 20 ksi) of the corresponding stress for the base metal specimens.

If failure did not occur before 500 cycles, the stress level was increased to 23 ksi for 100 additional cycles. If the specimen survived the additional cycling, the stress level was increased to 25 ksi for 400 more cycles. When a specimen was still intact at 1000 cycles, it was statically pulled to failure.

During some of the room temperature flaw enlargement tests, ultrasonic inspection techniques were used in an attempt to monitor crack growth. Sporadically specimens were removed from the test machine and radiographed to compare the x-ray indications with the other nondestructive test techniques.

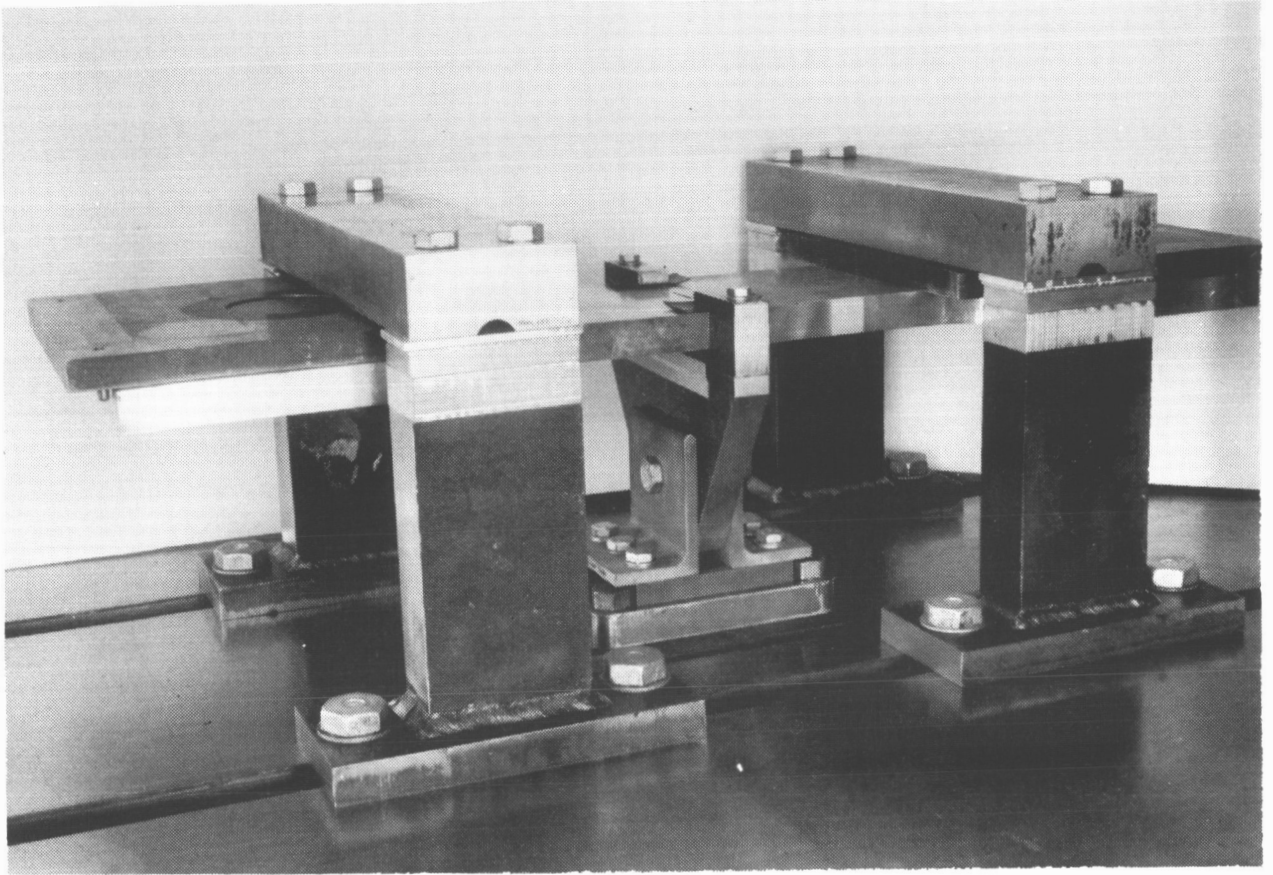


Figure 21. Test Setup for Bending Fatigue Crack Extension of 1.0-Inch Plate Material

7/TEST RESULTS

All test results are shown in either tabular or curve form in this report. Where possible, results are presented in more than one form. In many cases, the data do not give statistical comparative results. In those cases, the results are discussed on an individual basis.

MECHANICAL PROPERTIES

Base metal, weld metal, and repair weld properties were obtained on both the 0.063-inch sheet and the 1.0-inch plate materials at 75, -320, and -423° F. Ultimate tensile strength (F_{tu}); 0.02 percent offset and 0.2-percent offset tensile yield strength (F_{ty}); and percent elongation for base metal, heat-affected zones, weld zones, and repair weld zones are shown in Table 2 for 0.063-inch sheet and in Table 3 for 1.0-inch plate.

The variations of ultimate strength and yield strength with temperature are shown in Figure 22 for 2219-T81 sheet and in Figure 23 for the plate materials.

STATIC FRACTURE TOUGHNESS

Tests for determination of plane stress fracture toughness for material loaded in the longitudinal grain direction were performed on the base material, welded, and repair welded sheet materials at 75, -320, and -423° F. Data obtained from these tests are shown in Table 4. The 0.2 percent F_{ty} obtained from the mechanical properties tests are shown in comparison with the net fracture stress (σ_n). Since the net fracture stress for welded test specimens exceeded the yield strength, all fracture toughness values are listed as "apparent" values.

Net and gross fracture stresses are calculated as follows:

$$\sigma_G = \frac{P}{BW}$$

$$\sigma_n = \frac{P}{B(W - 2a)}$$

where

P = load at onset of rapid crack propagation (kips)

B = specimen thickness (inches)

W = specimen width (inches)

2a = critical crack length (inches)

Table 2. Mechanical Properties of 0.063-Inch 2219-T81 Aluminum Alloy

Test Temp. (° F)	Base Metal and As-Welded Conditions									
	Base Metal					As-Welded				
	F _{ty} (ksi)		F _{tu} (ksi)	F _{ty} (ksi)		F _{tu} (ksi)	Heat-Affected Zone		Weld Metal	
	0.02%	0.2%		0.02%	0.2%		0.02%	0.2%		
75	45.3	51.3	65.6	15.0	23.5	13.0	22.0	42.0		
	45.0	51.0	64.7	13.8	21.2	10.2	16.6	38.9		
Avg.	45.2	51.2	65.2	14.4	22.4	11.6	19.3	40.5		
	Estimated 0.2% F _{ty} @ FL = 20.9 ksi									
-320	57.1	63.3	84.0	19.7	29.0	19.8	27.5	59.8		
	54.9	61.4	82.4	17.5	26.2	15.3	23.5	58.6		
Avg.	56.0	62.4	83.2	18.6	27.6	17.6	25.5	59.2		
	Estimated 0.2% F _{ty} @ FL = 26.6 ksi									
-423	48.5	67.5	94.8	25.5	35.7	18.7	27.0	71.4		
	55.0	67.0	95.0	31.2	39.3	23.3	35.1	79.4		
Avg.	51.8	67.3	94.9	28.4	37.5	21.0	31.1	75.4		
	Estimated 0.2% F _{ty} @ FL = 34.3 ksi									

Table 2. Mechanical Properties of 0.063-Inch 2219-T81 Aluminum Alloy, Concluded

Test Temp. (°F)	Repair Welded Condition						F _{tu} (ksi)	Location of Fracture
	F _{ty} (ksi)							
	Heat-Affected Zone		Weld					
	0.02%	0.2%	0.02%	0.02%	0.2%	0.2%		
75	17.1	22.6	18.0	18.0	25.7	36.8	WM	
	17.8	24.6	15.0	15.0	21.8	39.0	WM	
			18.6	18.6	27.2	38.9	WM	
Avg.	17.5	23.6	17.2	17.2	24.9	38.2		
	Estimated 0.2% F _{ty} @ FL = 24.3 ksi							
-320	29.3	39.3	19.5	19.5	29.3	52.4	WM	
	17.0	24.3	21.7	21.7	30.3	51.9	WM	
			29.6	29.6	34.6	47.5	WM	
Avg.	23.2	31.8	23.6	23.6	31.4	50.6		
	Estimated 0.2% F _{ty} @ FL = 31.6 ksi							
-423	25.5	36.8	26.8	26.8	37.0	50.9	WM	
	30.5	36.1	27.3	27.3	36.1	62.5	WM	
			41.2	41.2	48.9	69.9	WM	
Avg.	28.0	36.5	31.8	31.8	40.7	61.1		
	Estimated 0.2% F _{ty} @ FL = 38.6 ksi							

Table 3. Mechanical Properties of 1.00-inch 2219-T81 Aluminum Alloy

Test Temp. (°F)	Base Metal and As-Welded Conditions									
	Base Metal					As Welded				
	F _{ty} (ksi)		Elongation in 2-inch (%)	F _{tu} (ksi)	F _{ty} (ksi)		Weld Metal	F _{tu} (ksi)		
	0.02%	0.2%			Heat-affected Zone	0.02%				
75	47.8	52.9	13.0	67.3	12.8	18.3	10.6	39.0		
	<u>48.0</u>	<u>52.8</u>	<u>5.5</u>	<u>66.5</u>	<u>15.0</u>	<u>21.6</u>	<u>12.2</u>	<u>42.3</u>		
Avg.	47.9	52.9	9.3	66.9	13.9	20.0	11.4	40.7		
					Estimated 0.2% F _{ty} @ FL = 18.4 ksi					
-320	58.4	62.0	16.5	81.1	19.5	24.8	15.3	57.1		
	<u>56.8</u>	<u>60.9</u>	<u>15.5</u>	<u>80.3</u>	<u>16.9</u>	<u>23.7</u>	<u>13.3</u>	<u>55.6</u>		
Avg.	57.6	61.5	16.0	80.7	18.2	24.3	14.3	56.4		
					Estimated 0.2% F _{ty} @ FL = 22.5					
-423	63.1	67.6	13.0	95.6	25.0	32.3	22.7	69.4		
	<u>61.1</u>	<u>66.5</u>	<u>13.5</u>	<u>94.3</u>	<u>23.6</u>	<u>25.2</u>	<u>22.6</u>	<u>57.9</u>		
Avg.	62.1	67.1	13.3	95.0	24.3	28.8	22.7	63.7		
					Estimated 0.2% F _{ty} @ FL = 28.7					

Table 3. Mechanical Properties of 1.00-inch 2219-T81 Aluminum Alloy, Concluded

Test Temp. (° F)	Repair Welded Condition						F _{tu} (ksi)
	F _{ty} (ksi)			Weld Metal			
	Heat-Affected Zone		0.02%	0.02%		0.2%	
	0.02%	0.2%		0.02%	0.2%		
75	15.2	22.0	11.8	19.3	32.3	32.3	
	<u>11.5</u>	<u>17.0</u>	<u>15.9</u>	<u>20.9</u>	<u>29.7</u>		
Avg.	13.4	19.5	13.9	20.1	31.0		
	Estimated 0.2% F _{ty} @ FL = 19.8 ksi						
-320	15.4	21.6	20.9	29.3	36.1	36.1	
	<u>12.3</u>	<u>16.6</u>	<u>14.8</u>	<u>22.9</u>	<u>33.1</u>		
Avg.	13.9	19.1	17.9	26.1	34.6		
	Estimated 0.2% F _{ty} @ FL = 22.6 ksi						
-423	14.2	19.2	22.3	29.8	35.9	35.9	
	<u>15.0</u>	<u>21.4</u>	<u>20.6</u>	<u>30.3</u>	<u>31.6</u>		
Avg.	14.6	20.3	21.5	30.1	33.8		
	Estimated 0.2% F _{ty} @ FL = 25.2 ksi						

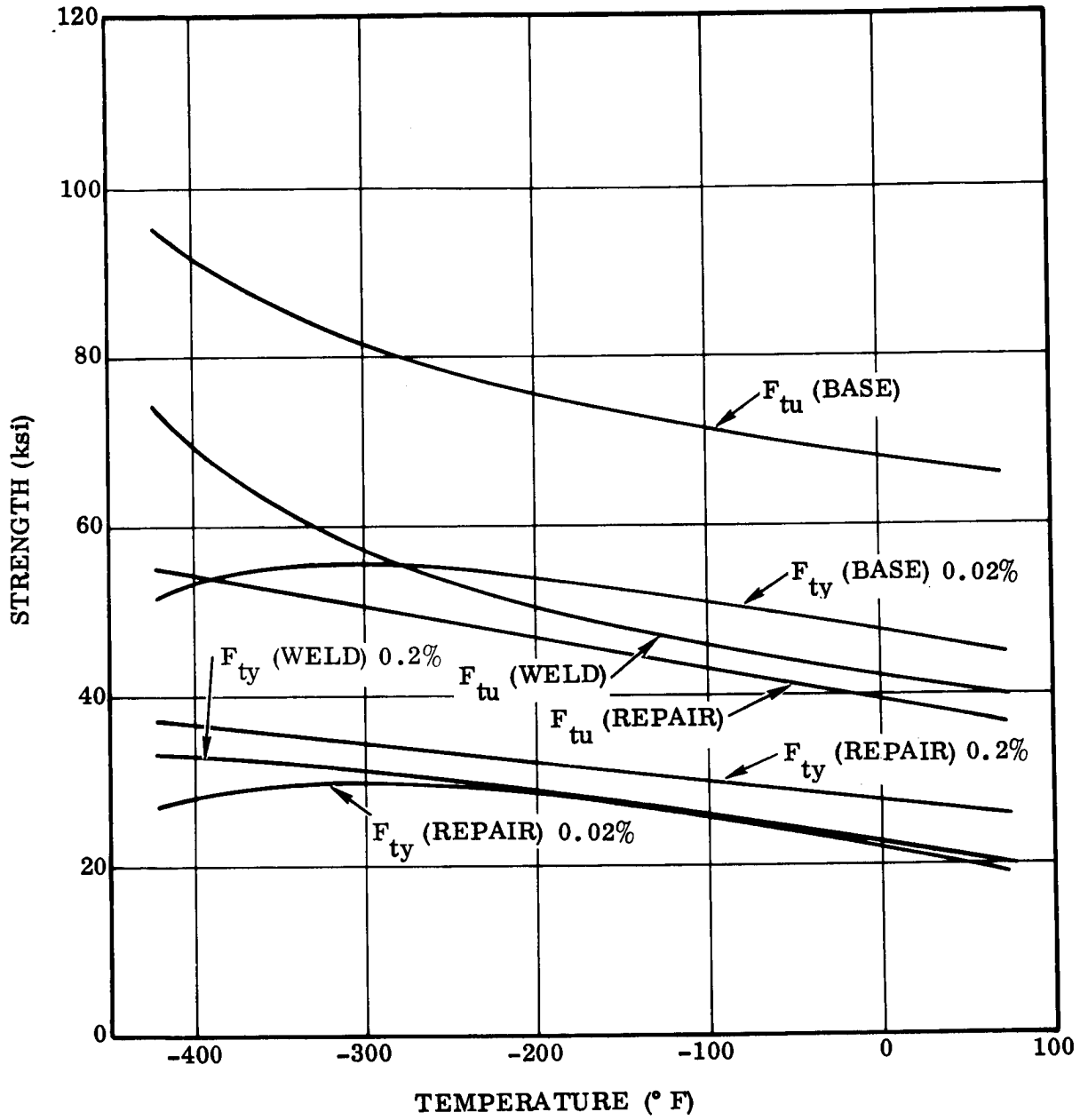


Figure 22. Variation of Strength With Temperature for 2219-T81 Sheet

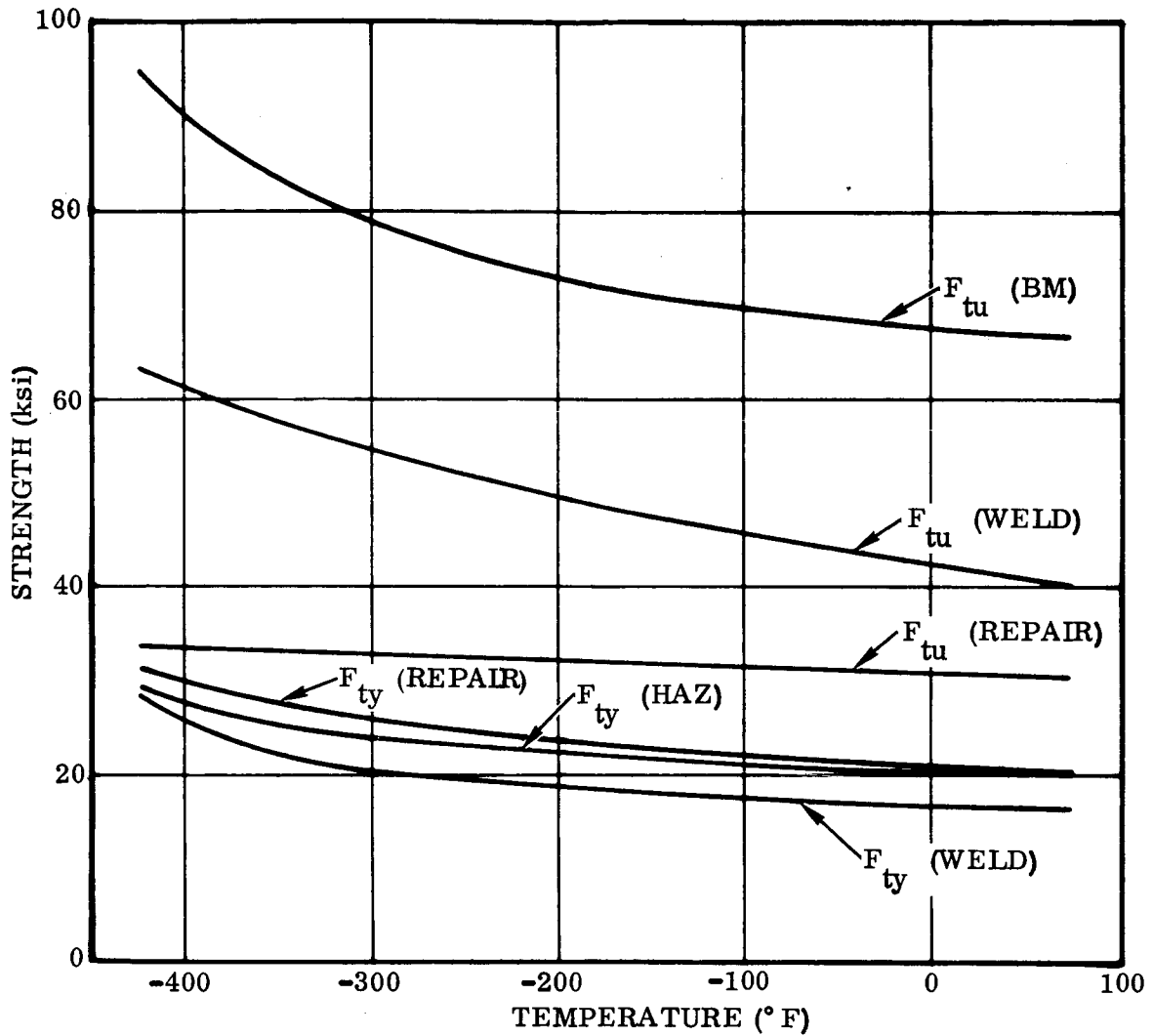


Figure 23. Variation of Strength with Temperature of 2219-T81 Aluminum Alloy 1-Inch Plate

The plane stress fracture toughness was calculated as follows:

$$K'_c = \sigma_G \sqrt{W \tan \frac{\pi a}{W}}$$

where

K'_c = fracture toughness uncorrected for plastic zone

Table 4. Static Fracture Tests of 2219-T81 Sheet Stock (t = 0.063 inch)

Test Temp. (°F)	Area Tested	2a _{CR} (in.)	σ_{ys} , 0.2% (ksi)	σ_n (ksi)	σ_G (ksi)	K' _c (ksi $\sqrt{\text{in.}}$)	a' (in.)	Apparent K* (ksi $\sqrt{\text{in.}}$)	Apparent K _{Ic} ** (ksi $\sqrt{\text{in.}}$)
75	Base Metal	5.3	51	38.1	22.5	70.5	3.0	76.6	41.6
	HAZ	4.4	22.4	32.5	21.6	59.8	3.33	79.6	52
	FL	5.0	21 est.	29.3	18	53.8	3.54	69.6	39.6
	WELD	4.4	22	28.3	18.8	51.8	3.1	69.1	36.2
-320	Base Metal	5.0	62	39.8	24.6	73.5	2.7	77.0	43.0
	HAZ	4.2	27.6	33.9	20.3	55.0	2.73	64.5	19.0
	FL	4.85	26.6 est.	30.0	18.8	56.5	3.14	66.0	36.2
	WELD	5.1	26	32.1	19.5	61.2	3.43	73.6	37.5
-423	Base Metal	6.1	67	54.6	29.0	99.5	3.4	108.5	74.2
	HAZ	4.8	37.5	42.2	26.5	77.8	3.1	91.8	61.1
	FL	5.8	34.3 est.	31.9	17.7	58.5	3.4	66.3	44.5
	WELD	4.5	31.1	27.8	18.3	51.1	2.7	58.8	33.2

* Corrected for plastic zone

** Pop-in determined by visual observation

Table 4. Static Fracture Tests of 2219-T81 Sheet Stock (t = 0.063 inch), Concluded

REPAIR WELDED CONDITION										
Test Temp. (°F)	Area Tested	2a CR (in.)	σ_{ys} , 0.2% (ksi)	σ_n (ksi)	σ_G (ksi)	K'_c (ksi $\sqrt{\text{in.}}$)	a' (in.)	Apparent K_c (ksi $\sqrt{\text{in.}}$)	Apparent K_{Ic} (ksi $\sqrt{\text{in.}}$)	
75	HAZ	4.40	23.6	33.3	21.0	58.04	3.16	74.13	36.25	
	FL	5.06	24.0	30.2	18.55	56.59	3.42	70.35	36.57	
	WELD	5.00	24.5	30.8	18.75	55.56	3.32	67.99	32.77	
-320	HAZ	4.42	31.0	35.7	23.5	65.17	2.91	78.09	48.76	
	FL	5.36	30.5	35.7	20.95	65.68	3.42	78.67	53.36	
	WELD	4.77	30.0	29.9	18.90	55.04	2.92	62.91	52.17	
-423	HAZ	4.57	23.6	43.5	28.1	79.52	3.04	96.41	59.08	
	FL	4.67	24.0	40.4	25.8	73.99	2.94	86.28	47.33	
	WELD	4.85	24.5	34.8	21.8	64.03	2.83	71.00	46.97	

Fracture toughness was corrected for the plastic zone by assuming that the final crack length is equal to the critical crack length plus the length of the plastic zone as follows:

$$r_y = \frac{(K'_c)^2}{2\pi(\sigma_{ys})^2}$$

$$a' = a + r_y$$

$$K_c = \sigma_G \sqrt{W \tan \frac{\pi a'}{W}}$$

where

- r_y = plastic zone correction
- σ_{ys} = yield strength of material containing the crack
- a' = crack length corrected for plastic zone
- K_c = fracture toughness corrected for plastic zone

For comparison purposes, an approximate plane strain fracture toughness (K_{Ic}) was calculated by determining the load at "pop-in" by optical methods (Figure 24). The K_{Ic} was calculated as follows:

$$K_{Ic} = \sigma_p \sqrt{W \tan \frac{2a_o}{W}}$$

where

- σ_p = gross stress at pop-in
- $2a_o$ = crack length at pop-in

The variation of plane stress fracture toughness with temperature for base metal and weldments is shown in Figure 25, and for repair welded sheet is shown in Figure 26.

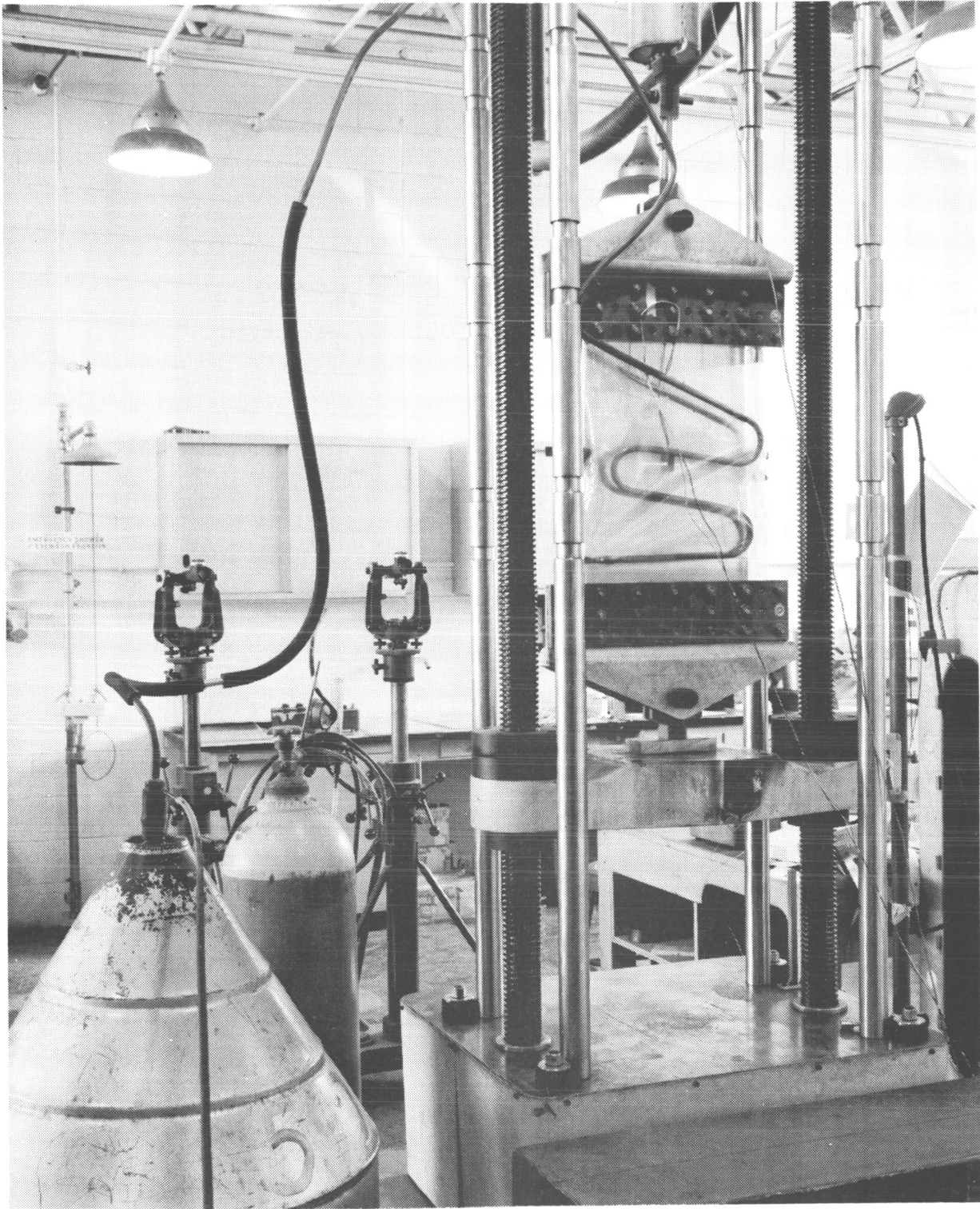


Figure 24. Center-Notched Fracture Toughness Specimen Test at -320°F .
Note Transits Used for Determination of Crack Growth

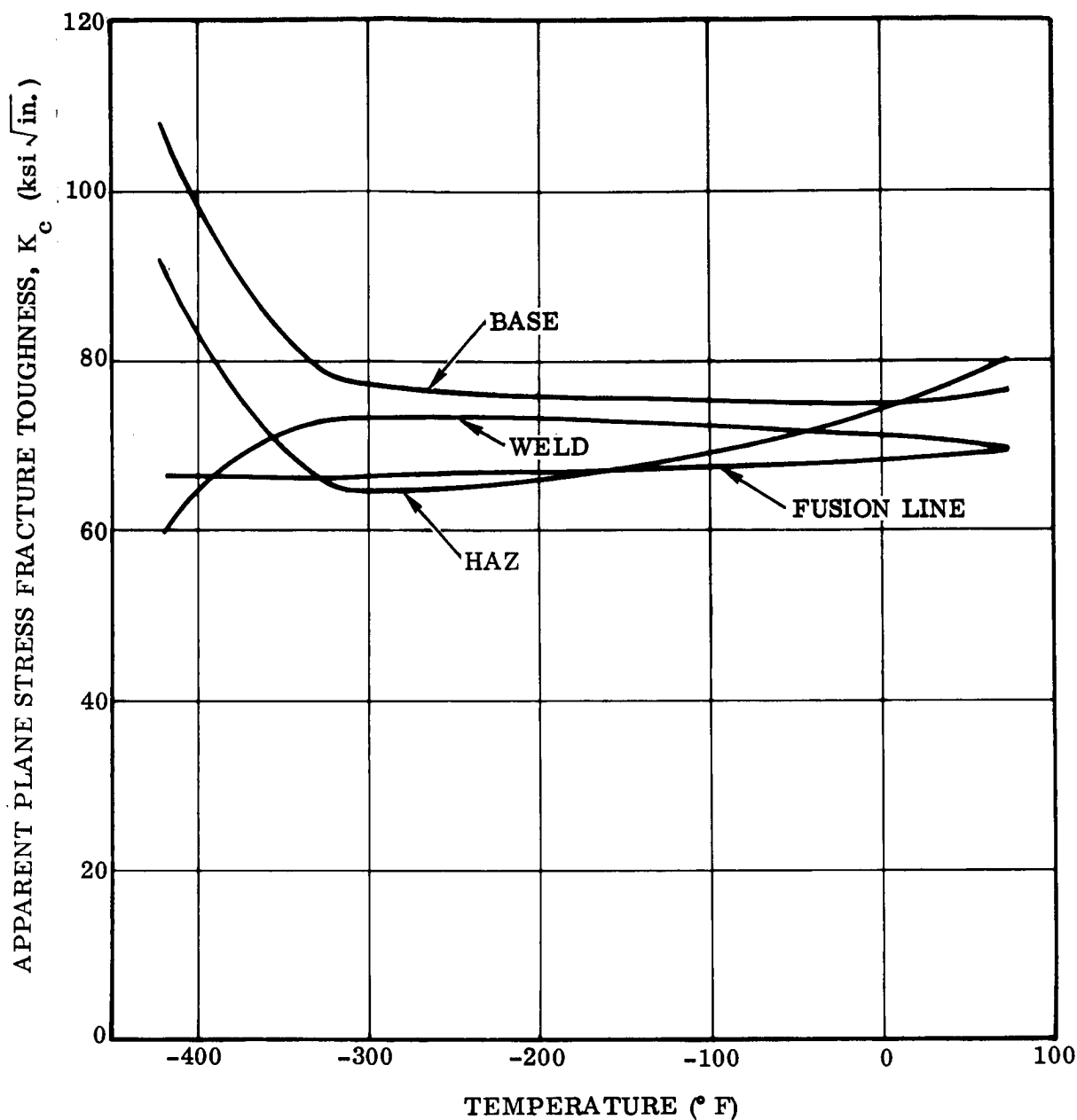


Figure 25. Variation of Apparent Plane Stress Fracture Toughness With Temperature for 2219-T81 Sheet

STATIC FRACTURE - PLATE MATERIAL

Although uniaxial static fracture testing of the plate paralleled the sheet testing, the specimen and test techniques were different. For the plate material, plane strain fracture toughness data were desired. The data were obtained through use of a surface-cracked tensile specimen. As in the sheet program, cracks were formed in four areas, namely: 1) base metal, 2) heat-affected zone (HAZ), 3) fusion line, and 4) in the center of the weldments. The results of the static fracture tests are shown in Table 5.

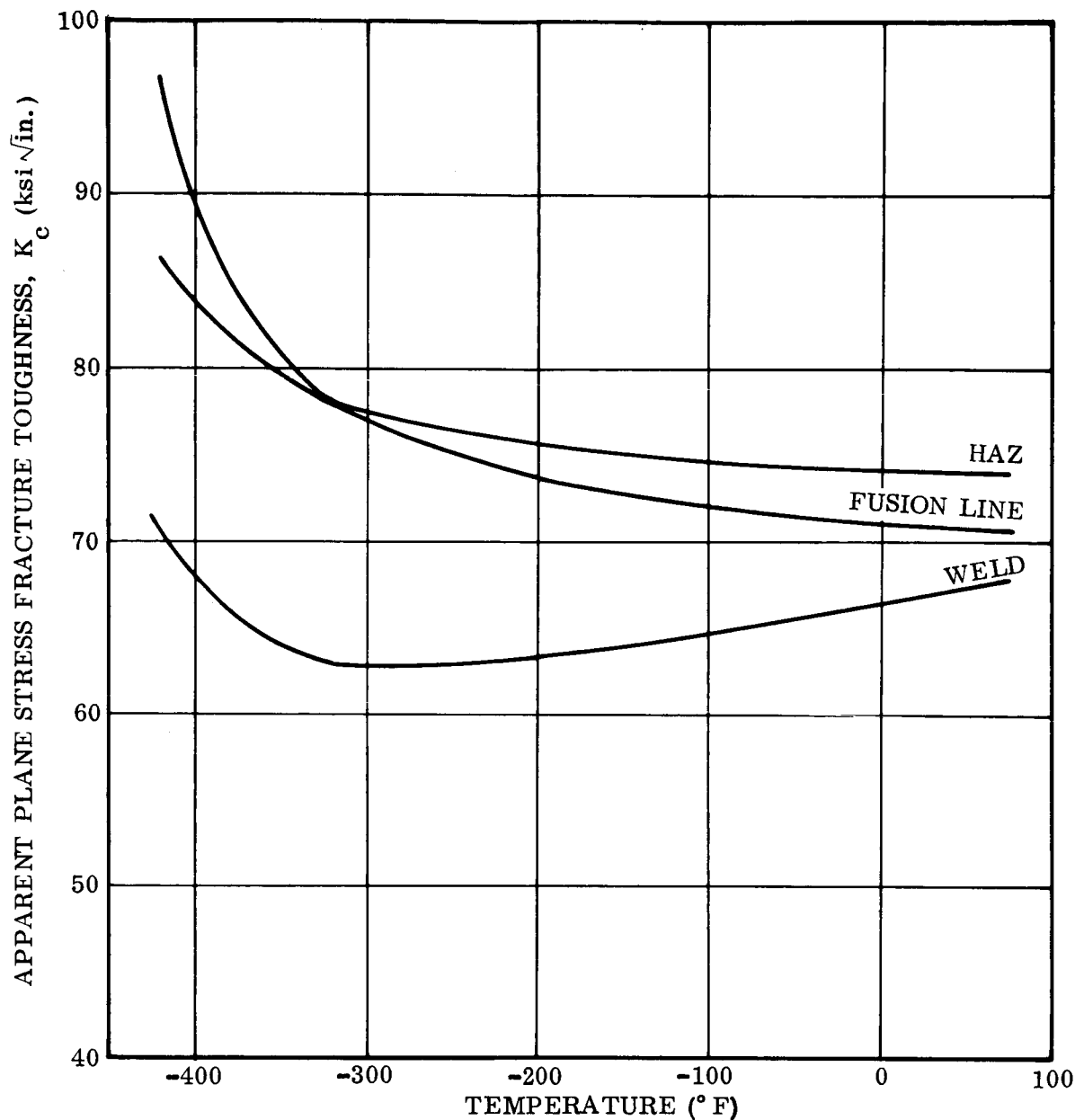


Figure 26. Variation of Apparent K_c With Temperature for Repair Welded 2219-T81 Sheet

Flaw dimension shown were obtained after fracture and reflect the greatest or critical dimensions of the crack. The direction of the maximum flaw growth is measured from the intersection of the semi-minor axis with the ellipse by angular degrees to the maximum flaw growth point. A 0° direction would indicate that the deepest penetration of the crack was directly below the center of the surface projection or on the minor axis of the semi-ellipse. The fracture stress is the gross value, with the reduction in total cross sectional area ignored. Two plane strain fracture toughness (K_{Ic}) values

Table 5. Static Fracture Toughness Test Results - 1.00-inch 2219-T81 Aluminum Alloy

Specimen Identification	Flaw Location	Specimen Size (inches)		Test Temperature (°F)	BASE METAL AND AS-WELDED CONDITIONS			Fracture Stress, σ (ksi)	Increment of Flaw Growth Along α (inches)	K_{Ic} at $\alpha = 0$ (ksi $\sqrt{\text{in.}}$)	K_{Ic} at $\alpha \neq 0$ (ksi $\sqrt{\text{in.}}$)
		Thickness, t	Width, W		Flaw Dimensions (inches)	Direction of Maximum Flaw Growth, α (deg)					
B3	Base metal	1.01	6.00	75	0.427	1.775	0.342	78	0.12	60.3	49.2
14	HAZ	1.03	6.00	75	0.503	1.925	0.456	75	0.38	39.0	33.4
13	FL	1.03	6.00	75	0.509	1.956	0.407	73	0.38	29.4	25.6
8	WM	1.06	6.00	75	0.526	1.871	0.438	74	0.23	33.7	29.6
B6	Base metal	1.01	6.01	-320	0.415	1.805	0.34	74	0.21	65.2	56.4
12	HAZ	1.02	5.99	-320	0.395	1.620	0.384	80	0.20	50.0	40.8
18	FL	1.02	6.00	-320	0.405	1.590	0.352	77	0.08	31.9	32.5
10	WM	1.06	6.01	-320	0.471	1.930	0.393	76	0.42	32.1	26.8
15	HAZ	1.02	6.00	-423	0.475	2.016	0.436	84	0.55	57.9	44.6
23	FL	1.03	6.01	-423	0.520	2.232	0.468	77	0.52	45.6	37.5
9	WM	1.04	6.00	-423	0.490	2.050	0.367	76	0.37	19.9	21.9

Specimen Identification	Flaw Location	Specimen Size (inches)		Test Temperature (°F)	REPAIR WELDED CONDITION			Fracture Stress, σ (ksi)	Increment of Flaw Growth Along α (inches)	K_{Ic} at $\alpha = 0$ (ksi $\sqrt{\text{in.}}$)	K_{Ic} at $\alpha \neq 0$ (ksi $\sqrt{\text{in.}}$)
		Thickness, t	Width, W		Flaw Dimensions (inches)	Direction of Maximum Flaw Growth, α (deg)					
R20	HAZ	1.06	5.98	75	0.471	1.750	0.357	76	0.212	24.1	20.5
R7	FL	1.01	5.99	75	0.488	1.839	0.390	77	0.243	31.5	26.8
16	WM	1.02	6.00	75	0.490	1.839	0.347	75	0.445	18.1	15.5
R4	HAZ	1.00	6.00	-320	0.490	1.897	0.423	82	0.346	36.0	28.1
R16	FL	Did not fail through flaw		-320						26.5	
R13	WM	1.07	5.99	-320	0.484	1.715	0.574	77	0.161	21.2	18.3
R11	HAZ	Did not fail through flaw		-423						21.2	
R17	FL	1.00	6.00	-423	0.400	1.574	0.328	77	0.054	34.8	29.2
R9	WM	1.05	6.01	-423	0.497	1.850	0.336	81	0.219	18.2	15.2

HAZ = Heat Affected Zone; FL = Fusion Line; WM = Weld Metal

are shown; the first for the flaw depth at the minor axis of the semi-ellipse ($\alpha = 0$), and the second for the flaw at the angle of greatest flaw growth ($\alpha \neq 0$).

Plane strain fracture toughness was calculated using the following equation:

$$K_{Ic}^2 = 1.21 \pi \sigma^2 \left(\frac{a}{Q} \right)$$

where

σ = gross stress on section at instability (ksi)

a = flaw depth (inches)

Q = flaw shape parameter

The flaw shape parameter can be obtained from curves found in various publications (References 1 and 3) or can be calculated as follows:

$$Q = \left[\Phi^2 - (0.212) \left(\frac{\sigma}{\sigma_{ys}} \right)^2 \right]$$

where

Φ = complete elliptical integral of the second kind

This equation was solved for several values of $\frac{\sigma}{\sigma_{ys}}$ and the results were plotted in Figure 27. If the stress intensity K_I is desired at a point not on the minor axis, the expanded form of the critical stress intensity factor may be used:

$$K_I = 1.1 \sqrt{\pi} \sigma \left(\frac{a}{Q} \right)^2 \left[\frac{1}{C^2} (a^2 \cos^2 \alpha + c^2 \sin^2 \alpha) \right]^{1/4}$$

Another method reported by Tiffany, Lorenz and Shah (Reference 8) and attributed to F. W. Smith (Reference 9) substitutes two multiplication factors as follows:

$$K_I = M_1' M_k' \sqrt{\pi} \sigma \left(\frac{a}{Q} \right)^{1/2}$$

where

M_1' = free surface coefficient

M_k' = finite thickness correction (sometimes called the deep flaw stress intensity magnification correction)

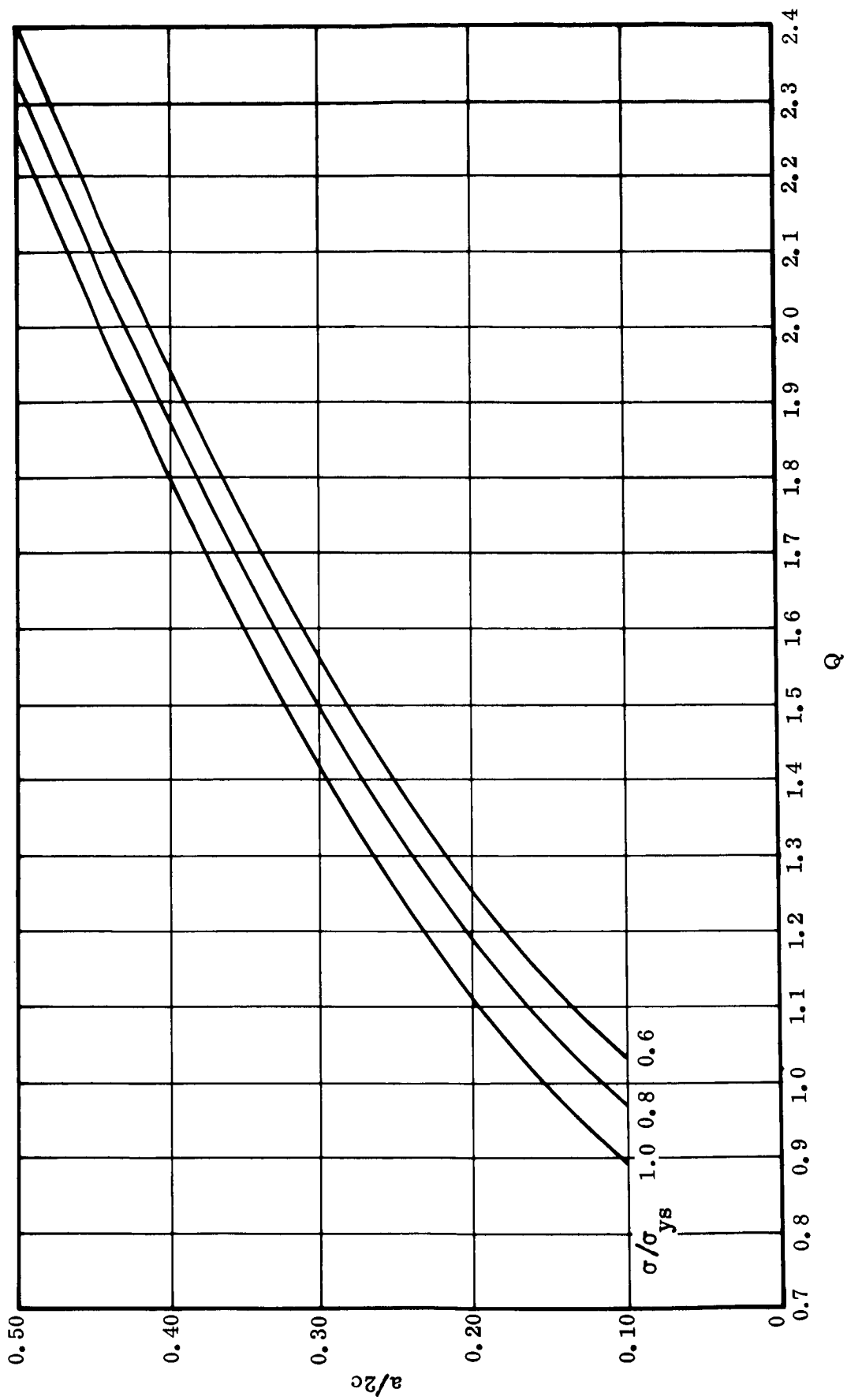


Figure 27. Variation of Q for Various Values of $\frac{\sigma}{\sigma_{ys}}$

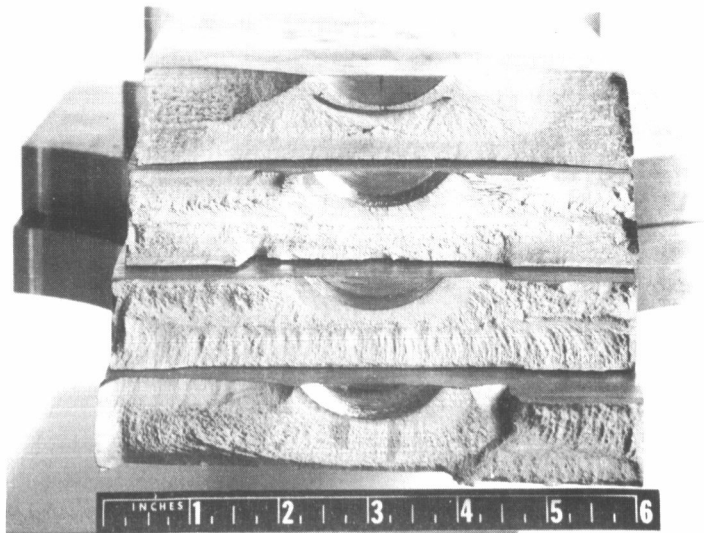
Smith calculated M_1' for various values of $\frac{a}{2c}$ and for values of α between 0 and 90 degrees. (See Reference 8, p 73.) For $\alpha = 0$ degrees and an $\frac{a}{2c}$ of 0.1, the M_1' value is about 1.09, slightly less than the 1.10 suggested by Irwin. (At 0 degrees, Smith's factors vary from 1.03 to 1.09 as $\frac{a}{2c}$ varies from 0.5 to 0.1.)

The finite thickness correction is based on the theory that as the crack grows through the thickness, the stress intensity is magnified by the back surface of the plate. (Irwin's equation neglected this magnification effect and was restricted to critical crack depths of less than 40 percent of the thickness.) Again Smith has calculated M_k' values for various combinations of $\frac{a}{2c}$, which are plotted by Tiffany, et al (Reference 7, p 74). In the case of a semicircular flaw ($\frac{a}{2c} = 0.5$), the magnification factor is negligible. However as the flaw becomes longer ($\frac{a}{2c}$ decreases), the M_k' increases to about 1.7 for $\frac{a}{2c}$ of 0.20 and an $\frac{a}{t}$ of 0.70.

This technique was used to calculate the K_{Ic} values when α was not zero ($\alpha \neq 0$).

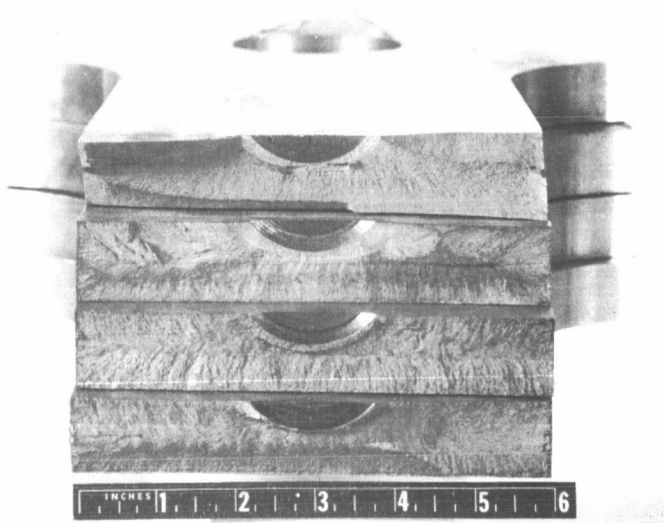
FRACTURE APPEARANCE

In many cases it becomes impossible to describe or tabulate the appearance of the fracture surfaces. Consequently it was deemed desirable to include photographs of the fractured surfaces themselves for the benefit of the reader. Figures 28 and 29 show fractured surfaces for all static plate tests at each test temperature. The reader can determine the resultant data for each test by use of the corresponding specimen identification number in Table 5.



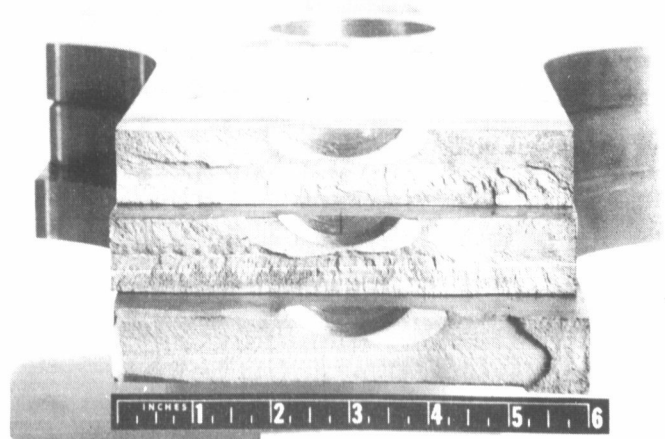
75° F

BASE METAL, B3
 WELD METAL, 8
 FUSION LINE, 13
 HEAT AFFECTED ZONE, 14



-320° F

BASE METAL, B6
 WELD METAL, 10
 FUSION LINE, 18
 HEAT AFFECTED ZONE, 12



-423° F

WELD METAL, 9
 FUSION LINE, 23
 HEAT AFFECTED ZONE, 15

Figure 28. Fracture Surfaces of 1.0-inch 2219-T81 Tested in Static Fracture at Various Temperatures. Marginal Notes Indicate Test Temperature and Location of Surface Flaw Relative to Weld Bead.

75°F

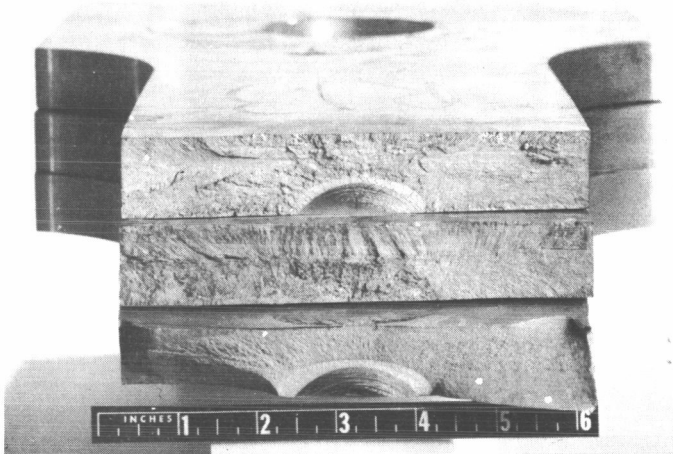


HEAT AFFECTED ZONE, R20

FUSION LINE, R7

WELD METAL, 16

-320°F



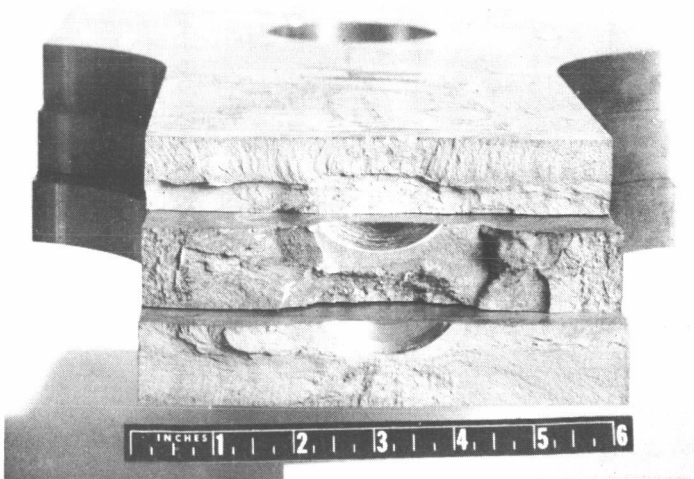
WELD METAL, R13

FUSION LINE, R16*

HEAT AFFECTED ZONE, R4

*Specimen did not fail through flaw.

-423°F



HEAT AFFECTED ZONE, R11*

FUSION LINE, R17

WELD METAL, R9

*Specimen did not fail through flaw.

Figure 29. Fracture Surfaces of Repair Welds in 1.0-inch 2219-T81 Tested in Static Fracture at Various Temperatures. Marginal Notes Indicate Test Temperature and Location of Surface Flaw Relative to the Repair Weld.

CYCLIC FLAW GROWTH TESTS - SHEET

Center-notched base metal, welded, and repair welded sheet specimens were cycled at room temperature, -320 and -423°F . Results of these tests are shown in Table 6.

Several tests were performed on the 0.063-inch sheet material using a 13-inch-wide specimen containing a semielliptical surface crack. The results of these tests are shown in Table 7.

Typical crack growth characteristics of the sheet materials are shown in Figures 30 through 37.

In one case (designated as the worst case situation), a group of specimens was tested under the same test conditions. These tests were of cyclic flaw growth in welded 2219-T81 sheets at -320°F . The history of crack growth with number of cycles is shown in Figure 35. The notch was located in the center line of the weld and the maximum stress level was 20.5 ksi. (The load was adjusted during testing to maintain a net stress of 20.5 ksi during crack growth.) For comparison, the crack growth of the repair welded sheet at -320°F is shown in Figure 36 for each of the areas tested.

Table 6. Cyclic Flaw Enlargement of 2219-T81 Sheet, Center Notched Tests

Test Temp. (°F)	Spec. No.	Spec. Type	Base Metal and As-Welded				Cyclic Net Stress (ksi)	Initial Flaw Length, 2a _i (in.)	Final Flaw Length, 2a _f (in.)	Cycles to Failure	Remarks	
			Spec. Size (in.)		Cyclic Net Stress (ksi)							
			t	w	Max.	Min.						
75	BC1	BASE	0.0618	13.00	40.5	2.0	0.51	4.20	293	No Failure		
	2-2-1	HAZ	0.0620	13.00	11.0	0.5	4.11	4.37	7000			
	2-10-1	FL	0.0620	13.00	20.5	1.0	4.37	7.63	345			
	3-4-2	W	0.0624	13.00	20.5	1.0	4.35	6.50	49			
	-320	BC2	BASE	0.0610	13.00	40.5	2.0	0.52	2.15		24,500	No Failure
		3-1-2	HAZ	0.0615	13.00	20.5	1.0	4.05	7.40		1788	
		3-3-1	FL	0.0610	13.00	20.5	1.0	4.25	8.85		640	
		1-7-1	W	0.0620	13.00	20.5	1.0	4.06	9.60		1060	
		1-1-1	W	0.0620	13.00	20.5	1.0	4.08	8.50		942	
		3-10-3	W	0.0620	13.00	20.5	1.0	4.07	8.75		369	
1-1-2		W	0.0615	13.00	20.5	1.0	4.04	9.30	1140			
3-5-1		W	0.0610	13.00	20.5	1.0	4.12	7.60	483			
-423		BC3	BASE	0.0610	13.00	20.5	1.0	4.30	6.70	466	Worst Case Specimens	
		2-10-2	HAZ	0.0615	13.00	21.0	1.0	4.16	4.66	1500		
	2-2-3	FL	0.0620	13.00	21.0	1.0	4.18	7.43	630			
	3-8-2	W	0.0615	13.00	21.0	1.0	6.20	9.10	917			
Repair Welded Condition												
75	4	W	0.0615	13.00	13.0	0.07	4.00	6.15	10,360	No Failure		
-320	3R	HAZ	0.0613	13.00	20.5	1.0	4.00	9.07	3600	Severe Buckling		
	11R	FL	0.0615	13.00	20.5	1.0	4.00	7.80	827	No Failure		
	9R	W	0.0615	13.00	20.9	1.0	4.00	7.40	489			
	-423	13	HAZ	0.0615	13.00	20.9	1.0	4.00	5.50	1000	No Failure	
7		FL	0.0620	13.00	21.5	1.0	4.00	6.50	1340	No Failure		
	6	W	0.0620	13.00	20.8	1.0	4.00	8.40	616	No Failure		

Table 7. Results of Surface-Notched 2219-T81 Sheet Cyclic Tests ($t = 0.062$ in., $W = 13.00$ in.)

Test Temp. ($^{\circ}$ F)	Specimen No.	Cyclic Gross Stress (ksi)		Initial Flaw Size		Final Flaw Size		Cycles to Failure	Remarks
		Maximum	Minimum	a_i (in.)	$2c_i$ (in.)	a_f (in.)	$2c_f$ (in.)		
75	CF-1	45	2	0.032	0.320	0.032	0.320	133	Failed twice in grip ends.
75	CF-2	25	1	0.040	0.400	0.040	0.400	9550	Cracked through thickness, no failure at 9645 cycles.
75	CF-4	25	1	0.040	0.400	0.040	0.400	110	No failure.
75	CF-4	38	2	0.040	0.400	0.062	0.500	570	Grip end failure at 688 cycles.
75	CF-3	25	1	0.032	0.320	0.032	0.340	2000	No failure.
-320	CF-3	38	1	0.032	0.340	0.062	0.340	887	Crack through thickness, grip end failure at 1452 cycles.

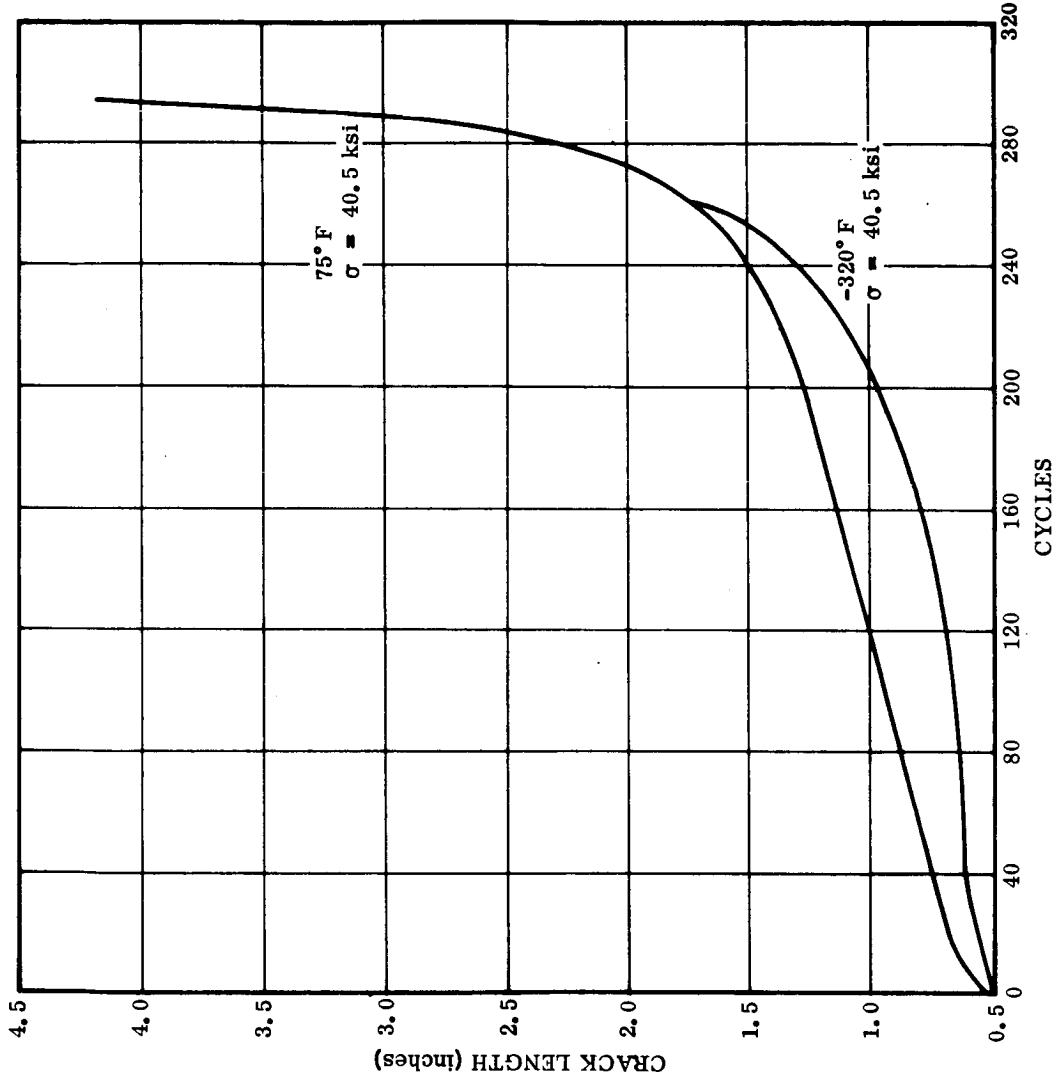


Figure 30. Cyclic Crack Growth, Base Metal Sheet

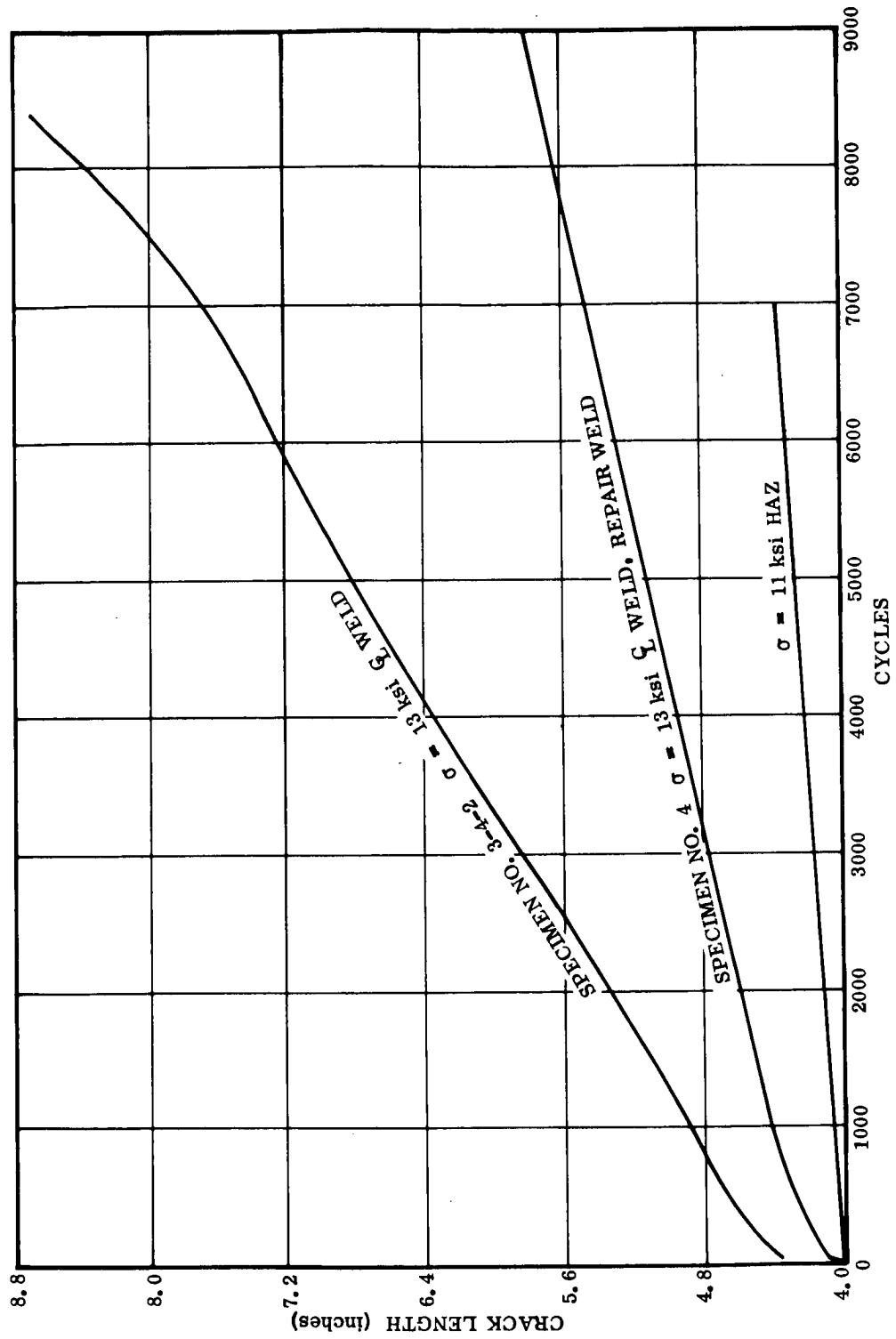


Figure 31. Cyclic Crack Growth, Welded Sheet, 75°F

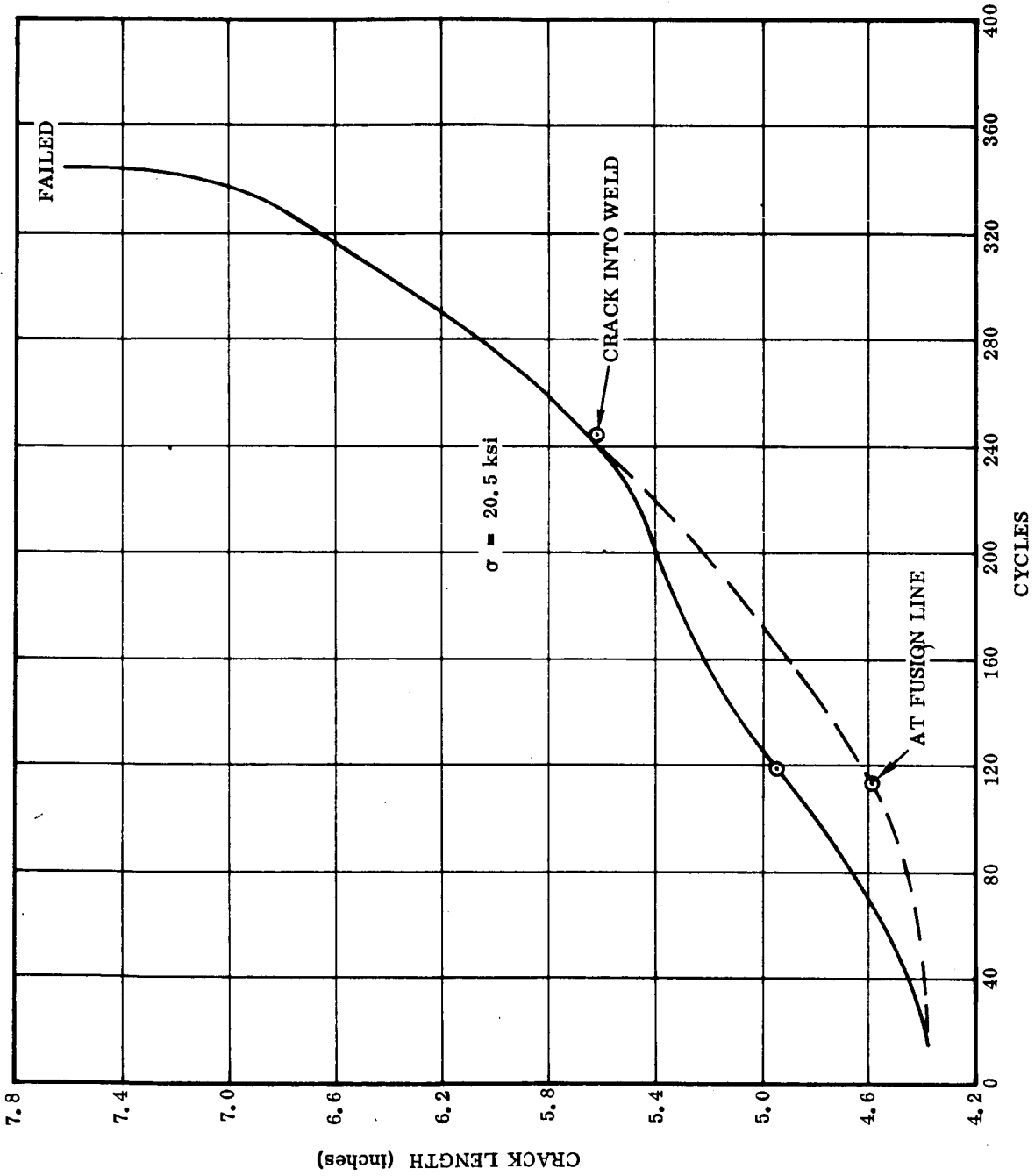


Figure 32. Cyclic Crack Growth, Welded Sheet (HAZ), 75°F

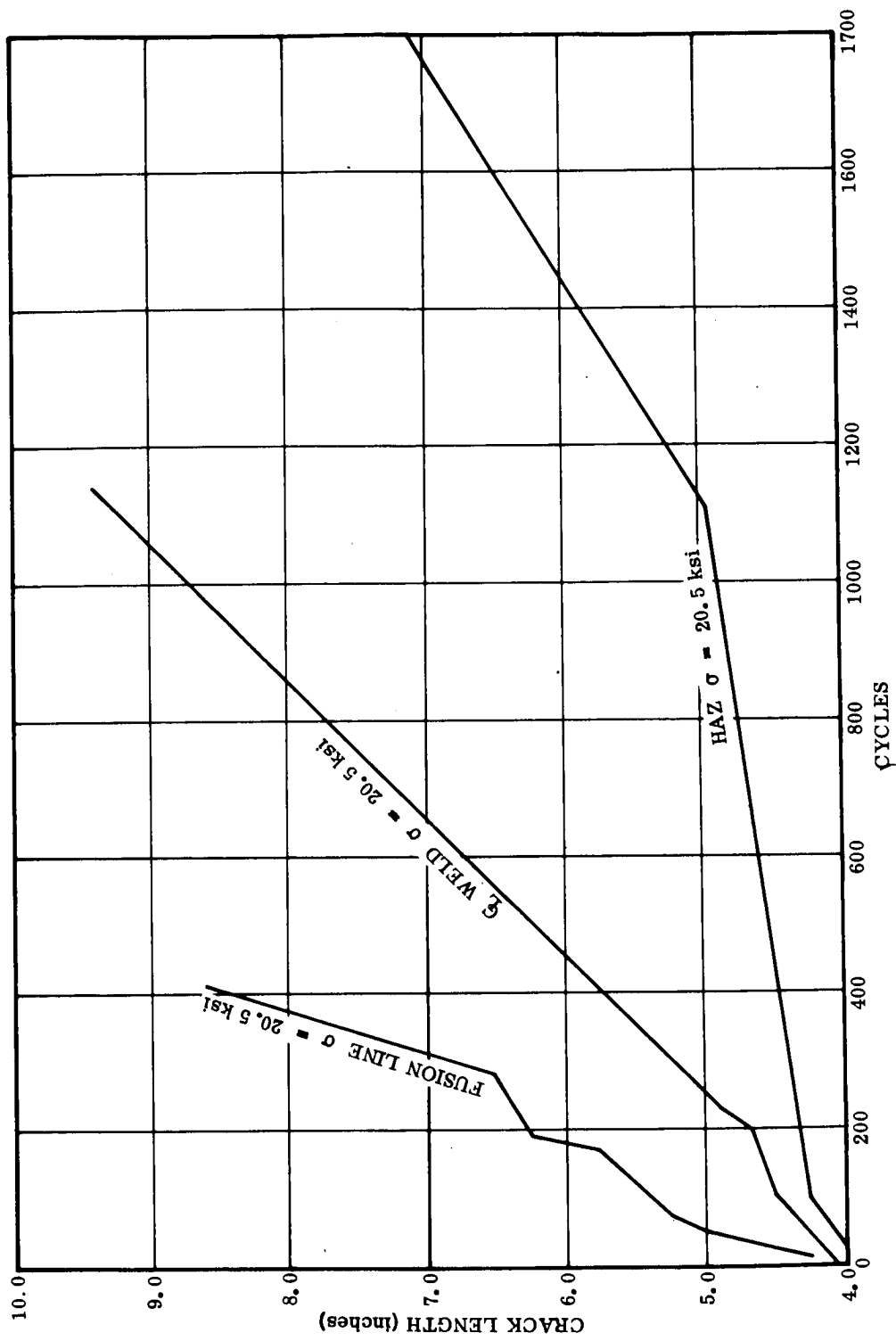


Figure 33. Cyclic Crack Growth, Welded Sheet, -320°F

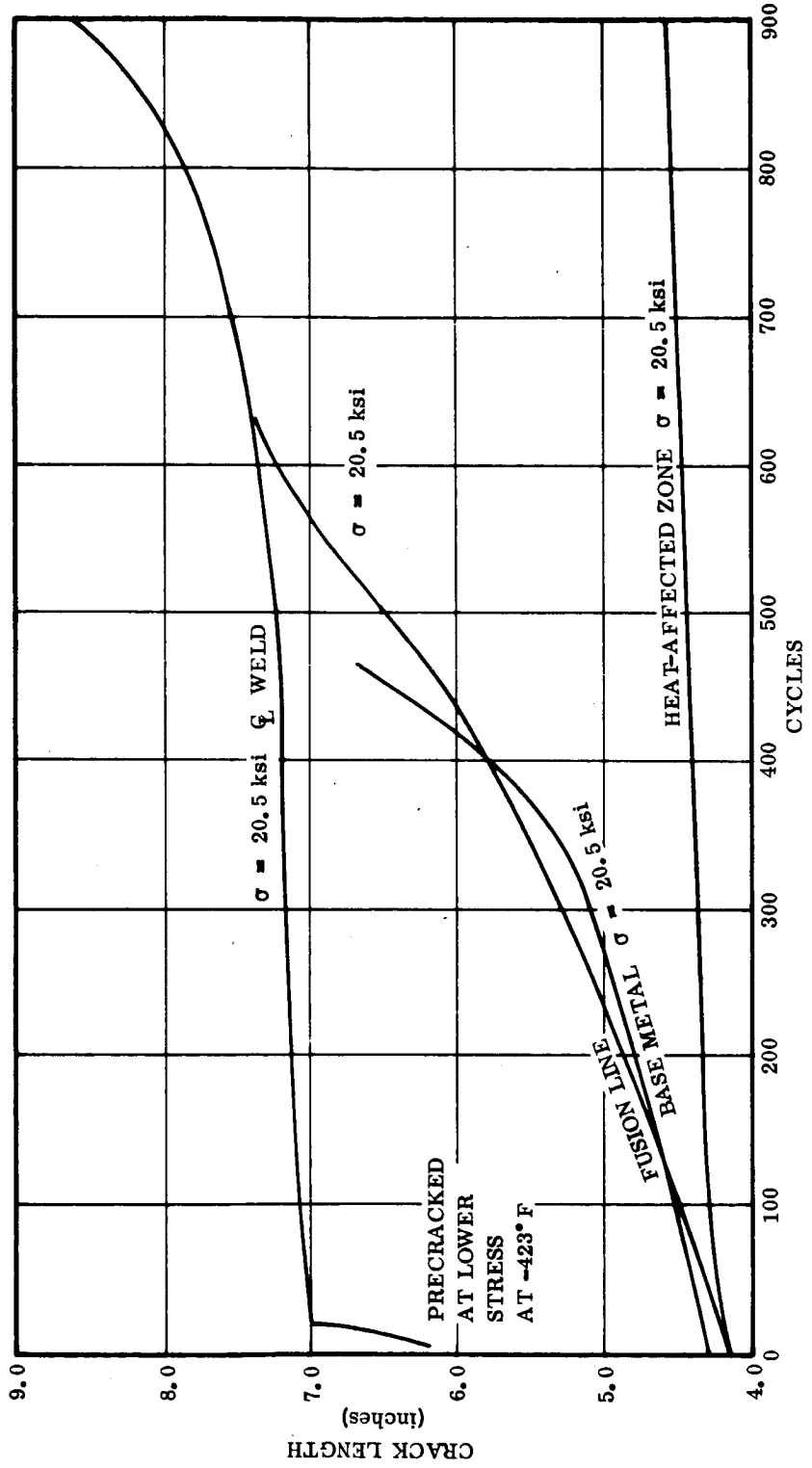


Figure 34. Cyclic Crack Growth, 2219-T81 Sheet, -423°F

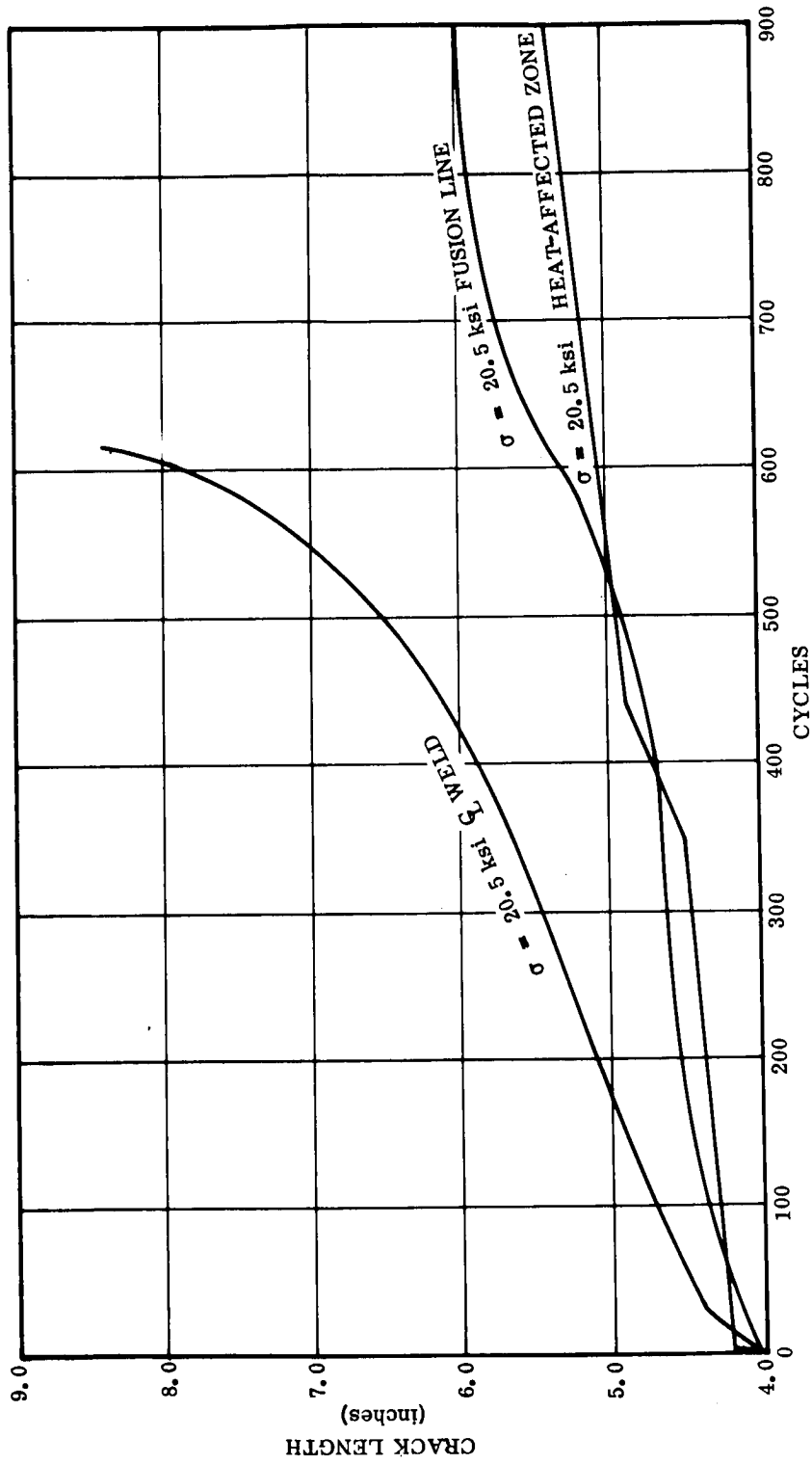


Figure 35. Cyclic Crack Growth, Repair Welded Sheet, -423°F

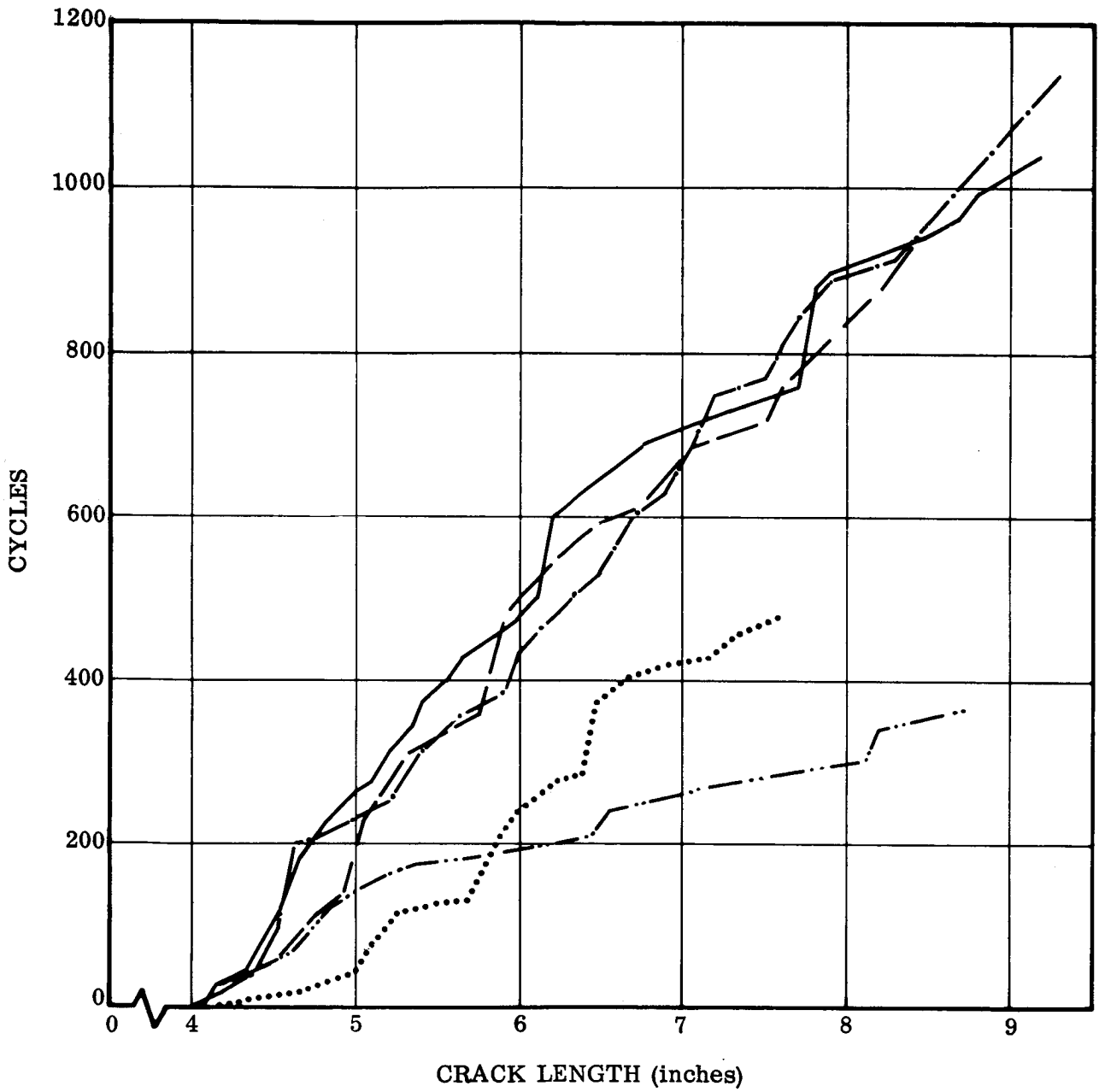


Figure 36. Crack Growth for Welded 2219-T81 Sheet at -320°F ($\sigma_m = 2.5$ ksi)

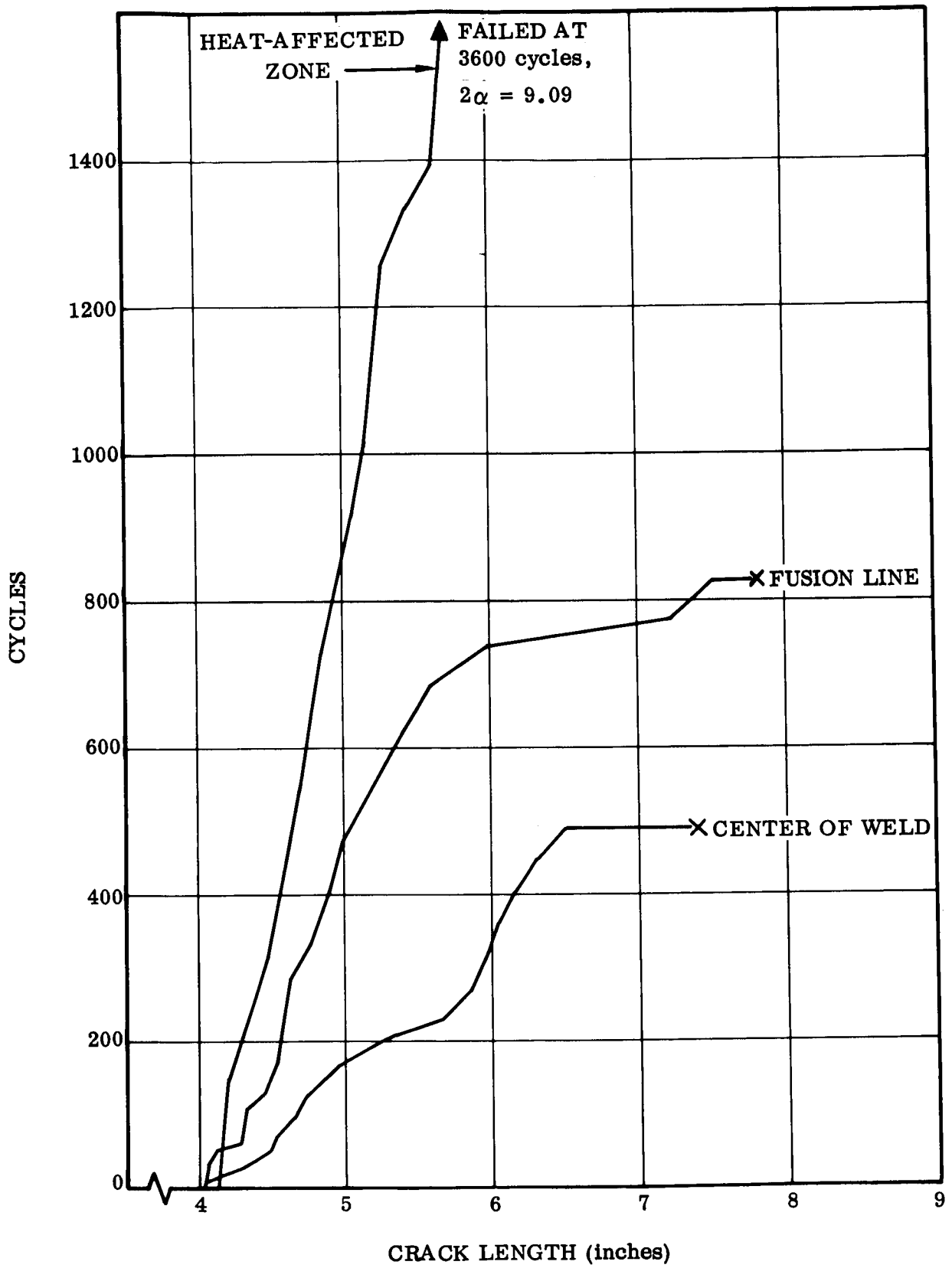


Figure 37. Crack Growth for Repair Welded 2219-T81 Sheet at -320°F ($\sigma_m = 20.5 \text{ ksi}$)

CYCLIC FLAW GROWTH TESTS - PLATE

All cyclic plate tests utilized either a semielliptical surface flaw or a totally imbedded flaw in the center of the weldments. Because of time and financial restrictions, it was not always possible to fatigue a specimen to failure at a single stress level. As a consequence, the following procedures were used for welded and repair welded specimens:

- a. Cycle at 20 ksi to failure or 500 cycles (whichever occurred first).
- b. If specimen survived 500 cycles, increase stress to 23 ksi and cycle to failure or 100 additional cycles.
- c. If specimen survived 600 cycles, increase stress to 25 ksi and cycle to failure or 300 additional cycles.
- d. If specimen survived 900 cycles, it was statically pulled to failure.

In some cases, Steps c and d were modified slightly to permit additional cycling. A summary of all plate fracture tests is shown in Table 8.

Since it was virtually impossible to measure flaw depth growth during testing, no curves are available that parallel those obtained from testing of the sheet material.

Flaw enlargement data for all 1.0-inch plate fatigue tests are shown in Table 9. All flaw measurements were determined after fracture of the specimens. Initial flaw size is considered to be that flaw size that occurred immediately after low stress notch extension. Final flaw size is either the critical flaw size if fracture occurred due to cycling or the maximum flaw obtained during cycling. In some cases it was possible to obtain several flaw sizes for various stress levels when failure did not occur within 500 cycles. A substantial amount of engineering judgement was required to determine the initial and final flaw sizes. In addition, the crack growth behavior is quite erratic in weldments and repair weldments. The reliability of the data presented is a function of such erratic behavior.

In several cases, the repair welded specimens survived less than one cycle. The cause of these apparently premature failures was a combination of variability of the repair weld material and the scatter in mechanical properties data.

The appearance of fractured surfaces is shown in Figures 38, 39, and 40 for plate flaw enlargement test specimens.

Table 8. Fracture Tests of 2219-T81 Plate

Base Metal and Weld Metal						
Temperature (° F)	Specimen Identification	Test Type	Area Tested	Stress (ksi)	Cycles to Failure	Additional Cycles and Remarks
75	B3	S	BM	48.5	Pop-in	
	8	S	W	25.7	Pop-in 25.3 ksi	
	13	S	FL	21.6	Pop-in	
	14	S	HAZ	30.2	28.3 psi	
-320	B6	S	BM	52.5	Pop-in	
	18	S	FL	32.4	Pop-in	
	10	S	W	25.2	Pop-in 22.4 ksi	
	12	S	HAZ	39.0	Pop-in 22.8 ksi	
-423	-	-	BM			This specimen cycled @ -423° F
	9	S	W	20.6		
	15	S	HAZ	40.5		
	23	S	FL	29.7		
75	B5	F	BM	43	539	Failed in grip end.
	5	F	W	20	NF at 500	100 cycles at 21.6 ksi; 79 cycles at 23 ksi
	24	F	FL	20	NF at 970	1000 cycles at 23 ksi; 100 cycles at 25 ksi; 100 cycles at 26.6;
						100 cycles at 30 ksi; Static test 30.2 ksi
-320	R5	F	HAZ	20	NF at 750	20 cycles at 23 ksi; 450 cycles at 25 ksi; Pull rod failure at 28 ksi
	B4	F	BM	45	47	
	2	F	WM	20	NF at 500	100 cycles at 23 ksi; 3 cycles at 25 ksi
	R12	F	HAZ	20	NF at 500	100 cycles at 23 ksi; 300 cycles at 25 ksi; one cycle to 44.1 ksi;
-423	20	F	FL	20	NF at 500	One cycle to 45.3 ksi; 97 cycles at 25 ksi; NF at 50 cycles at 45 ksi
						100 cycles at 23 ksi; 400 cycles at 25 ksi; one cycle to 31.5 ksi;
						50 cycles at 25 ksi; Static test 31.5 ksi NF
						Cracks visible after 22 cycles
	B2	F	BM	45	24	100 cycles at 23, NF; 300 cycles at 25 NF; No visible cracks
	17	F	FL	20	NF at 500	100 cycles at 23, NF; 270 cycles at 25, Failed; Cracks grew
	11	F	HAZ	20	NF at 500	100 cycles at 23, NF; 16 cycles at 25, Failed
	4	F	W	20	NF at 500	

NF = No failure
 S = Static
 F = Fatigue

Table 8. Fracture Tests of 2219-T81 Plate, Continued

Base Metal and Weld Metal						
Temperature (° F)	Specimen Identification	Test Type	Area Tested	Stress (ksi)	Cycles to Failure	Additional Cycles and Remarks
-423	R2*	F	Internal W incl.	20	NF at 500	2 cycles at 23, Failed
-423 Worst Case	R19*	F		20	NF at 500	100 cycles at 23 ksi; 416 cycles at 25 ksi, NF; 500 cycles at 30, NF; Static test failure at 33.6 ksi
	R1	F	W	20	313	
	3	F	W	20	NF at 500	100 cycles at 23 ksi, NF; 300 cycles at 25 ksi; NF; Static test failure at 34.16 ksi
	6	F	W	20	NF at 500	100 cycles at 23 ksi, NF; 65 cycles at 25 ksi, Failed
	1	F	W	20	NF at 500	100 cycles at 23 ksi, NF; 300 cycles at 25 ksi, NF; Static test failure at 25.66 ksi
-423	B1	F	BM	43	72	
75	R6*	F	W incl.	4.17	NF at 100	Twelve stress levels used, up to 18.3 ksi; failed at 19.5 ksi; total 703 cycles
	R14*		Int. ck.			
	19*		W incl.			
	R22*	F	Mech. notch	10	NF at 125	Failed during notch extension Failed at 20 ksi

Weld Repair Phase III

75	I6*	S	W	14.6	-	
	R7*	S	FL	23.8	Pop-in 23.6	
	R20*	S	HAZ	20.3	Pop-in 14.8 & 19.8	
-320	R13*	S	WM	19.2	-	
	R16*	S	FL	26.6	Pop-in 18.5 ksi	
	R4*	S	HAZ	25.8	-	
-423	R9*	S	W	15.35		
	R17*	S	FL	29.4		
	R11*	S	HAZ	21.2		

NF = No failure
 S = Static
 F = Fatigue
 * = Repair weld specimen

Table 8. Fracture Tests of 2219-T81 Plate, Concluded

Weld Repair Phase III						
Temperature (° F)	Specimen Identification	Test Type	Area Tested	Stress (ksi)	Cycles to Failure	Additional Cycles and Remarks
75	R15*	F	W	22.9	Failed	217 cycles +0.02 growth, 310 cycles +0.05 growth Static failure at 23.2 ksi
	R3*	F	F	19.8	812	
	7*	F	HAZ	20.0	NF at 500	
-423	R18*	F	W	15.2†	<1	100 cycles at 23, NF; 16 cycles at 25 ksi; Crack grew 12 cycles at 23 ksi; Crack grew
	R21*	F	F	20.0	NF at 500	
	R8*	F	HAZ	20.0	NF at 500	

NF = No failure
 S = Static
 F = Fatigue
 * Repair weld specimen
 † Failed during first cycle

Table 9. Cyclic Flaw Growth Data for 1.0-Inch 2219-T81 Aluminum Alloy

Test Temp. (°F)	Specimen Number	Spec. Type	Spec. Size (in.)		Cyclic Gross Stress, σ_G (ksi)		Initial Flaw Size		Final Flaw Size		K_{II} (ksi $\sqrt{\text{in.}}$)	K_{II}/K_{IF}	Cycles to Failure	Remarks (load in ksi)		
			t	W	Max.	Min.	a_1 (in.)	$2c_1$ (in.)	Q_1	a_f (in.)					$2c_f$ (in.)	Q_f
75	B5 (FB)*	Base	1.010	5.995	43.0	0.82	0.515	1.835	1.38	0.515	2.535	1.20	54.9	0.934	539 (NF)	**
	R5 (FB)	HAZ	1.01	6.00	20.0	0.008	0.352	2.176	1.02	0.625	2.452	1.27	21.3	-	750 (NF)	*
	24	FL	1.01	6.00	20.0	0.008	0.235	1.50	0.95	0.420†	1.503	1.29	22.2	0.875	970 (NF)	1000 ~ @ 23 (NF) 100 ~ @ 25 (NF) 100 @ 26.6 (NF) 100 @ 30.0 (NF) Stat. Fail. @ 31.0
-320	5	WM	1.010	6.01	20.0	0.008	0.255	1.530	0.93	0.305	1.530	1.01	20.4	0.955	500 (NF)	100 ~ @ 21.6 (NF) 79 @ 23.3 (F)
	B4	Base	1.01	6.00	45.0	0.025	0.512	1.859	1.44	0.730‡	2.30	1.59	52.2	0.88	47 (F)	100 ~ @ 23 (NF) 397 @ 25 (NF) 50 @ 45 (NF)*
	R12 (FB)	HAZ	1.01	6.01	20.0	0.025	0.170	1.483	0.98	0.217	1.492	0.72	16.8	0.34	500 (NF)	100 ~ @ 23 (NF) 397 @ 25 (NF) 50 @ 45 (NF)*
-423	20 (FB)	FL	1.01	5.99	20.0	0.025	0.181	1.547	0.96	0.181	1.547	0.82	17.2	0.58	500 (NF)	100 ~ @ 23 (NF) 400 @ 25 (NF) 1 @ 31.5 (NF) 60 @ 25 (NF) 1 @ 31.5 (NF)*
	2	WM	1.01	6.00	20.0	0.025	0.300	1.50	1.19	0.450	1.93	1.27	19.6	0.845	500 (NF)	100 ~ @ 23 (NF) 3 @ 25 (F)
	B2	Base	1.01	6.01	45.0	0.025	0.520	1.98	1.42	0.665	2.13	1.55	53.0	0.925	24 (F)	100 ~ @ 23 (NF) 300 @ 25 (NF)*
-423	B1	Base	1.01	6.01	43.0	0.025	0.454	1.780	1.46	0.790	2.604	1.55	51.0	0.676	72 (F)	100 ~ @ 23 (NF) 270 @ 25 (F)
	11	HAZ	1.01	6.00	20.0	0.025	0.570	1.875	1.53	0.720	2.12	1.67	23.8	0.93	500 (NF)	100 ~ @ 23 (NF) 300 @ 25 (NF)*
-423	17 (FB)	FL	1.01	6.02	20.0	0.025	0.585	1.60	1.77	0.655	2.33	1.41	21.8	0.56	500 (NF)	100 ~ @ 23 (NF) 300 @ 25 (NF)*
	4	WM	1.01	6.01	20.0	0.025	0.290	1.505	1.19	0.415	1.55	1.42	19.2	0.910	500 (NF)	100 ~ @ 23 (NF) 16 @ 25 (F)

* FB = Failure by Bending

**Grip end fractured. Specimen was broken in two by static bending. Flaw size measurements were made by comparing surface crack extensions at various cycles with flaw depth after fracture.

The critical flaw depth could not be accurately determined.

NF = No Failure

F = Failed

† $\Delta = 0.22$ -inch, $\alpha = 67^\circ$

‡ $\Delta = 0.35$ -inch, $\alpha = 72^\circ$

Table 9. Cyclic Flaw Growth Data for 1.0-Inch 2219-T81 Aluminum Alloy, Contd

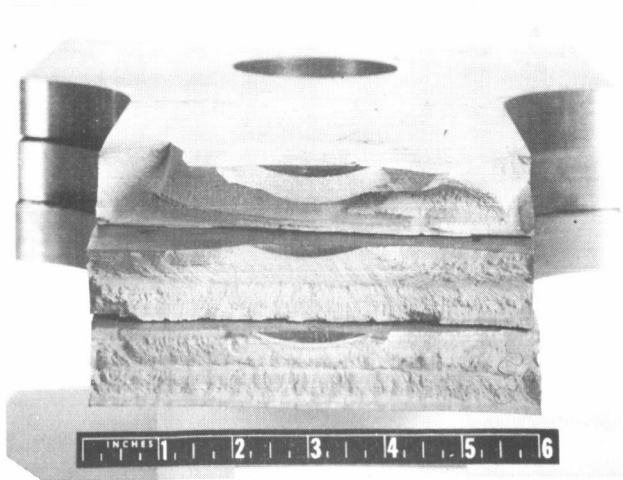
Test Temp. (°F)	Specimen Number	Spec. Type	Spec. Size (in.)		Cyclic Gross Stress, σ_c (ksi)		Initial Flaw Size		Final Flaw Size		K_{II} (ksi $\sqrt{in.}$)	K_{II}/K_{If}	Cycles to Failure	Remarks (load in ksi)			
			t	W	Max.	Min.	a_i (in.)	$2c_i$ (in.)	Q_i	a_f (in.)					$2c_f$ (in.)	Q_f	
75	7	HAZ	1.00	5.98	20.0	0.008	0.485	1.94	1.25	0.580	2.03	1.36	24.4	0.953	500 (NF)	Static fail @ 23.2	
	R3	FL	1.01	6.01	19.8	0.008	0.575	2.51	1.19	0.835	2.98	1.35	26.8	0.883	812 (F)		
	R15	WM	1.01	5.98	22.9		0.26	1.565		0.26	1.565	1.03			1 (F)		
	R8	HAZ	1.02	5.98	20.0	0.025	0.520	1.98	1.29	0.640	2.12	1.41	24.8	0.944	500 (NF)		12 ~ @ 23 (F)
-423	R21	FL	1.00	6.018	20.0	0.025	0.455	1.873	1.30	0.619	2.10	1.48	23.1	0.920	500 (NF)	100 ~ @ 23 (NF) 16 @ 25 (F)	
	R18	WM	1.055	5.985	14.4		0.457	1.726		0.746	2.27	1.60		0.757	1 (F)		
Repair Welded Condition																	
-423	R1	Repair	1.06	6.00	20.0	0.025	0.507	1.753	1.54	0.507	1.753	1.54	22.2	1.0	313 (F)	100 ~ @ 23 (NF) 300 @ 25 (NF) Static fail @ 25.7	
	1	As-Welded	1.06	6.00	20.0	0.025	0.460	1.839	1.36	0.480	1.839	1.44	22.2	0.91	500 (NF)		
	3	As-Welded	1.02	5.97	20.0	0.025	0.275	1.560	1.16	0.275	1.560	1.16	20.4	1.0	500 (NF)		
	6	As-Welded	1.05	5.99	20.0	0.025	0.438	1.775	1.35	0.496	1.804	1.44	23.6	0.98	500 (NF)		100 ~ @ 23 (NF) 300 @ 25 (NF) Static fail @ 34.2
As-Welded and Repair Welded Worst Case Condition (Surface Flaw in Weld Tested at -423 °F)																	

Table 9. Cyclic Flaw Growth Data for 1.0-Inch 2219-T81 Aluminum Alloy, Concluded

Test Temp. (°F)	Specimen Number	Internal Defect Type	Specimen Size (in.)	Cyclic Gross Stress, σ_G (ksi)		Initial Internal Flaw Size		K_{Ic} (ksi $\sqrt{in.}$)	Cycles to Failure (load in ksi)	Remarks		
				Max.	Min.	a_i (in.)	$2c_i$ (in.)				Q (in.)	
				t	W							
75	R22*	Machined Notch	1.00	6.00	20.0	0.008	0.21	1.07	1.1	17.4	125 ~ @ 6.0 (NF) 8 @ 16.7 (NF) Static fail @ 20	No visible growth
	R6*	Tungsten Incl.	1.00	6.00	19.5	0.008	0.26	1.10	1.21	18.0	703 ~ @ 4 to 18.3 (NF) Static fail @ 19.5**	No visible growth
	19*	Tungsten Incl.	1.01	5.95	7.4		0.28 0.77	1.03 2.10	1.32 1.66	6.6 (tungsten) 11.7 (surface flaw)	Failed on first cycle	Two visible growth areas not located in inclusion area
	R19	Linear Porosity	1.00	5.96	20.0	0.008					500 (NF) 100 ~ @ 23 (NF) 400 @ 25 (NF) 500 @ 30 (NF) Static fail @ 33.6	Visible linear porosity plus lack of fusion, but no growth
-423	R2	Tungsten Incl.	1.01	5.99	20.0	0.008	0.275	1.41	1.26	19.0 (K_{II}) 21.8 (K_{Ic})	500 (NF) failed @ 23	No visible growth

* These specimens were instrumented for ultrasonic crack detection tests.

**Stress levels ranging from 4 to 16.7 ksi for a total of 700 cycles were used in an attempt to enlarge the internal flaw.

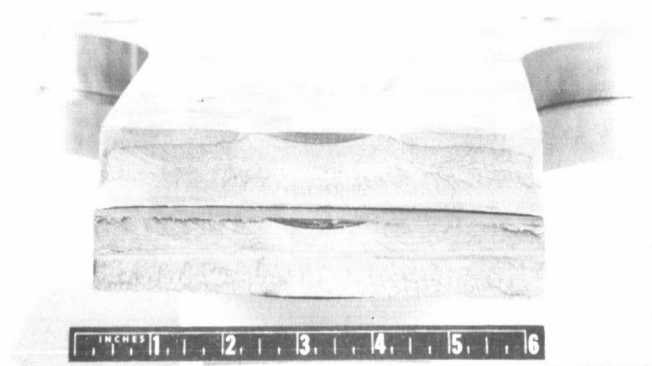


75° F

BASE METAL, B5

WELD METAL, 5

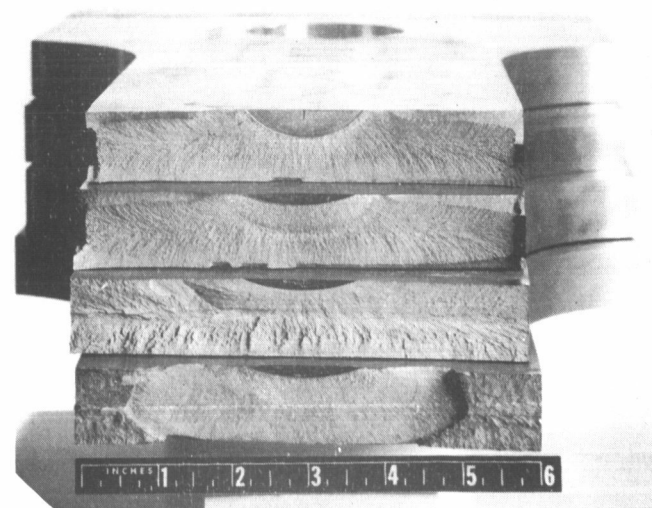
FUSION LINE, 24



-320° F

BASE METAL, B4

WELD METAL, 2



-423° F

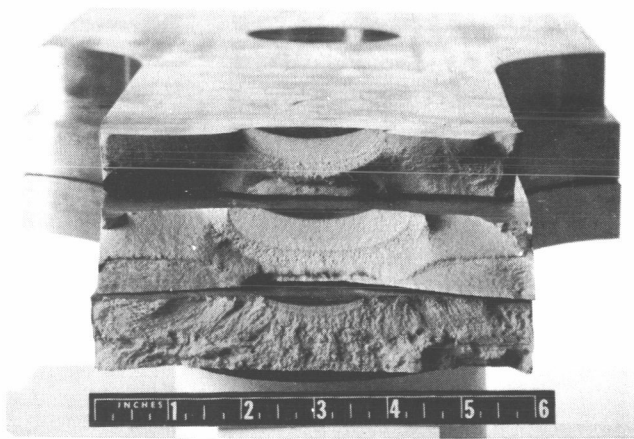
BASE METAL, B1

BASE METAL, B2

WELD METAL, 4

HEAT AFFECTED ZONE, 11

Figure 38. Fracture Surfaces of 1.0-inch 2219-T81 Tested in Cyclic Fracture at Various Temperatures. Marginal Notes Indicate Test Temperature and Location of Surface Flaw Relative to Weld Bead.



75° F

HEAT AFFECTED ZONE, 7

FUSION LINE, R3

WELD METAL, R15



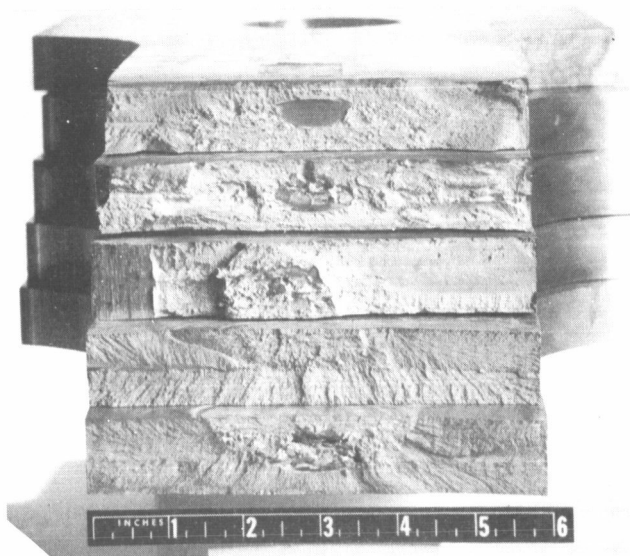
-423° F

HEAT AFFECTED ZONE, R8

FUSION LINE, R21

WELD METAL, R18

Figure 39. Fracture Surfaces of Repair Welds in 1.0-inch 2219-T81 Tested in Cyclic Fracture at Various Temperatures. Marginal Notes Indicate Test Temperature and Location of Surface Flaw Relative to the Repair Weld.



75° F

MACHINED NOTCH, R22

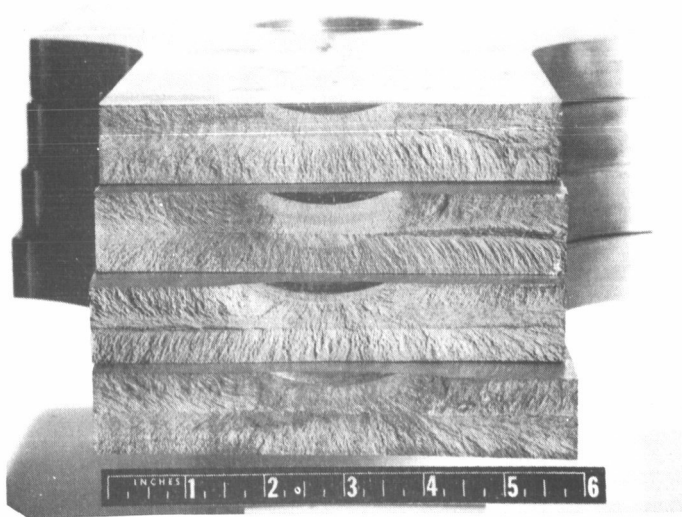
TUNGSTEN INCLUSION, R6

TUNGSTEN INCLUSION, 19

-423° F

LINEAR POROSITY, R19

TUNGSTEN INCLUSION, R2



WORST CASE: FLAW IN WELD
METAL TESTED
AT -423° F.

NUMBERS: R1

1

3

6

Figure 40. Fracture Surfaces of Repair Welds in 1.0-inch 2219-T81 Tested in Cyclic Fracture at Various Temperatures. Marginal Notes Indicate Test Temperature and Type of Internal Flaw in the Repair Welds.

8/DISCUSSION OF RESULTS

MECHANICAL PROPERTIES - SHEET

The strength of 2219-T81 sheet increases with a decrease in temperature between 75 and -423°F (Table 2, Figure 22). The same generalization can be made for both the automatic TIG welds and the manual repair welded sheet. The results obtained show small scatter for the base metal (whose ultimate strength varied from 65.2 ksi at 75°F to 94.9 ksi at -423°F) but a great deal more for the 0.02 percent and 0.2 percent offset yield strengths of the weldments. Inasmuch as a single specimen was used to obtain stress-strain curves for both heat-affected zone (HAZ) and weld metal zones, the ultimate strength for the welded specimen represents only the strength of the weakest section, namely the weld metal. For purpose of calculating the plastic zone correction at the weld fusion line for center-notched specimen tests, the average yield strength between the HAZ and the weld metal was used. Perhaps the most significant portion of the mechanical property data is the ratio of the yield strength to ultimate strength. For comparison purposes, these ratios are listed as follows:

	Base Metal	Weld	Heat-Affected Zone
75° F	0.785	0.475	0.553
-320° F	0.75	0.430	0.329
-423° F	0.71	0.413	0.498

The values used for obtaining the yield strength to ultimate strength ratios were average values for 0.2 percent offset.

Several interesting observations can be made. First, the yield strength of base metal is about three-quarters of the ultimate strength. At the same time, the yield strength of the weld metal is almost always less than half the ultimate strength of the joint.

For both the base metal and the weld metal, the ratio decreases with a decrease in temperature.

The similar ratios for the repair welded sheets fall between the base metal and the automatic welded material.

A typical stress-strain curve is shown in Figure 41. In the lower elastic region, the curves for the weld metal and heat-affected zone are almost identical. As the proportional limit is passed, the curves draw apart but then continue at the same slope. In most cases, the modulus of elasticity is the same in both zones.

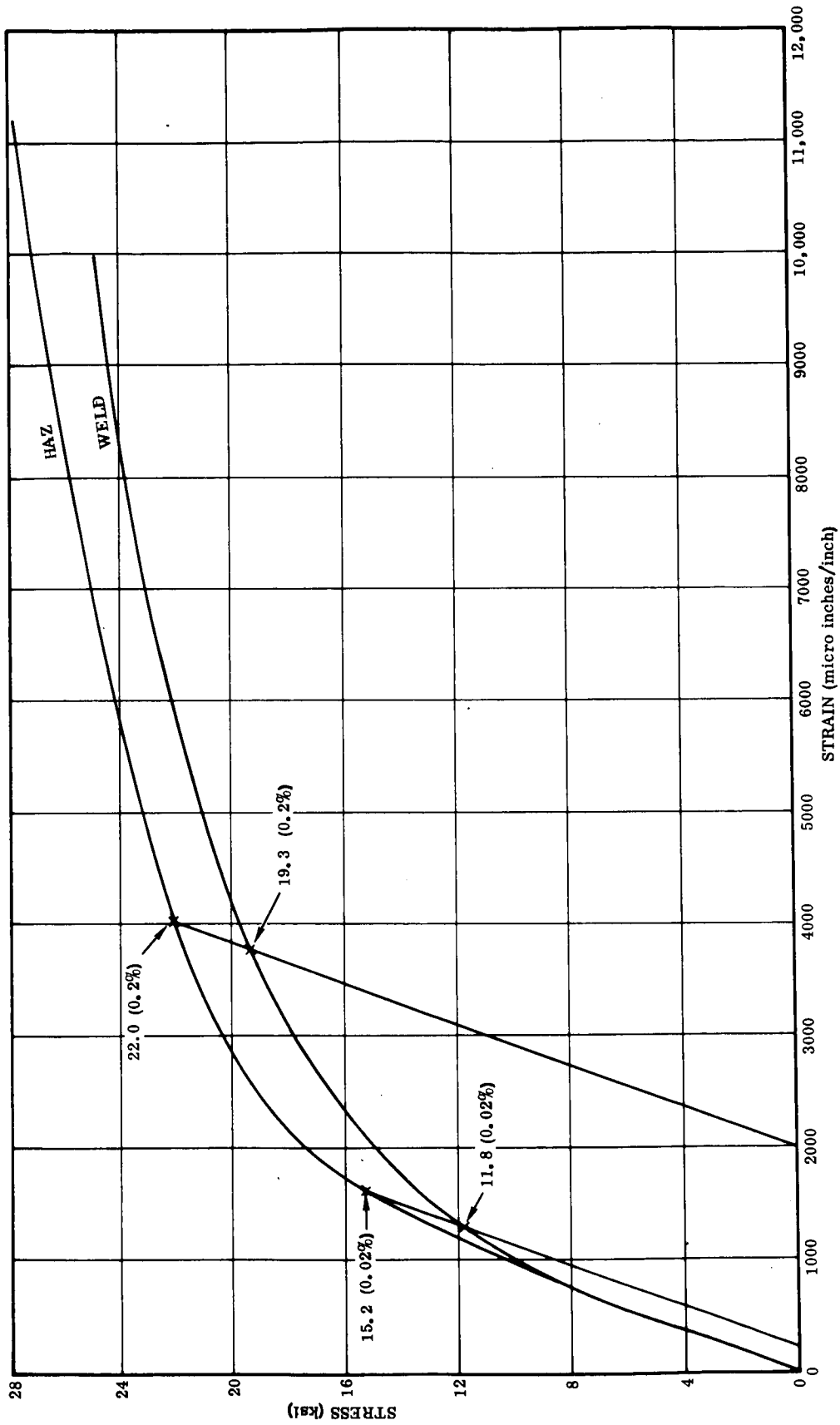


Figure 41. Stress-Strain Curve, 2219-T81 Aluminum Weldment at Room Temperature

MECHANICAL PROPERTIES - PLATE

The mechanical property characteristics of plate were very similar to those of the sheet (Table 3 and Figure 23) for the base metal and automatic welded materials. However, when the plate was repair welded, the properties became very erratic. For example, the ultimate strength of the welded plate increased from 41 ksi at 75° F to 64 ksi at -423° F. However, when the same material was manually repair welded three times, the variation was from 31 ksi at 75° F to only 34 ksi at -423° F.

PLANE STRESS FRACTURE TOUGHNESS (K_{IC})

Variation of the K_{IC} with temperature for base metal and welded sheet is shown in Figure 25. At room temperature, the static fracture toughness (corrected for plastic zone) of the heat-affected zone (HAZ) is greater than that of the base metal. However, at -423° F, the K_{IC} of the base metal is 108 ksi $\sqrt{\text{in.}}$ compared to 92 ksi $\sqrt{\text{in.}}$ for the HAZ. In general, the toughness of this alloy increases with a decrease in temperature. However, the corrected K_{IC} for the automatic TIG welded sheet shows a decrease at -423° F. For the manual repair welds, except for the fusion line, the K_{IC} (corrected) increases continuously with a decrease in temperature.

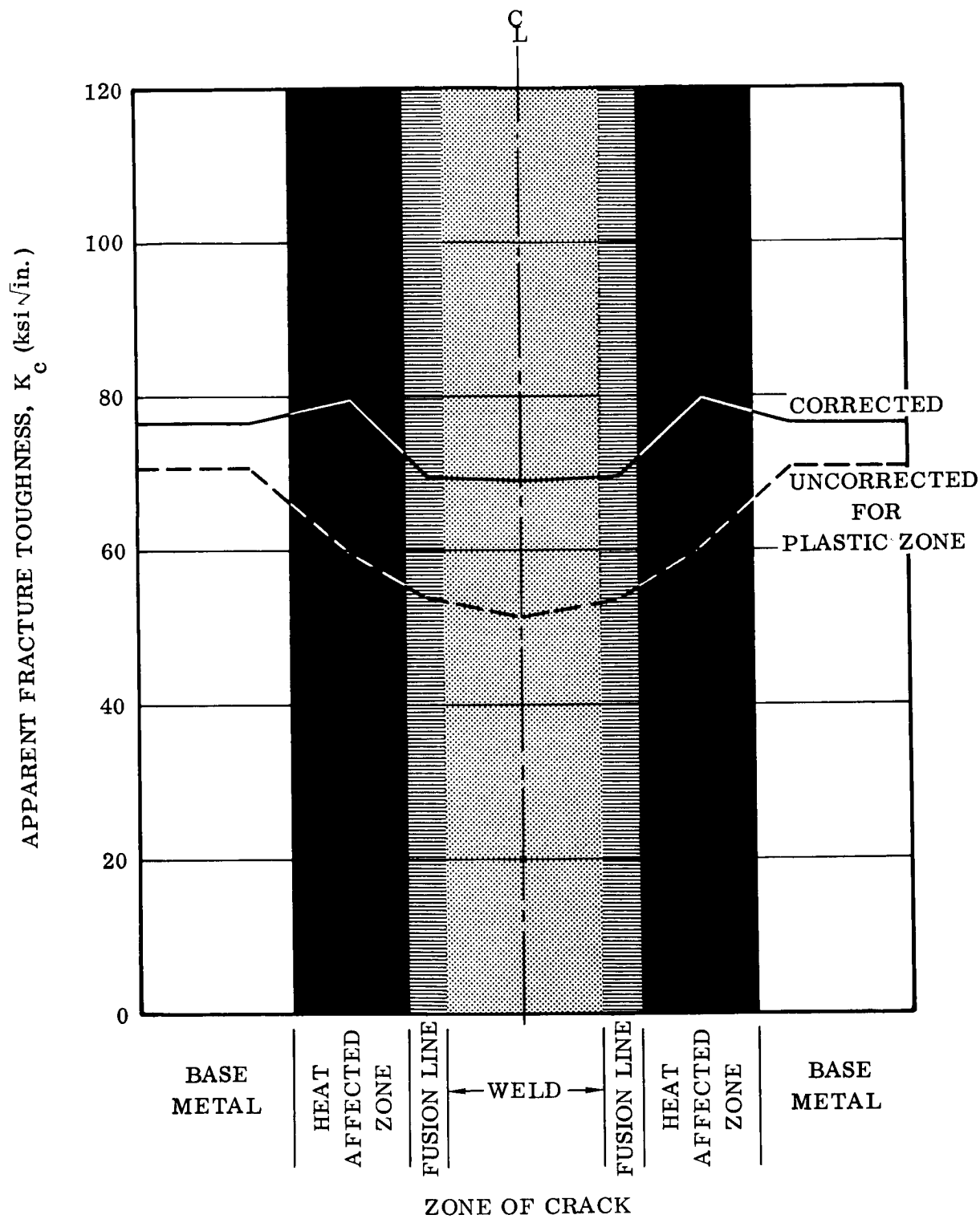
VARIATION OF PLANE STRESS FRACTURE TOUGHNESS WITH LOCATION OF CRACK

One of the important phases of this program concerned the relative fracture toughness of various zones in the vicinity of the welds. Representations of the K_{IC} variation with weld zones are shown in Figure 42. All K_{IC} values shown are corrected for the plastic zone. In addition, the uncorrected values are shown at room temperature. Again, the values obtained were for only one test for each test condition and are statistically unacceptable. In the case of room temperature, a small amount of scatter could vary the ranking of the various zones. The results shown for room temperature tests indicate that the corrected K_{IC} for the heat-affected zone is tougher than any other zone including the base metal. However, at -320° F the corrected K_{IC} values of the HAZ are the lowest of all zones. The results at -423° F behave as one might expect with the K_{IC} decreasing from the parent metal down to the center line of the weld. The apparent K_{IC} values obtained from the center notched specimen tests are also plotted (Figure 42c) to show the similarity between the two fracture toughness concepts. Another examination of the results (Table 4) shows some interesting trends.

When the uncorrected K_{IC} values are plotted at 75° F (Figure 42), the resulting curve is more like what one expects with the highest value at the base metal zone decreasing continuously to the center of the weld.

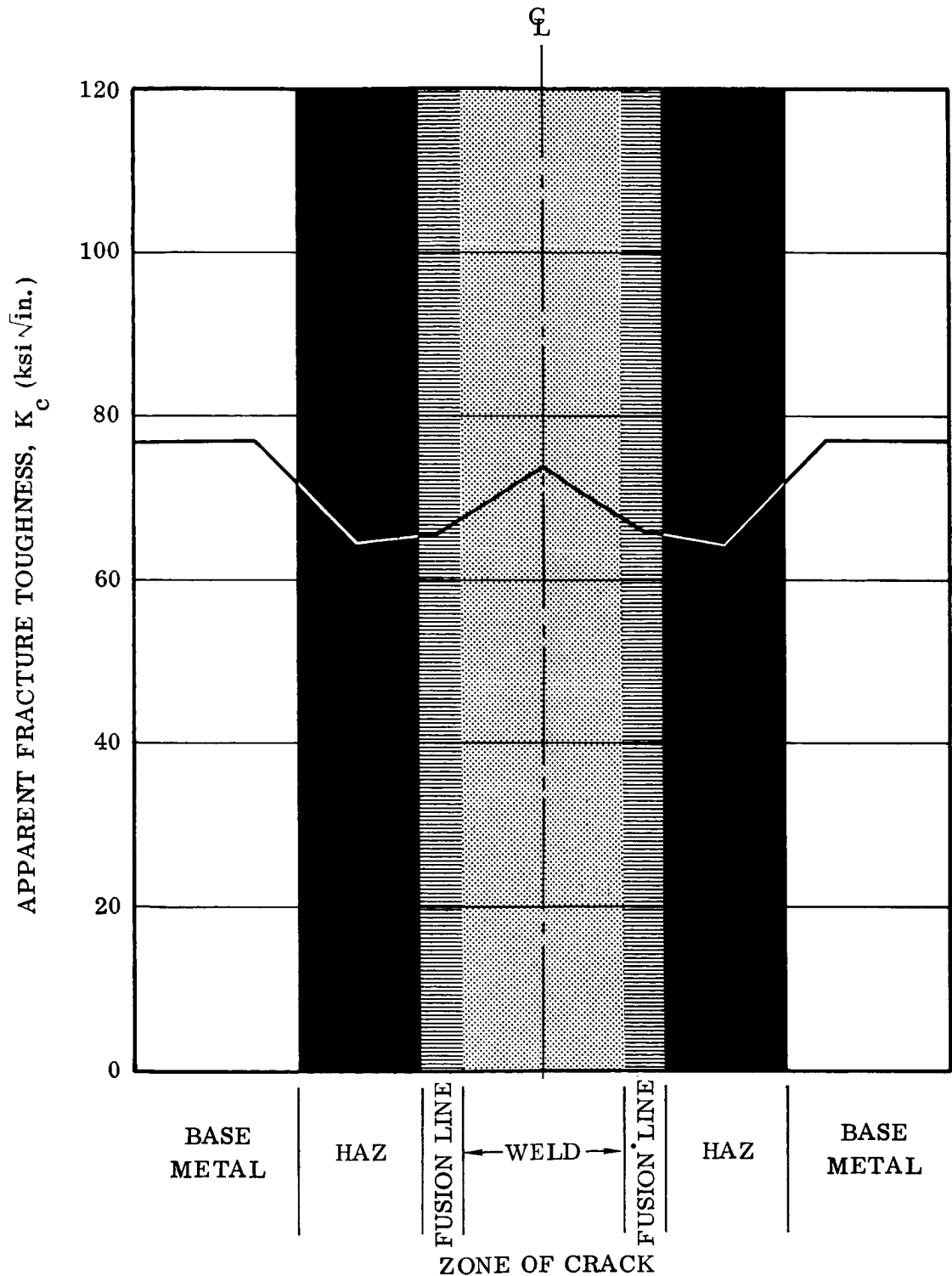
The only difference between the two sets of values is the plastic zone correction:

$$\frac{K_{IC}^2}{2\pi\sigma_{ys}^2}$$



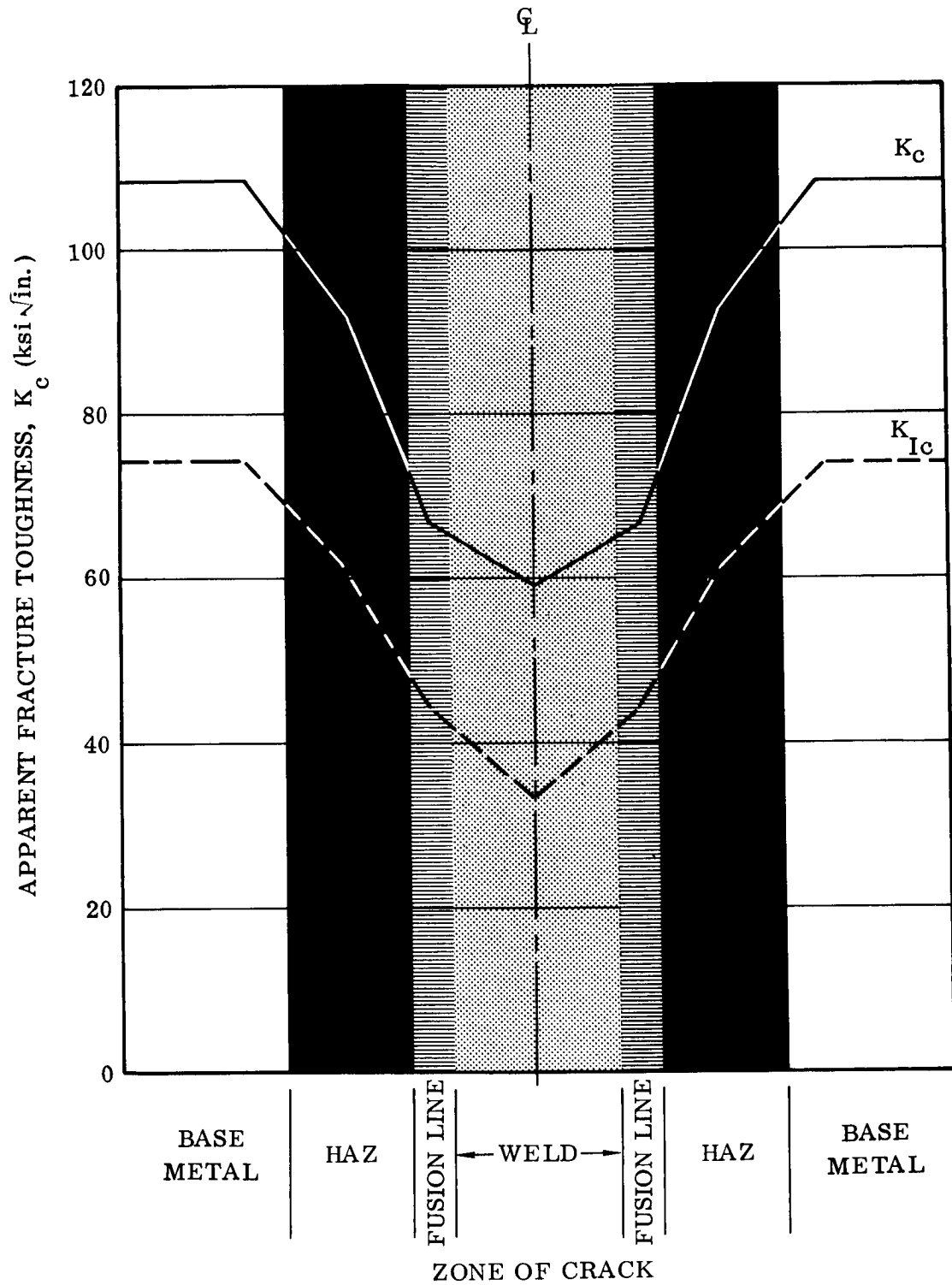
a. Temperature = 75° F (t = 0.063 Inch)

Figure 42. Distribution of Apparent K_c With Weld Zones



b. Temperature = -320° F (t = 0.063 Inch)

Figure 42. Distribution of Apparent K_c With Weld Zones, Continued



c. Temperature = -423° F (t = 0.063 Inch)

Figure 42. Distribution of Apparent K_c With Weld Zones, Concluded

The only term that can cause a change in the relative ranking of the corrected K_{IC} values is the yield strength. As has been discussed, the yield strength of either the weld or heat-affected zones is less than half the base metal yield strength. At the same time, the ultimate strength in the weld area is about two-thirds the ultimate strength in the parent material. It appears that the correction for plastic zone is too severe for the weld zones. It may be that the substitution of ultimate strength for yield strength in the plastic zone correction would be more accurate despite the apparent discrepancy.

PLANE STRAIN FRACTURE TOUGHNESS OF 1.0-INCH PLATES

Results for static fracture tests on 1.0-inch-plate material are shown in Table 5. All tests performed in this portion were plane strain surface-notched tests. The variation of plane strain fracture toughness with temperature is shown in Figure 43 for base metal and automatic welded specimens and in Figure 44 for manual repair welded specimens. Actually the base metal specimen test at -423°F was not performed since the anticipated load exceeded the capacity of the test machine. In addition, the repair welded HAZ specimen tested at -423°F and the repair welded fusion line specimen tested at -320°F did not fail through the surface notch. The odd failures of these two tests are an indication of the erratic behavior of 2219-T81 plate that has been subjected to three repair welds.

For purposes of discussion, the K_{IC} value obtained from the base metal sheet test is used in Figure 43 to complete the curve.

Nevertheless, the results are quite revealing. The K_{IC} of the base material is substantially greater than that of any other zone at all test temperatures. As was expected, the toughness of the heat-affected zone (HAZ) is higher than any part of the weld for the automatic welded plate. Not expected was the lower ranking of the HAZ tests after the plate had been subjected to repair welding. Again the problems associated with locating the notch in the HAZ and the fusion line of the plate material could cause the discrepancy, particularly after repair welding, which causes broadening and overlapping of the weld zones.

The K_{IC} for all zones except the weld metal increases with a decrease in temperature. However, the toughness of the weld metal, either as-welded or repair welded, shows a distinct reduction between -320° and -423°F . In fact, the as-welded plate (weld zone) toughness decreases continuously with a decrease in temperature.

This loss of toughness in the weld metal at -423°F was observed in the sheet tests also (Figure 25).

NET FRACTURE STRESS

A great deal has been written about the relationship of the net fracture stress to the yield strength of the material as a criterion for acceptable fracture toughness data

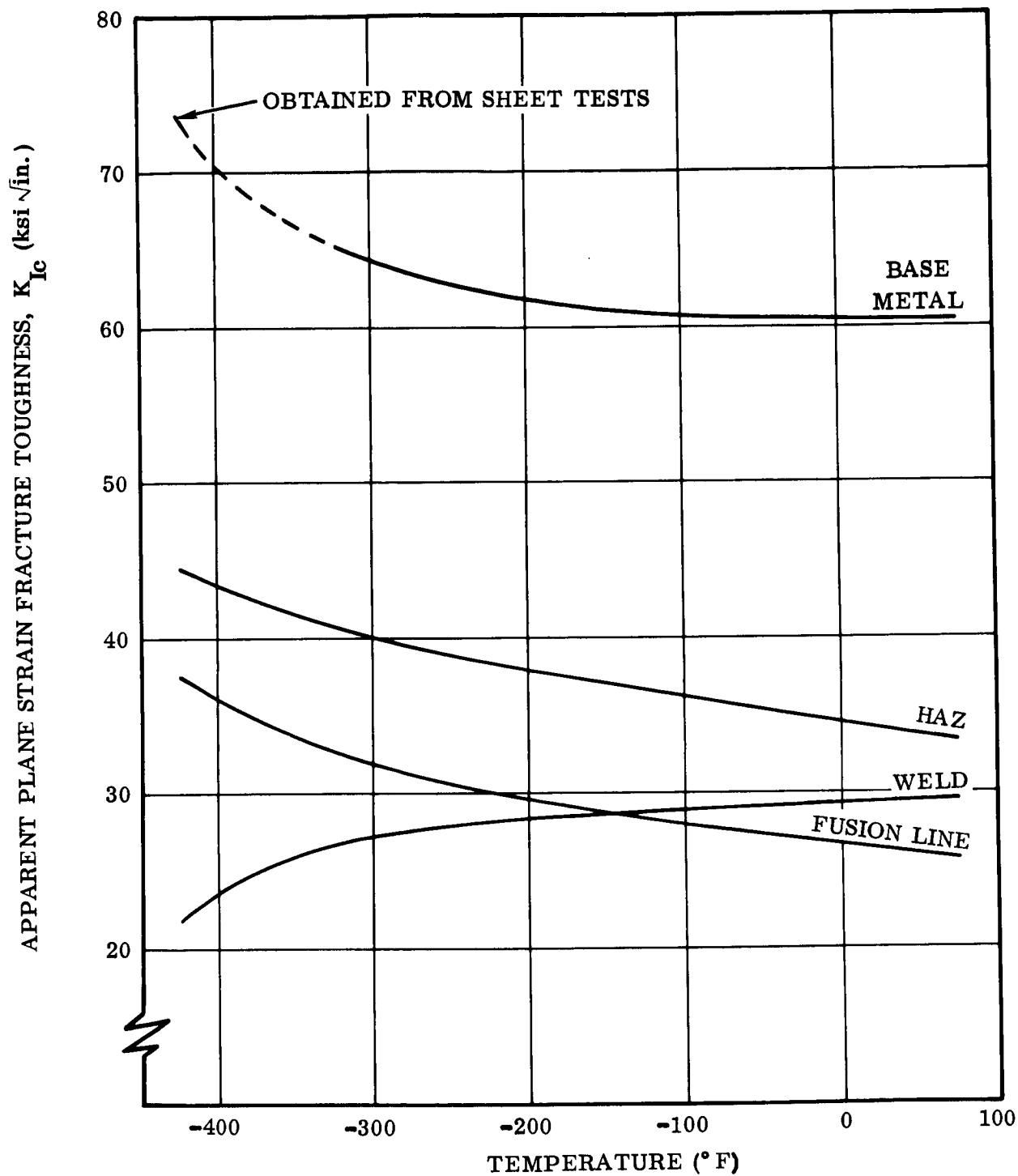


Figure 43. Variation of Apparent Plane Strain Fracture Toughness with Temperature for 2219-T81 Plate

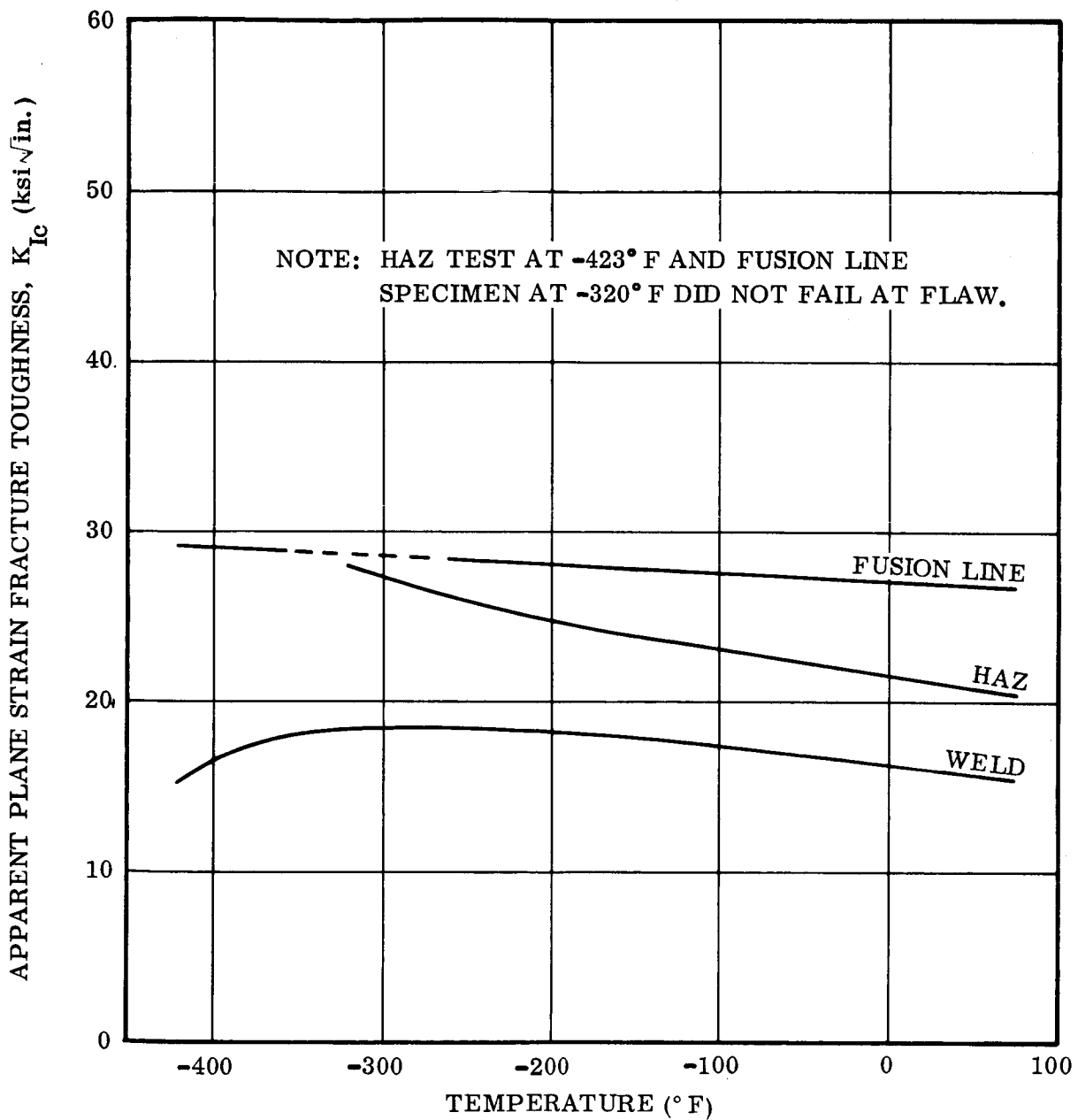


Figure 44. Variation of Apparent K_{Ic} with Temperature for Repair Welded 2219-T81 Plate

(Reference 1). In general, most investigators believe that the net fracture stress should not exceed 80 percent of the yield strength for plane stress tests and should not exceed 100 percent of yield strength for plane strain tests. Two reasons are suggested for this requirement, namely: 1) the basic stress analysis is based on linear elastic theory, and 2) as the average stress approaches yield strength, stress concentrations cause the stress in a portion of the material to be elevated into the plastic region resulting in progressive failure due to general yielding.

The plastic region of welded material does not resemble the same region in parent materials however, particularly when the base metal has been subjected to a complex tempering process and the weld metal has not. Without performing sustained load testing in the plastic region, it is not entirely proper to say that the weld metal will fail by general yielding when the stress exceeds an arbitrary yield strength obtained by an off-set method.

It was not the intent of this program to design a new plastic theory of fracture mechanics. However, it is necessary to understand the limitations of the data. A comparison of net stress to yield strengths for various tests is desirable.

For sheet tests the following ratios are obtained:

<u>Temperature (°F)</u>	<u>Zone</u>	<u>Net Stress/ Yield Strength (0.2%)</u>	<u>Net Stress/ Ultimate Strength</u>
75	Base Metal	0.74	0.58
	HAZ	1.44	0.80
	Fusion line	1.40	0.72
	Weld	1.47	0.70
-320	BM	0.64	0.48
	HAZ	1.23	0.57
	FL	1.13	0.51
	W	1.26	0.54
-423	BM	0.81	0.57
	HAZ	1.12	0.56
	FL	0.93	0.42
	W	0.90	0.37

At all temperatures, the base material meets (or practically meets) the 80 percent requirement. However, in no case does any other zone qualify. In fact, only at -423°F does the yield strength exceed the net stress. A rather interesting observation can be made concerning the net stress to ultimate strength ratio. In all cases, this ratio is

0.80 or less. Although the ratio for base metal is noticeably less than for all other zones at room temperature, this difference minimizes at -320°F and is reversed at -423°F where all other zones show lower ratios than the base metal.

At room temperature the net stress to yield strength ratio for all weld zones is about twice as high as the base metal ratio. At the same time the net stress to ultimate strength ratio for weld zones is only 1.2 to 1.4 that of the base metal. Again, the reason for these discrepancies is the large decrease of yield strength that is suffered by the 2219-T91 alloy due to welding.

The corresponding results for 1.0-inch plate are:

<u>Temperature (°F)</u>	<u>Zone</u>	<u>σ_N/σ_{ys}</u>	<u>σ_N/σ_u</u>
75	BM	0.91	0.72
	HAZ	1.38	0.68
	FL	1.14	0.50
	W	1.46	0.59
-320	BM	0.84	0.64
	HAZ	1.58	0.68
	FL	1.42	0.57
	W	1.15	0.42
-423	HAZ	1.39	0.63
	FL	1.0	0.46
	W	0.70	0.32

The results are even more striking here. In all cases but one, the net stress to ultimate strength ratio is less for welded zones than for the base metal, while the net stress to yield strength ratio is always greater for welded zones than for the base metal.

Although the usual fracture criteria are violated in the aluminum weld tests, it is unrealistic to attempt to meet them since the required stresses would be far below those found in aerospace application which, after all, is the real problem area.

As may be seen from a typical weld stress-strain curve shown in Figure 41, the behavior of an aluminum weldment can not be expected to be well characterized by a linear-elastic stress analysis. Thus the difficulty arises in interpreting the data, but as these conditions are typical of those found in welded aluminum structures, these problems are real. It is expected that behavior of the surface flawed specimens in this program, even under general yielding, should be similar to the same type of flaw's behavior in an actual vehicle. The through-the-thickness flaws may be subject to greater errors because of the finite-width effect, but past experience with 2219 aluminum indicates the results are conservative. Much work needs to be done in the area of plastic fracture mechanics to alleviate this problem.

CYCLIC CRACK GROWTH - SHEET

The crack growth of the sheet was determined under a maximum stress level (tension) that was virtually constant during testing. The minimum stress level (tension) was applied simply to prevent the sheet from being subjected to compression loading or buckling due to a change in length (caused by deformation or slippage). Some of the crack growth is shown in Figures 30 through 36.

In the early part of the program there was some consideration given to the size of the initial crack length. Some of the specimens were machined with a crack length of about 30 percent of the sheet width. However, it was desired to limit the maximum fatigue stress to 90 percent of yield strength (or 71.5 percent of ultimate). At the same time it was desired to limit the net fracture stress of the static fracture specimens to 80 percent of the yield strength. Consequently, a fatigue specimen with a 30 percent crack length should fail before one cycle was completed. For this reason, the length of the crack was changed to 1/2 inch to provide some crack growth at higher stress levels before failure. Nevertheless, some tests were performed with a 30-percent initial crack length. After the program began, the cyclic maximum stress level was set at 40.5 ksi for base metal tests and 20.5 ksi for welded specimen tests.

The general crack growth characteristics of the base metal sheet are similar at the three test temperatures. It appears that there are two distinct rates of growth; the initial rate is slow, but speeds up as fracture approaches. The initial rate is approximately 300 cycles/inch, which speeds up to a maximum of about 10 cycles/inch as fracture becomes imminent for the sheet material at 75 and -320°F .

The growth rate in the center of the welded sheet is somewhat greater than the rate of crack growth in the heat-affected zone. In fact, at -423°F , the crack grew slower in the HAZ than it did in the base metal (Figure 34). In addition the HAZ sustained many more cycles than the base metal at -423°F .

Ironically, the repair welded sheet lasted longer and cracked at a slower rate than did the automatic welded sheet at room temperature when the crack was located in the center of the weld (Figure 31). This was not the case at -423°F however, where the total cycles to failure of the welded sheet (center of weld) exceeded the cycles to failure of the repair welded sheet (Figures 34 and 35). It should be noted that at -423°F , the specimen with a notch in the center of the weld was inadvertently cycled (at -423°F) at a lower stress level for several thousand cycles before the maximum stress was increased to 20.5 ksi. At that time the crack growth rate was very high (about 20 cycles/inch) but quickly changed (after 20 cycles) to a very slow crack growth rate (2500 cycles/inch) for about 600 cycles. At this temperature, the repair welded sheet assumed growth characteristics that resembled the growth rate of the as-welded fusion line at -423°F . Again, at -423° , the growth rate in the repair welded HAZ is the lowest of all tests performed. One might expect to find erratic results for crack growth in the

HAZ and at the fusion line because of the difficulty in identifying these areas. In addition, the HAZ and fusion line become even more complicated as multiple weld passes are utilized (as they are in repair welding). Furthermore, the repair process frequently calls for removal of the weld material before additional repairs can be made. This process only multiplies the possibility of errors.

Crack growth rates at -320°F show the same sort of erratic behavior as did those rates at other temperatures (Figure 33). At this temperature, the crack in the HAZ started growing at the same low rate as at other temperatures but increased drastically at about 1100 cycles. Even then, the rate of growth of the crack in HAZ was less than the rates in other zones.

A rather interesting phenomenon occurred in the heat-affected zone of the welded sheet at 75°F . One test, cycled at 11 ksi (90 percent of F_{ty}) grew at the usual low rate (Figure 31). However, a similar specimen tested at 20.5 ksi showed some remarkable growth characteristics. For the first 110 cycles, the crack growth rate was about 320 cycles/inch. At that point the crack extended suddenly 0.4 inch in the next 5 or 6 cycles. Here the growth rate reverted to the original rate until about 240 cycles were completed. At 250 cycles, the crack grew into the weld metal, and the growth increased to a rate resembling that of other cracks in weldments.

The statistical problems associated with testing insufficient numbers of specimens are demonstrated in Figure 36, which shows the crack growth variation with cycles for five welded sheet specimens at -320°F . Four of the five specimens have approximately the same growth rates, although one of these started erratically. In addition, four of the five fractured at about the same final crack length. However only three of the five show the kind of behavior that is suitable for good statistical accuracy. All five of the specimens contained the same type of initial crack in the center of the weld metal. The behavior of the repair welded sheet on the same scale (Figure 37), which is what one might predict, shows that the difference between the growth characteristics of, say, the fusion line and center line of the weld is comparable to the scatter obtained from the five welded specimens with the crack at one location.

Nevertheless it appears possible to obtain good crack growth data if sufficient tests are performed.

CYCLIC CRACK GROWTH - PLATE

The behavior of welded and repair welded 2219-T81 aluminum plate is quite erratic when subjected to cyclic loading (Table 9, Figures 38, 39, 40 and 47).

In some cases specimens survived 1000 cycles at more than 20 ksi maximum stress. In several cases, repair welded specimens fractured while the load was being applied for the first cycle. In other tests, fractures occurred in areas away from the notched

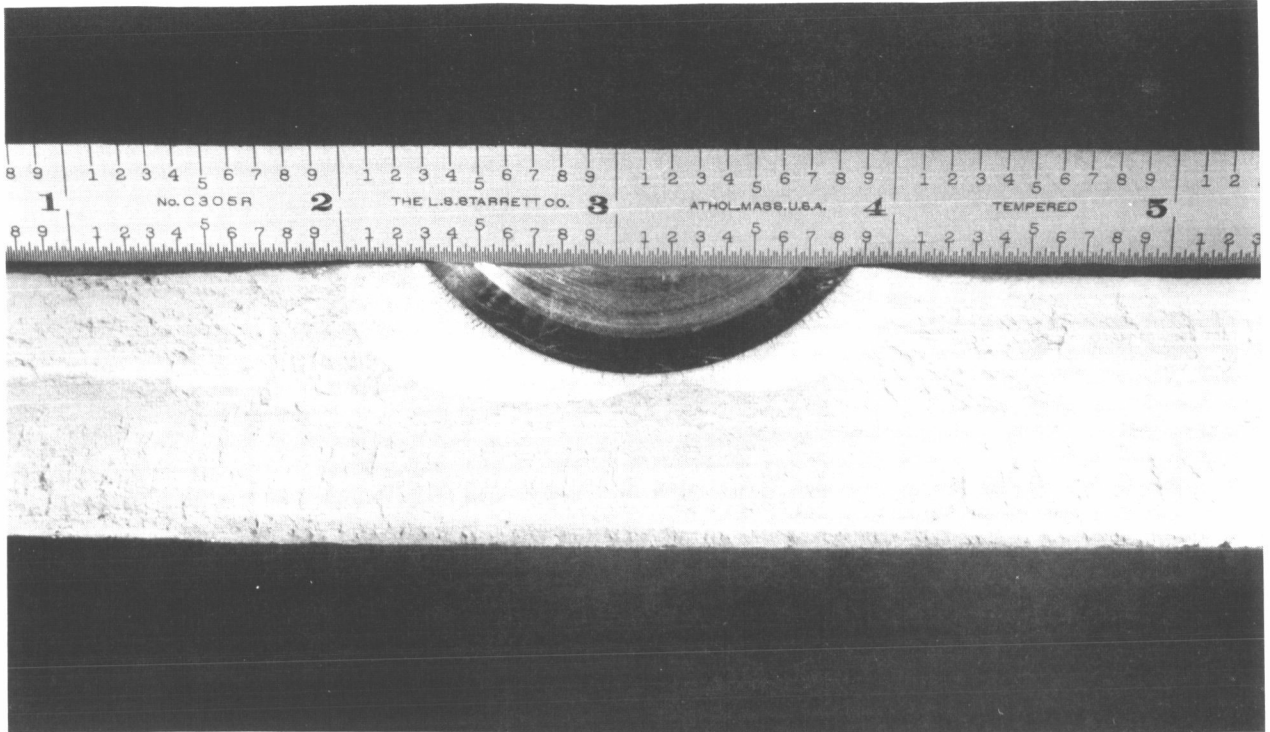


Figure 45. Fracture Surface of Welded 2219-T81 Aluminum Plate (Crack in Fusion Line, 75° F)

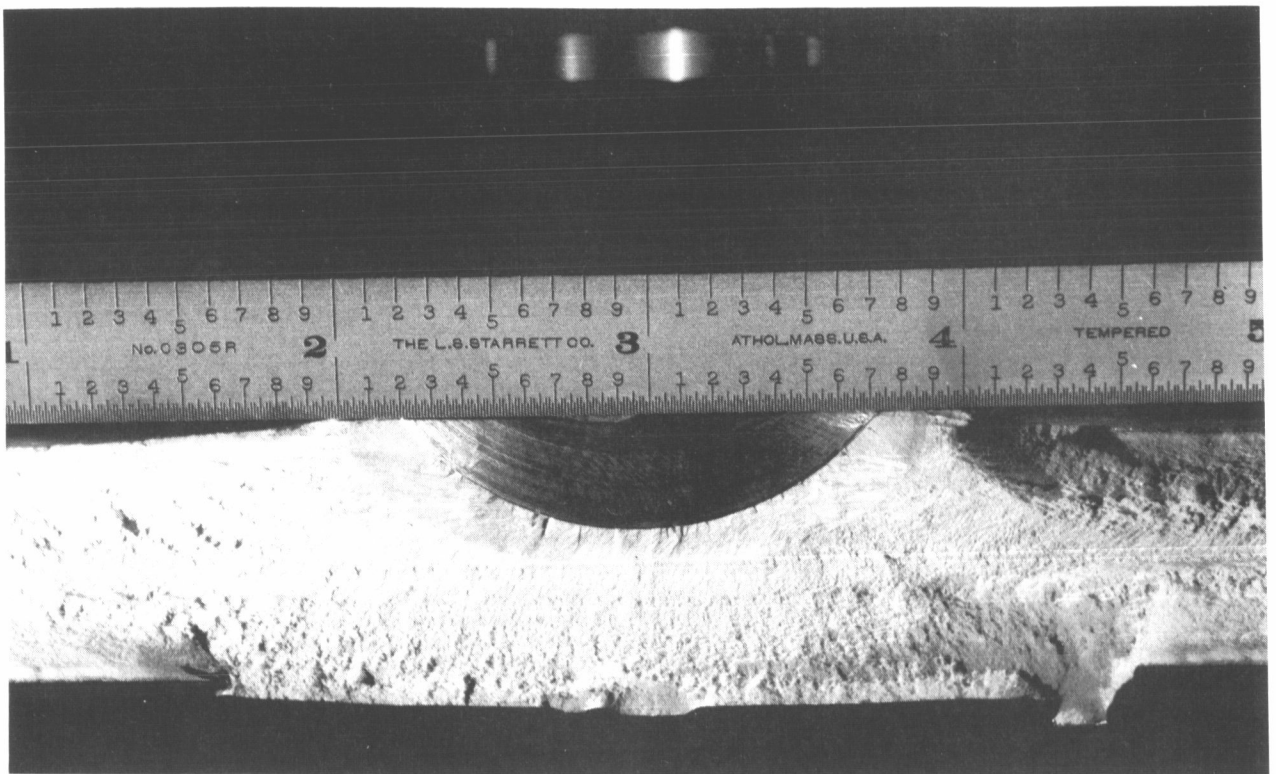


Figure 46. Fracture Surface of Welded 2219-T81 Aluminum Plate (Crack in Weld Metal, 75° F)

section of the specimen. In one case, during initial fatigue crack extension, a crack grew from the corner of the weld rather than from the sharp notch. Observation of the fractured surfaces demonstrates the erratic behavior of the welded specimens.

One specimen (Number 11, Figure 38), with the notch in the heat-affected zone, which was tested at -423°F , shows a large, bean-shaped crack path that appears to have propagated through the thickness. The roughness of the repair weld metal is clearly shown in Figure 39.

Fracture surfaces of repair welded specimens containing internal flaws (Figure 40) show distinctly different characteristics from those of the automatic welded specimens. In one case, the crack propagated in a section completely removed from the rather severe tungsten inclusion. Higher magnification of several fractured specimens, shown in Figures 45 and 46, permits closer observation.

The specimen that was notched in the fusion line (Figure 45) and cycled at room temperature shows a peculiar unsymmetric fatigue growth pattern. It is possible that such behavior was due to the fact that the fusion zone is not planar but curves through the thickness of the plate.

In the case of the crack in the center of the weld (Figure 46), a more classic semi-elliptical fatigue pattern is clearly visible. The heterogeneity of the weld metal is also visible.

An attempt was made to use the polarized light technique described by Tiffany, Lorenz, and Hall (Reference 3) for determination of flaw growth. However, those portions of the flaw growth that were not distinct under white lighting were also not distinct under polarized lighting.

Convair agrees with Tiffany, Lorenz, and Hall (Reference 3, p 19) that neither of these methods is reliable for measuring the flaw size and shape.

STRESS INTENSITY RATIO

According to Tiffany, Lorenz, and Hall (Reference 3), the cyclic life of material containing a flaw is a simple function of the ratio of the initial crack intensity factor K_{II} to the critical crack intensity factor K_{Ic} (Figure 47). Assuming that the welded material is reasonably homogeneous, and that Tiffany, Lorenz, and Hall are correct, one might conclude that a welded plate (particularly 2219 aluminum) would behave in the same fashion. Unfortunately, some of the specimens fatigued under this program did not fail and others failed only after the maximum stress was increased. Nevertheless, the variation of the log of the cyclic life with $\frac{K_{II}}{K_{Ic}}$ is shown schematically in Figure 47 for various tests.

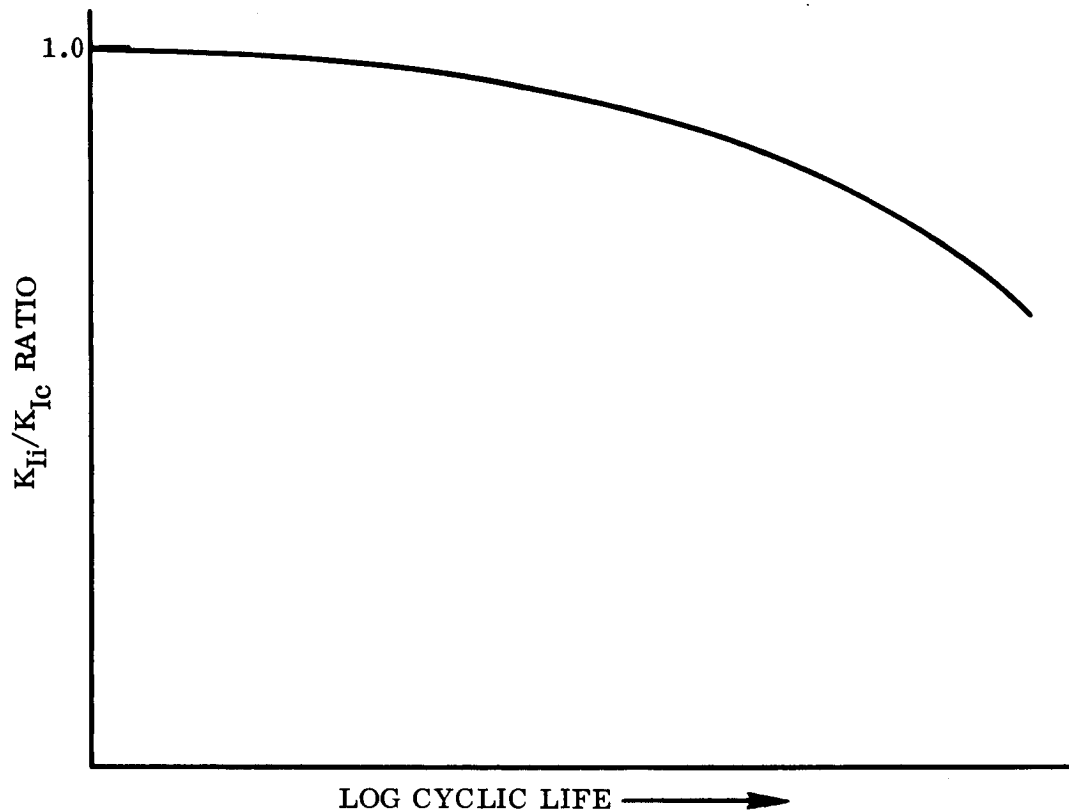


Figure 47. Schematic of Cycle Life Variation

In the cases where the cyclic stress level was raised during testing, the K_{II} value was obtained as follows.

- 1) After fracture, the cracked surface was examined for evidence of crack growth. In most cases, arrest lines were visible and, by prudent examination and interpretation, it was possible to relate the arrest line and crack depth to a particular cycle.
- 2) The K_{II} value was calculated by using the crack depth associated with last arrest line prior to fracture.

In those cases where a fatigue specimen was fractured by a static load, the same procedure was used for calculation of K_{II} . However, since failure did not occur due to fatigue, the true cyclic life is greater than the cycles recorded. This condition is illustrated by an appropriate symbol (containing a horizontal arrow) on the curve of Figure 48.

The tests that were performed represented many different conditions (temperature, stress, etc.) and locations of cracks. There was little duplication of conditions in the program. Nevertheless, many of the tests are plotted on the same graph in Figure 48.

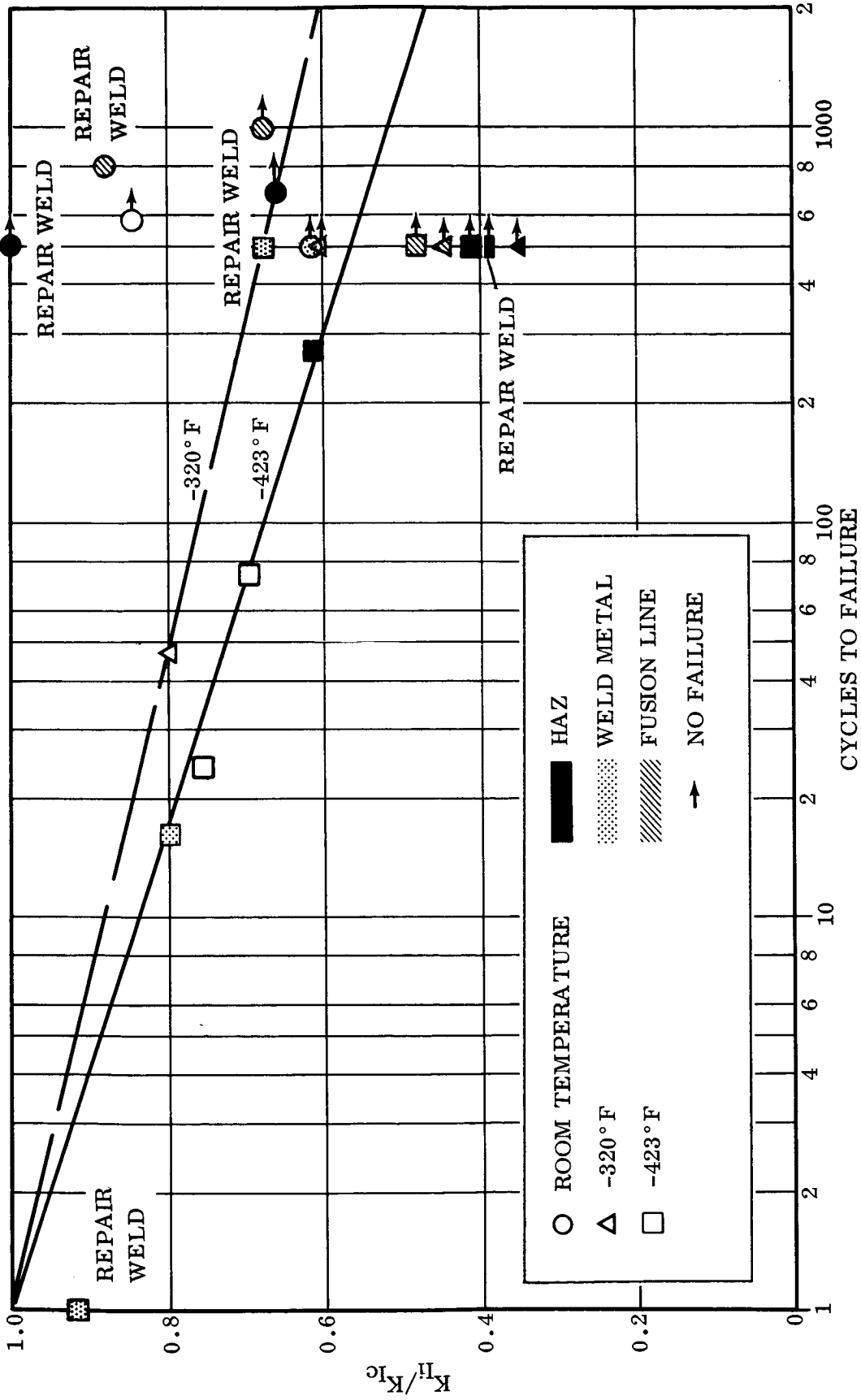


Figure 48. Variation of Stress Intensity Ratio With Cycles to Failure for 2219-T81 Plate

The results are somewhat surprising. For example, at -423°F , virtually all of the points (except the repair weld results) fall on a straight line. Furthermore, it is possible that a curve could be constructed for the results at -320°F . However, at room temperature, insufficient fractures prevent any sort of accurate curve to be drawn. Still, one might consider the results obtained by Tiffany, Lorenz, and Hall which show a curve that could be compatible with some of the results obtained in this program.

At any rate, it appears that for a given K_{II}/K_{IC} ratio, the 2219-T81 plate can withstand less cycles at -423°F than at any other temperature, and that this relationship is somewhat independent of whether the material is welded or not. However, when several repair welds are made, the results are virtually unpredictable.

9/CONCLUSIONS AND RECOMMENDATION

1. The yield strength of 2219-T81 sheet and plate decreases significantly when welded. The reduction of yield strength is much greater than the corresponding reduction in ultimate strength.
2. Base metal 2219-T81 sheet and plate toughness increases with a decrease in temperature. Plane stress and plane strain fracture toughness of the heat-affected zone increases with a decrease in temperature; the HAZ is less tough than the base metal but tougher than any other zone. The weld metal region has the lowest fracture toughness of any of the regions tested.
3. The weld area fracture toughness (plane stress or plane strain) of automatic welded 2219-T81 sheet or plate decreases significantly between -320 and -423°F.
4. The behavior of welded 2219-T81 aluminum plate is quite erratic after three repair welds have been made. The toughness values of repair welded 2219-T81 aluminum can be substantially lower than those of the new welds [K_{Ic} (Repair) \approx 15 ksi $\sqrt{\text{in.}}$, K_{Ic} (Weld) \approx 22 ksi $\sqrt{\text{in.}}$].
5. Cyclic flaw growth rates are generally higher on the weld metal than any other region tested.
6. At normal operating stresses, the critical flaw size for 2219-T81 parent metal and welds is quite large ($a \approx 1/2$ inch, $2c \approx 2$ inches) given the standard 2:1 weld land buildup.
7. Due to the very low possible toughness of repair welds, it is recommended that repair welding be kept to a minimum with 2219 aluminum as serious material property degradation is possible. Note that all repair welds (except for the flaw simulation tests) on this program meet all government specifications for welds and would be fully acceptable in an aerospace vehicle.
8. Tungsten inclusions appear to reduce the fracture toughness of the welds quite considerably and thus should always be removed. Further examination of this problem would be useful.

10/REFERENCES

1. Fracture Toughness Testing and Its Applications, ASTM STP. No. 381, April 1965.
2. Brown, W. F., and Srawley, J. E., Plane Strain Crack Toughness Testing of High Strength Materials, ASTM Special Publication No. 410, March 1967.
3. Tiffany, C. F., Lorenz, P. M., and Hall, L. R., Investigation of Plane Strain Flaw Growth in Thick Walled Tanks, NASA CR-54837, D2-20467-1, February 1966.
4. Eitman, D. A. and Rawe, R. A., Plane Stress Cyclic Flaw Growth of 2219-T87 Aluminum and 5Al-2.5Sn ELI Titanium Alloys at Room and Cryogenic Temperatures, NASA CR-54956, September 1966.
5. Christian, J. L., Yang, C. T., and Witzell, W. E., Physical and Mechanical Properties of Pressure Vessel Materials for Application in a Cryogenic Environment, Part III, ASD-TDR-62-258, December 1964.
6. Mayer, L. W., Alcoa Aluminum Alloy 2219, Alcoa Green Letter, September 1965.
7. Witzell, W. E., Hersh, M. S., and Anderson, R. T., A Survey of Welding and Inspection Techniques for 2219-T81 Aluminum Alloy, NASA CR-72097, January 1967.
8. Tiffany, C. F., Lorenz, P. M., and Shah, R. C., Extended Loading of Cryogenic Tanks, NASA CR-72252, 1967.
9. Smith, F. W., Stresses Near a Semi-Circular Edge Crack, Ph. D. thesis, University of Washington, 1966. University of Michigan Microfilm Inc. No. 66-7901.

11/BIBLIOGRAPHY

Benjamin, W. D., and Steigerwald, E. A., Stress Corrosion Cracking Mechanisms in Martensitic High Strength Steels, AFML-TR-67-98, April 1967.

Boyle, R. W., "A Method for Determining Crack Growth in Notched Sheet Specimens," Materials Research and Standards, August 1962.

Brown, B. F., "A New Stress-Corrosion Cracking Test for High-Strength Alloys," Materials Research and Standards, Vol. 6, No. 3, March 1966.

Campbell, J. E., Current Methods of Fracture-Toughness Testing of High-Strength Alloys with Emphasis on Plane Strain, DMIC Report 207, 31 August 1964.

Carman, C. M., Plane Strain Fracture Toughness of 5Al-2.5Sn ELI Titanium and 2219-T87 Aluminum Alloy Weldments, NASA P.O. C-35060A, Quarterly Progress Report, Frankfort Arsenal, October 1964.

Carman, C. M., Forney, J. W., and Katlin, J. M., Plane Strain Fracture Toughness of 2219-T87 Aluminum Alloy at Room and Cryogenic Temperature, NASA CR-54297, NASA LeRC, Cleveland, Ohio, August 1966.

Christensen, R. H., and Denke, P. H., Crack Strength and Crack Propagation Characteristics of High Strength Materials, ASD-TR 61-207, May 1961.

Christian, J. L. and Hurlich A., Physical and Mechanical Properties of Pressure Vessel Materials for Application in a Cryogenic Environment, Part II, ASD-TRD-62-258, April 1963.

Christian, J. L. and Witzell, W. E., "Evaluation of the Effects of Specimen Configuration and Testing Variables on Crack Propagation Properties," Cryogenic Engineering Conference, 17 August 1964.

D'Annessa, A. T., Fracture Toughness of X7039-T6 Aluminum Alloy Plate Weldments, Technical Report 6-62-64-6, Lockheed MSD, Sunnyvale, Calif.

Hahn, G. T. and Rosenfield, A. R., Sources of Fracture Toughness: The Relation Between K_{Ic} and the Ordinary Tensile Properties of Metals, Metal Science Group, Battelle Memorial Institute, April 1967.

Hanna, G. L. and Steigerwald, E. A., Development of Standardized Test Methods to Determine Plane Strain Fracture Toughness, AFML-TR-65-213, September 1965.

BIBLIOGRAPHY, Contd

- Hanna, G. L. and Steigerwald, E. A., Influence of Working Hardening Exponent on Crack Propagation in High-Strength Materials, AFML-TR-66-139, October 1966.
- Kobayashi, A. S., On the Magnification Factors of Deep Surface Flaws, Boeing Co. Structural Development Research Memo No. 16.
- Lanta, F. J. and Steigerwald, E. A., Influence of Work Hardening Coefficient on Crack Propagation in High-Strength Steels, AFML-TR-65-31, May 1965.
- Paris, P. and Erodogan, P. E., "A Critical Analysis of Crack Propagation Law," Trans. ASME, T of Basic Engineering, December 1963.
- Parker, E. R., Brittle Behavior of Engineering Structures, John Wiley and Sons, New York 1957.
- Srawley, J. E. and Brown, W. F., Jr., Fracture Toughness Testing, NASA Technical Note TN D-2599, January 1965.
- Srawley, J. E., Jones, M. H., and Brown, W. F., Determination of Plane Strain Fracture Toughness, Materials Research and Standards, Vol. 7 No. 6, June 1967.
- Srawley, J. E., Jones, M. H., and Gross, B., Experimental Determination of the Dependence of Crack Extension Force on Crack Length for a Single Edge Notch Tension Specimen, NASA Technical Note TN D-2396, August 1964.
- Tetelman, A. S. and McEvily, A. J., Jr., Fracture of Structural Materials, John Wiley and Sons, New York, 1967.
- Tiffany, C. F. and Masters, J. N., Investigation of the Flaw Growth Characteristics of 6A1-4V Titanium Used in Apollo Spacecraft Pressure Vessels, NASA CR-65586, NASA MSC, March 1967.
- Witzell, W. E., Fracture Toughness of Stainless Steel Sheet at Cryogenic Temperatures, American Rocket Society Paper 2418-62, 4 April 1962.
- Witzell, W. E., Fracture Mechanics — Development of Single Edge Notch and Slow Bend Evaluation Techniques, Convair Report GDA-ERR-AN-701, 31 December 1964.
- Witzell, W. E., An Introduction to Crack Propagation in High Strength Sheet Materials, Convair Report MRG-286, 2 February 1962.

BIBLIOGRAPHY, Contd

Yang, C. T., A Study of Law of Crack Propagation, Convair Report ERR-AN-64-489, ASME Paper No. 64, WA/Met-6.

Yang, C. T., Use of Critical Gross Stress as a Design Limit — A Design Concept for Brittle Fracture, Convair Report GDC-ERR-AN-1005, December 1966.

APPENDIX I

NONDESTRUCTIVE TESTING

APPENDIX I

NONDESTRUCTIVE TESTING

Nondestructive testing was conducted throughout all phases of the program and served two basic functions: 1) as an inspection and quality evaluation tool, and 2) as a means for assessing and monitoring flaw characteristics.

I-1/TEST METHODS

The test methods and procedures used for quality evaluation are outlined below.

PENETRANT TESTING

The 0.063-inch sheet was tested with water-washable fluorescent penetrants. Very minor indications of isolated pits were seen in Sheets 2-6, 2-8, and 3-4. More extensive corrosion pits, although not a severe attack, were noted in Sheet 4-6. Some weld joint preparations were also tested but due to the pre-weld preparation, which involved fairly heavy scraping, the test was discontinued.

The welds in 0.063-inch sheet were penetrant tested with solvent-removable, visible red dye. The penetrant aided significantly in establishing an optimum weld schedule. Selection of the repair weld specimens was, to some extent, based upon the penetrant results. Porosity was the major defect type noted; however, small crater cracks were also noted. Care was exercised to assure coverage for a full inch on either side of the weld centerline.

Both visible red dye and fluorescent penetrants were used to assess the quality of the weld filler wire. Prior to each weld, a sample of up to 10 feet of wire was run off and tested. One spool of wire found to contain an intermittent seam was rejected on the basis of the penetrant test.

The same procedures were followed for the 1.00-inch plates. No significant surface or edge indications were noted. No cracks were found in the welds, although some surface porosity was identified.

ULTRASONIC TESTING

The 0.063-inch-thick sheet was tested with an ultrasonic technique in which the incident energy was passed through the sheet and reflected from a smooth metal plate. The amount of energy reflected varied according to the homogeneity of the sheet through which the transmitted energy was directed. This technique is extremely sensitive to laminar discontinuities. As a gauge of sensitivity, two wires, 0.012- and

0.018-inch diameter, were placed on one end of the sheet. Figure I-1 shows the ultrasonic C-scan image of the two wires. No discontinuities were found in any of the 0.063-inch material.

The 1.00-inch plate was ultrasonically tested by conventional pulse-echo immersion techniques. Both longitudinal and 45-degree shear wave techniques were used. The test sensitivity was established on 2/64-inch-diameter, flat-bottom drill reference standard blocks of 7075-T6 aluminum. Several discrete discontinuities, probably inclusions, were found in 1.00-inch plate parent metal. However, each was noted and welding arranged such that the position of these defects would be away from the weld areas. The defects were small, providing reflections less than the reflections from 5/64-inch diameter flat-bottom holes in the reference standards.

After welding the 1.00-inch plates, contact ultrasonic tests were conducted on all welds. Numerous discontinuities were noted. However, all were correlated with radiographic indications. The test frequency was 2.25 MHz and both 45- and 60-degree refracted shear wave angles were used.

RADIOGRAPHIC TESTING

All welds were radiographically inspected. Radiography enabled immediate assessment of the weld schedule. Specimen selection was largely based upon the combined results of the radiographic and ultrasonic tests. Lengths of welds containing defects were segregated by the NDT and used for weld repair specimens.

EDDY CURRENT TESTING

Eddy current tests were conducted on one 0.063-inch sheet weld. However, because of the inherent conductivity changes associated with the weld, the sensitivity at which practical operation could be obtained was too low to detect any but surface-connected defects. Subsurface linear porosity was not detectible.

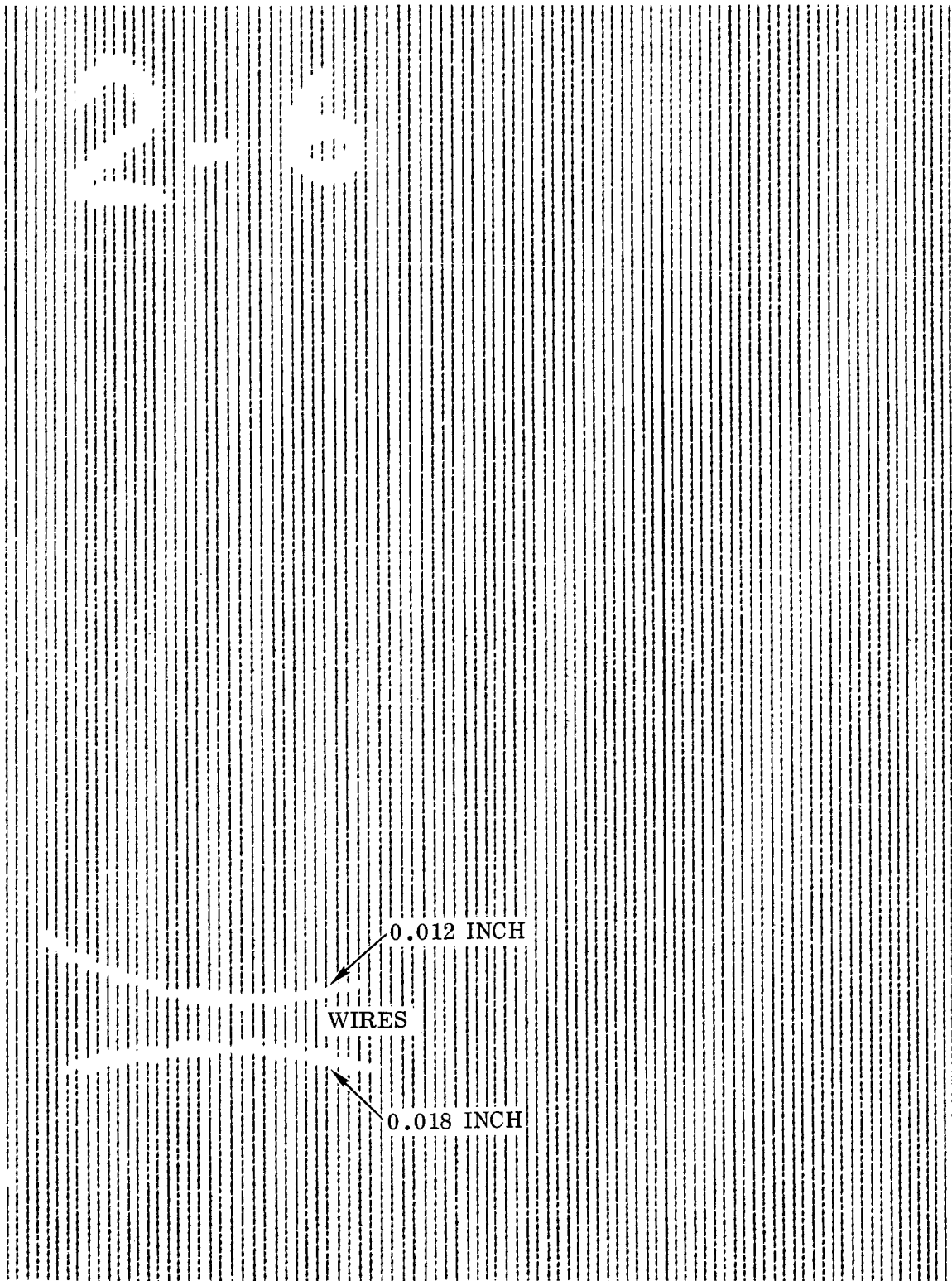


Figure I-1. Ultrasonic C-Scan, Sheet 2-6 (0.063-Inch), Showing 0.012- and 0.018-Inch-Diameter Wires

I-2/FLAW GROWTH TESTS

The remainder of the nondestructive testing was associated with flaw growth and characterization. Ultrasonic, radiographic, and eddy current tests were used to monitor flaw growth. On some static fracture specimens in room temperature tests, penetrant tests were compared with visual examinations. The techniques used and results of these tests are summarized below.

ULTRASONIC TESTS ON 0.063-INCH SHEET FLAWS

A 70-degree shear wedge block (Figure I-2) was fabricated so that lateral movement of the transducer could be made. The 0.063-inch center-notched specimens were prepared prior to entry into the testing machine by finding the position toward and away from the notch that provided maximum pulse-echo response from the notch. The block was then bonded to the specimen using Eastman 910 adhesive. This adhesive was found effective to bond the acrylic wedge to the aluminum surface. One disadvantage, however, was that, in the removal of the wedge, the edges tended to chip away. Since the block was intended for subsequent reuse, this breakage, even though of minor extent, was undesirable. It was later found that several of the clear silicone adhesives were effective as couplants and did not cause breakage of the block upon removal. The silicone adhesives were used for the majority of the tests with the only objectionable feature being the one- to two-hour cure time at room temperature.

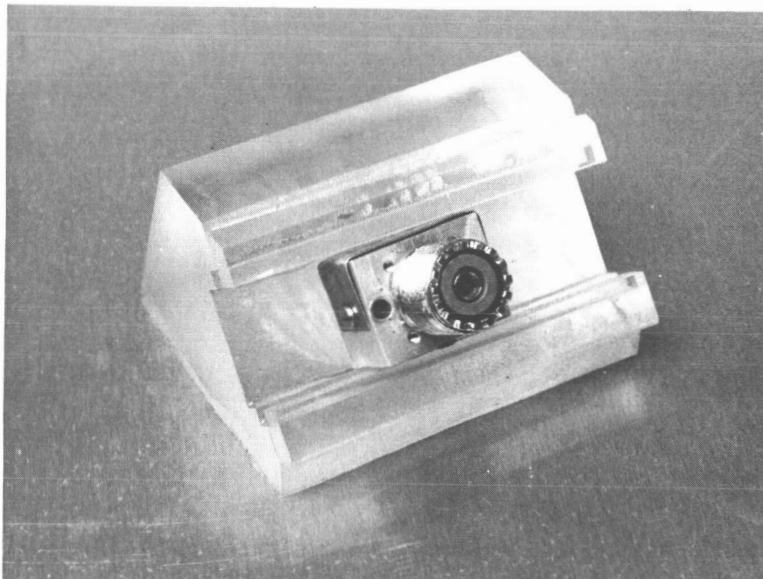


Figure I-2. Shear Wedge Block (70 Degrees) Fabricated to Provide Lateral Transducer Adjustment

Neither the pulse-echo nor the through-transmission techniques yielded greater than a 2 to 1 ratio between ultrasonic amplitude change and actual flaw growth. On thicker specimens (0.250- and 0.375-inch titanium) previous experience demonstrated a 6 to 1 maximum response ratio. At this order of response, measurements of amplitude change provide accuracy of about 0.005-inch in determining flaw extension. It is assumed that the failure to obtain greater response was primarily influenced by the thinness of the 0.063-inch specimen. Phasing, multiple mode conversion, and wave-guiding reduce the effectiveness of the transverse wave in thin materials.

With only a 2 to 1 response ratio available from the instrumentation, visual observation is more accurate. The amplitude of the ultrasonic A-scan signals can only be measured within about 0.050 inch.

ULTRASONIC TESTING OF ARTIFICIAL FLAWS IN ONE-INCH-THICK SPECIMENS

An ultrasonic through-transmission shear wave test was used to detect crack propagation during fatigue testing of the 1.00-inch specimens. It consisted of two transducers on either side of the defect in the weld as shown in Figure I-3.

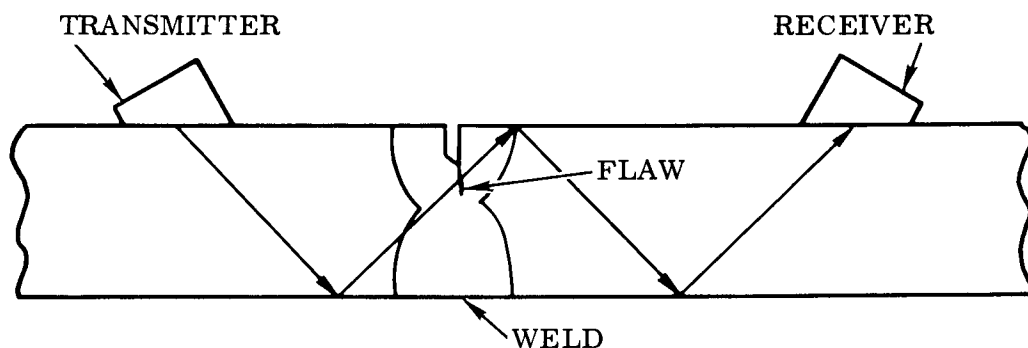


Figure I-3. Schematic of Shear Wave Test Setup

The transmitting transducer sends an angle beam through the thickness of the specimen which reflects off the bottom surface and is intercepted by the defect. Since the beam is wide compared to the size of the defect, part of the beam travels around the defect and reflects off the top and bottom surfaces before reception by the receiving transducer. When a crack initiates and propagates from the defect, more of the beam is intercepted and, therefore, a reduction in signal amplitude results. Conversely, when the transmitting transducer is converted to the pulse-echo mode, the portion of the beam that reflects from the defect and subsequently the bottom surface, as shown

in Figure I-3, returns to the transmitting transducer. The signal response is the opposite, because more of the beam is reflected as a crack enlarges, and an increase in reflection amplitude results.

A specimen undergoing a bending fatigue test is shown in Figure I-4. The transmitting and receiving transducers are shown both on the top surface. The wedges are bonded to the specimen with silicone rubber adhesive, which stays intact during test. Figure I-5 shows the complete test setup, which includes the fatigue testing machine and the ultrasonic instrumentation.

It was assumed that the crack would initiate from the defect in the weld. This was not the case for one of the specimens (Specimen 19). In Specimen 19, the crack started from the edge of the specimen and was not detected ultrasonically until it had

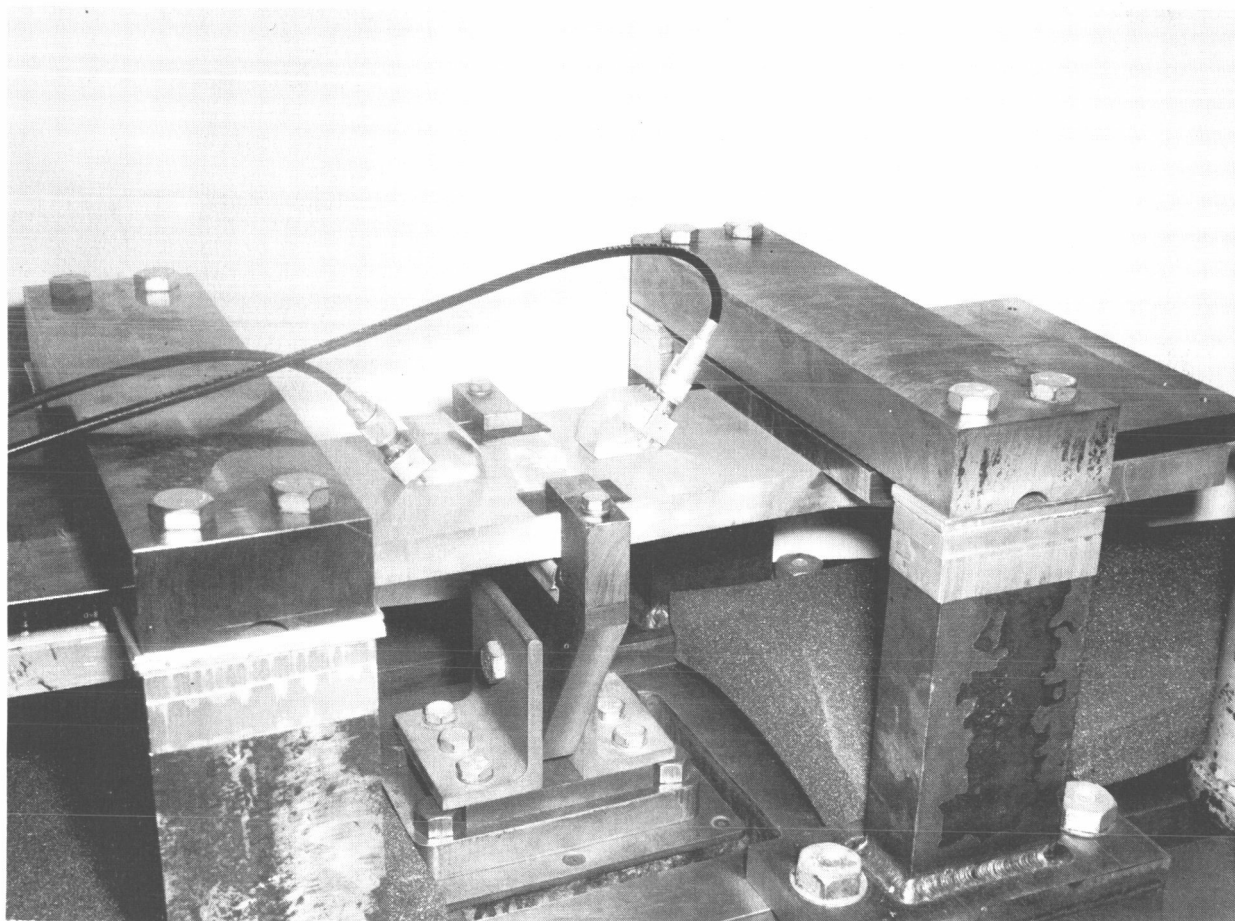


Figure I-4. Ultrasonic Transducers for Through-Transmission Test In-Situ on the Fatigue Test Machine

propagated towards the weld and intercepted the acoustic beam. The effect was a decrease in the through-transmission signal from 2.3 to 2.1 inches amplitude.

Specimens R6 and R22 were fatigue tested in slow cycle tension-tension with the same ultrasonic setup. Both specimens broke during the first cycle at the highest load. The cracks propagated too rapidly to enable distinguishing between crack initiation, crack growth, and failure by the ultrasonic technique, except with automatic signal monitoring and recording. It was assumed all three events took place in a few seconds at most.

Of six plate specimens ultrasonically tested while undergoing cyclic fatigue notch sharpening, significant data were only obtained from one. This specimen was instrumented with a single transducer, and amplitude data were taken in the reflection mode only. These data are as follows.



Figure I-5. Ultrasonic Test Instrumentation Used During Cyclic Flaw Enlargement on the One-Inch-Thick Plate Specimens

<u>Cycles</u>	<u>Reflection Amplitude (inches)</u>
1,200	0.80
1,865	0.90
9,000	1.00
2,800	1.00
12,000	1.25
13,700	1.30
15,000	1.25
17,000	1.20
18,000	1.20
19,500	1.20
20,170	1.20

A definite increase was noted with a maximum at 13,700 cycles. At less than 21,000 cycles, the adhesive bond between the transducer wedge and the specimen started to fail. It is probable that the apparent decrease reflected in the data was, in fact, an early indication of this bond failure.

EDDY CURRENT MONITOR FOR FLAW GROWTH IN 0.063-INCH SHEET

A probe holder was fabricated to provide accurate positioning for the eddy current probe. Figure I-6 shows the holder, which provides X and Y motion transmitted by the adjustment screws provided. The probe holder was adhesively bonded to the

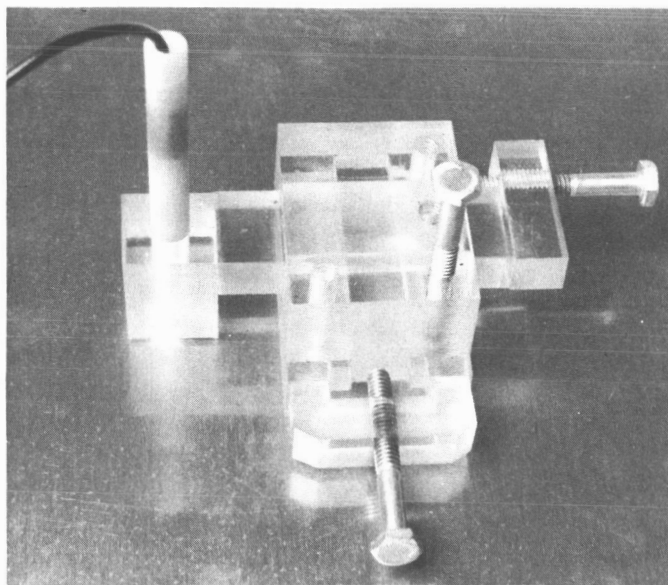


Figure I-6. Eddy Current Probe Holder

specimen and adjusted so that the edge of the starter notch just perceptibly influenced the instrument meter. Both X and Y datum lines were established at this point. The probe was then moved approximately 1/2-inch to a fixed stop on the holder. This provided an unaffected area, which could be used to zero or calibrate the instrument. With the probe in the calibrate area, a reading was taken and established as a reference point. Just prior to taking readings to assess flaw growth, the instrument was calibrated to the reference reading on the unaffected material. The probe was then moved to the original X, Y datum and a reading taken. If the reading was found to vary from the previous reading, the probe was moved some measured distance along the X and Y axes until the original reading was obtained. Then ΔX and ΔY were read. In this manner the tip of an advancing flaw was tracked. The eddy current instrument used was an impedance tester.

Specimen 2-2-1 was tested as described above and the data follow.

<u>Cycles</u>	<u>Inches</u>	
	<u>X</u>	<u>Y</u>
0	0	0
10	0	0
15	0	0
25	0	0
35	0	0
45	0	0
60	0.04	0
70	0.06	0
85	0.06	0
108	0.07	0
1,250	0.10	0.005
2,470	0.13	0.005
3,250	0.18	0.005
5,200	0.19	0.010
7,000	0.19	0.010

The final X measurement of 0.19 inch compares with 0.20 measured optically and 0.205 measured radiographically. The only limiting factor in the precision of the method is in the manipulating device. Further refinement of the probe holder would permit noncontacting measurements to be recorded automatically and even establish feedback to the testing machine to change load or shut down.

RADIOGRAPHIC TESTING FOR FLAW ENLARGEMENT STUDIES

High-resolution radiographs on single-emulsion Eastman Kodak Type R film provided images that could be measured within less than 0.005 inch. On the center-notched sheet, radio-opaque putty carefully inserted in the notch afforded much more accurate measurements.

Measurements were made radiographically at periodic intervals on one of the room-temperature specimens (2-2-1). Radiographic measurements were in agreement with visual observations within 0.020 inch. Two of the 0.063-inch specimens with part-through or "thumb-nail" notches were radiographically tested. On parent metal Specimen CF1 no crack extension was noted. Figure I-7 shows the measurements taken from the radiograph of Specimen CF2. These cracks were not visually apparent.

A radiograph of Specimen 3-4-2, made at 830 cycles, proved an interesting subject for microdensitometry. Crack extensions measured on the radiograph were 0.530 and 0.350 inch compared with 0.468 and 0.305 inch measured visually. The longer crack lay in an almost vertical plane for about 0.130 inch, then transitioned to a plane estimated at about 30 degrees from vertical. Figure I-8 is a reproduction of the radiograph in that area. Two microdensitometric scans were made, one at each arrow. Figure I-8 shows the recordings that resulted.

Figure I-9 is a scan of a radiograph from Specimen 20, a 1.00-inch plate weldment with the flaw in the fusion line. Note the indication from the opposite edge of the weld.

Figure I-10 is a scan across the part-through notch of Specimen CF2. Note the sharp spike corresponding with an almost-through crack.

Figure I-11 is a scan across Specimen R12, a 1.00-inch-thick specimen notched in the heat-affected zone. Note the symmetrical shape across the width of the weld, which had been machined flush.

These scans illustrate the feasibility of densitometric scanning as a potential means of automatically interpreting films.

Another contribution from radiography was initiated as a result of examination of the post-fracture appearance of Specimen B3. The protruding tongue or lip led to some conjecture whether the 1.00-inch plate might not be affected by a condition noted previously by Convair on other programs involving 2219 alloy. A 0.500-inch-thick



Figure I-7. Measurements From Radiograph of Specimen CF2
(Looking Down on the Specimen)

plate of 2219-T81 had exhibited a band through the center that was deficient of copper. An X-ray fluorescence analysis revealed copper variation of greater than 1 percent, with the least amount in the exact center plane. To test for this condition on this program, three cut-out sections remaining from the "dog-bone" machining were selected. One was from base metal Specimen B3, in which the odd fracture occurred, and the other two from Specimens B2 and B6, which failed in a "normal" manner. An "end-on" radiograph of all three pieces in simultaneous exposure revealed a strip of slightly higher film density about 1/4-inch wide in the exact center of B3. B2 and B6 did not contain any evidence of this condition. Figure I-12 shows the microdensitometric scan, which reveals the difference from B2 and B6. The 0.04 D shown on the B3 specimen is indicative of copper deficiency in and about the center plane of the original plate.

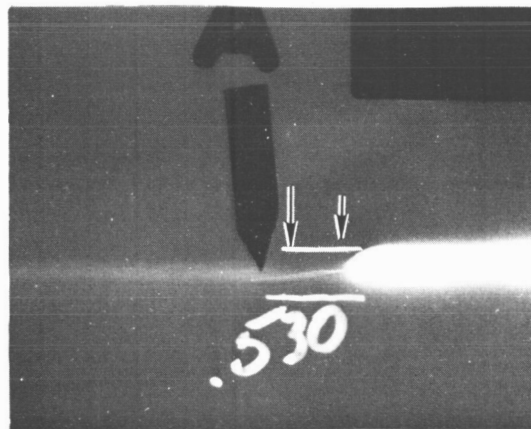
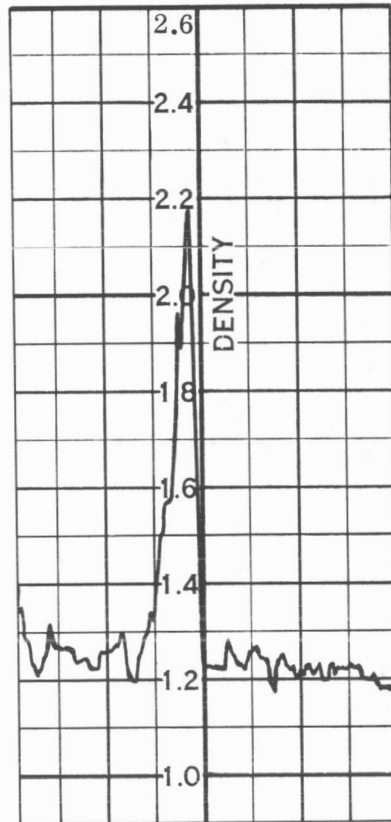
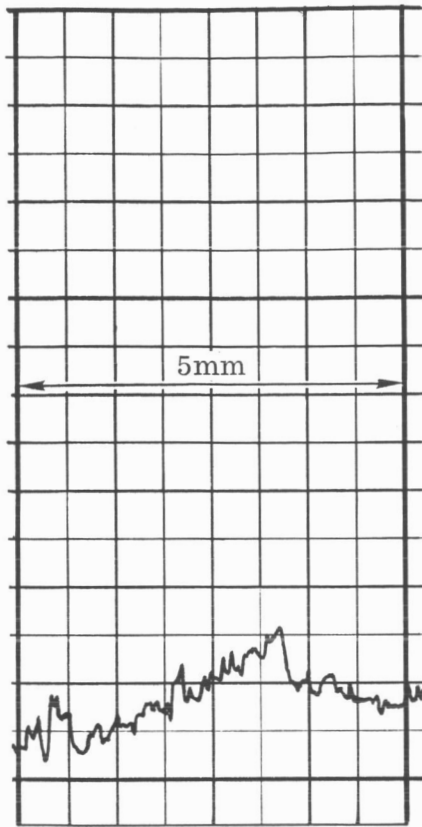


Figure I-8. Microdensitometric Scans of Cracks in Specimen 3-4-2

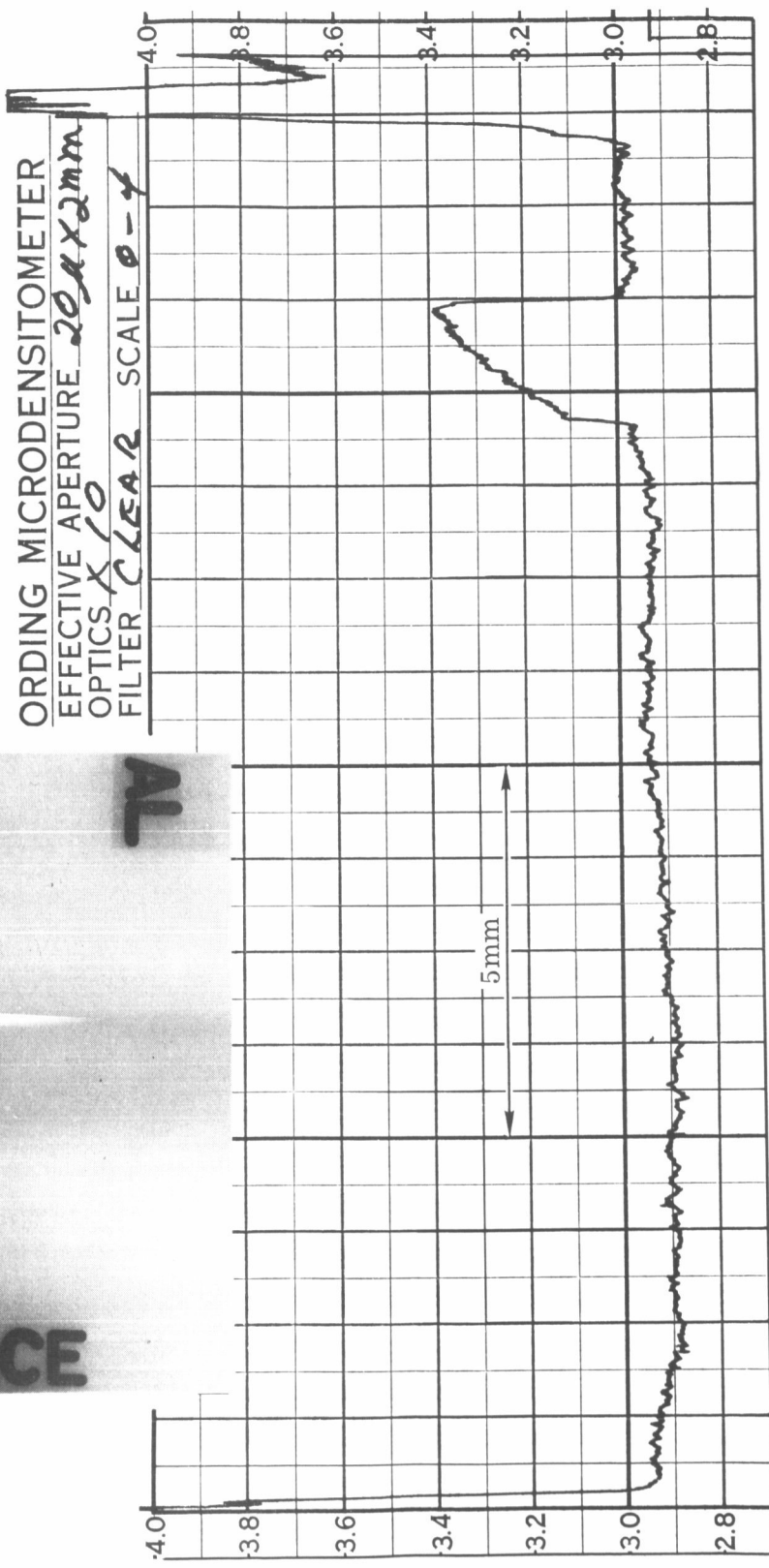
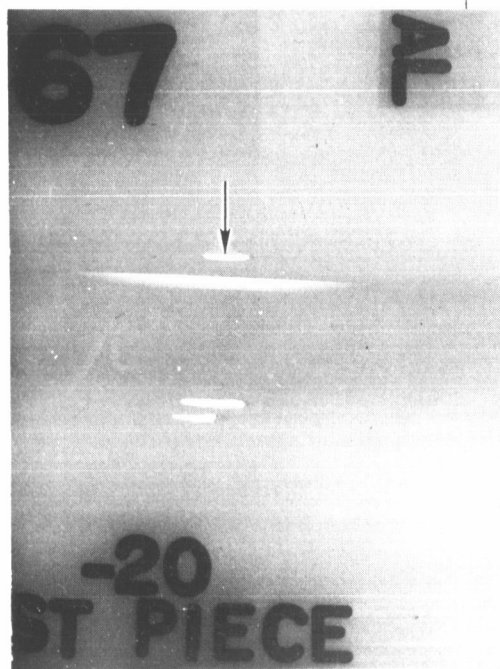


Figure I-9. Microdensitometric Scan of Starter Notch in Specimen 20

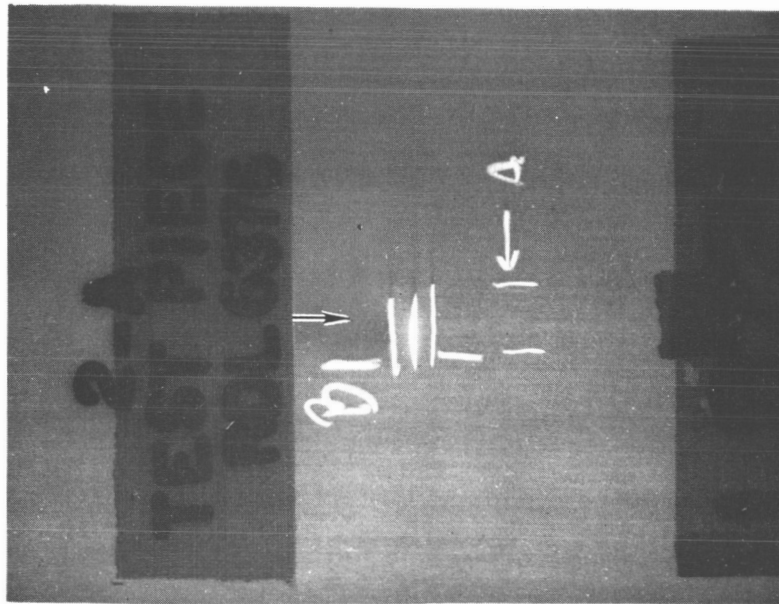
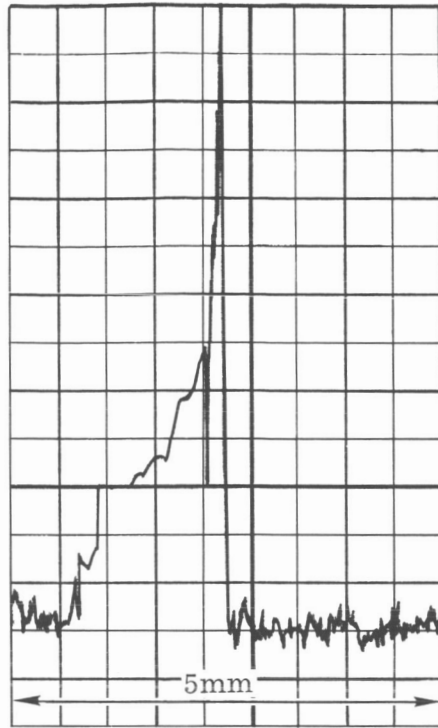


Figure I-10. Microdensitometric Scan

ORDING MICRODENSITOMETER

EFFECTIVE APERTURE 4 μ X .4 mm

OPTICS 50X

FILTER OPEN SCALE 0-4

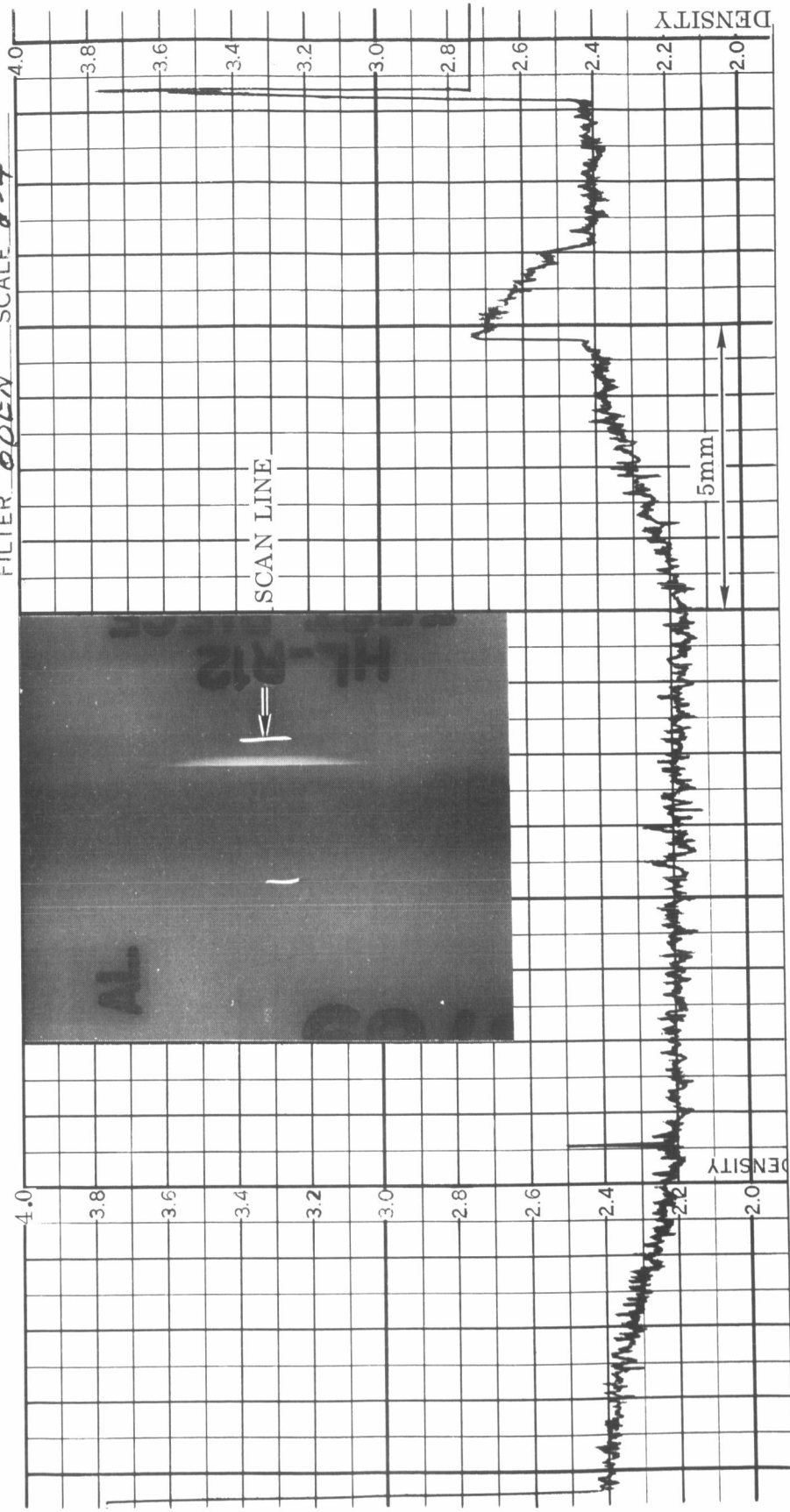


Figure I-11. Microdensitometric Scan of Specimen R12

FOLDOUT FRAME 1

FOLDOUT FRAME 2

TOMATIC RECORDING MICRODENSITOMET
EFFECTIVE APERTURE 20X
OPTICS OPEN
FILTER OPEN SCALE 0-

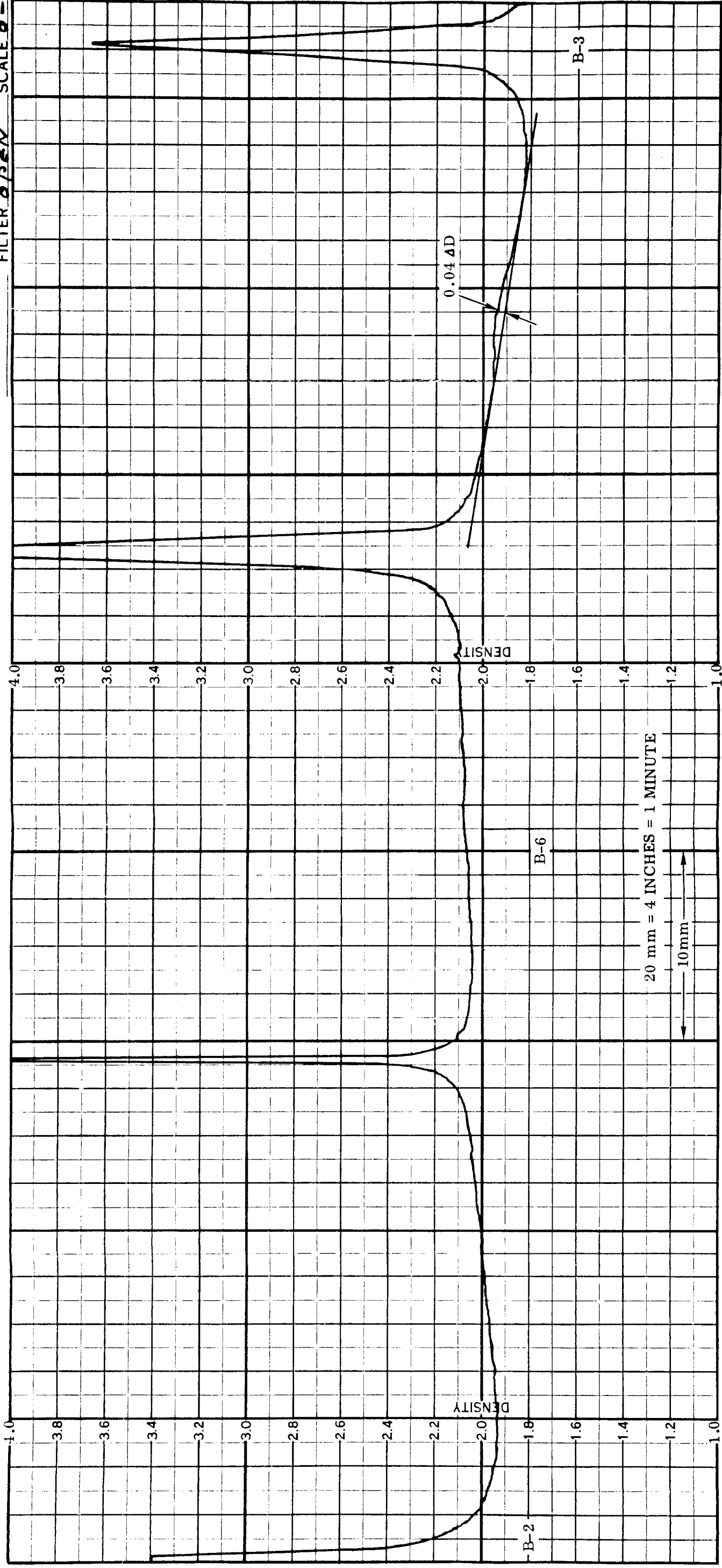


Figure I-12. Microdensitometric Scans of Cut-Outs From Specimens B2, B3, and B6. The 0.04 Density Gradient is an Indication of Copper Migration in 2219-T81 Aluminum Alloy

DISTRIBUTION

Copies

National Aeronautics and Space Administration
Lewis Research Center
21000 Brookpark Road
Cleveland, Ohio 44135

Attention:	Contracting Officer, MS 500-210	1
	Liquid Rocket Technology Branch, MS 500-209	8
	Technical Report Control Office, MS 5-5	1
	W. E. Roberts, MS 3-17	1
	Technology Utilization Office, MS 3-16	1
	D. L. Nored, MS 500-209	1
	AFSC Liaison Office, MS 4-1	2
	T. Moore, MS 105-1	1
	Library	2
	W. Russell, MS 14-1	1
	Office of Reliability & Quality Assurance, MS 500-203	1
	Richard H. Kemp, MS 49-1	1
	J. E. Srawley, MS 105-1	1
	R. Swallow, MS 501-2	1
	W. Brown, MS 105-1	1

National Aeronautics and Space Administration
Washington, D.C. 20546

Attention:	Code MT	1
	RPX	2
	RPL	2
	SV	1
	RV-2	1

Scientific and Technical Information Facility
P.O. Box 33
College Park, Maryland 20740

Attention:	NASA Representative	
	Code CRT	6

National Aeronautics and Space Administration
Ames Research Center
Moffett Field, California 94035

Attention:	Library	1
------------	---------	---

National Aeronautics and Space Administration
Flight Research Center
P.O. Box 273
Edwards, California 93523

Attention: Library 1

National Aeronautics and Space Administration
Goddard Space Flight Center
Greenbelt, Maryland 20771

Attention: Library 1

National Aeronautics and Space Administration
John F. Kennedy Space Center
Cocoa Beach, Florida 32931

Attention: Library 1

National Aeronautics and Space Administration
Langley Research Center
Langley Station
Hampton, Virginia 23365

Attention: Library 1

National Aeronautics and Space Administration
Manned Spacecraft Center
Houston, Texas 77001

Attention: Library 1

National Aeronautics and Space Administration
George C. Marshall Space Flight Center
Huntsville, Alabama 35812

Attention: Library 1
Keith Chandler, R-P&VE-PA 1
Robert Hoppes, R-ME-MW 1

National Aeronautics and Space Administration
Western Operations Office
150 Pico Boulevard
Santa Monica, California 90406

Attention: Library 1

Jet Propulsion Laboratory
 4800 Oak Grove Drive
 Pasadena, California 91103
 Attention: Library 1

Office of the Director of Defense Research & Engineering
 Washington, D.C. 20301
 Attention: Dr. H. W. Schulz, Office of Asst. Dir.
 (Chem. Technology) 1

Defense Documentation Center
 Cameron Station
 Alexandria, Virginia 22314 1

Arnold Engineering Development Center
 Air Force Systems Command
 Tullahoma, Tennessee 37389
 Attention: AEOIM 1

Advanced Research Projects Agency
 Washington, D.C. 20525
 Attention: D. E. Mock 1

Air Force Materials Lab.
 Wright-Patterson Air Force Base
 Dayton, Ohio 45433
 Attention: M. Knight (MAAM) 1
 Sidney Davis (MAAM) 1

Air Force Rocket Propulsion Laboratory (RPR)
 Edwards, California 93523 1

Air Force Rocket Propulsion Laboratory
 Edwards, California 93523
 Attention: W. F. Payne 1

Air Force FTC (FTAT-2)
 Edwards Air Force Base, California 93523 1

Air Force Office of Scientific Research
 Washington, D.C. 20333
 Attention: SREP, Dr. J. F. Masi 1

Commanding Officer U.S. Army Research Office (Durham) Box CM Duke Station Durham, North Carolina 27706	1
U.S. Army Missile Command Redstone Scientific Information Center Redstone Arsenal, Alabama 35808 Attention: Chief, Document Section	1
Commander U.S. Naval Ordnance Test Station China Lake, California 93557 Attention: Code 45	1
Commanding Officer Office of Naval Research 1030 E. Green Street Pasadena, California 91101	1
Director (Code 6180) U.S. Naval Research Laboratory Washington, D.C. 20390 Attention: H. W. Carbart J. M. Krafft (Mechanics)	1 1
U.S. Atomic Energy Commission Technical Information Services Box 62 Oak Ridge, Tennessee Attention: A. P. Huber, Code ORGDP Box P	1
Air Force Aero Propulsion Laboratory Research & Technology Division Air Force Systems Command United States Air Force Wright-Patterson AFB, Ohio 45433 Attention: APRP (C. M. Donaldson)	1

Aerojet-General Corporation
P.O. Box 296
Azusa, California 91703

Attention: Librarian 1
E. J. Morgan 1

Aerojet-General Corporation
11711 South Woodruff Avenue
Downey, California 90241

Attention: F. M. West, Chief Librarian 1

Aerojet-General Corporation
P.O. Box 1947
Sacramento, California 95809

Attention: Technical Library, 2484-2015A 1
C. E. Hartbower 1

Aerospace Corporation
P.O. Box 95085
Los Angeles, California 90045

Attention: J. G. Wilder, MS-2293 1
Library-Documents 1

ARO, Incorporated
Arnold Engineering Development Center
Arnold AF Station, Tennessee 37389

Attention: Dr. B. H. Goethert, Chief Scientist 1

Atlantic Research Corporation
Shirley Highway & Edsall Road
Alexandria, Virginia 22314

Attention: A. Scurlock 1
Security Office for Library 1

Battelle Memorial Institute
505 King Avenue
Columbus, Ohio 43201

Attention: Report Library, Room 6A 1
R. E. Monroe, Materials Joining Division 1

Battelle-Northwest 3000 Stevens Drive P.O. Box 999 Richland, Washington 99352 Attention: R. G. Hoagland	1
Beech Aircraft Corporation Boulder Facility Box 631 Boulder, Colorado Attention: J. H. Rodgers	1
Bell Aerosystems, Inc. Box 1 Buffalo, New York 14205 Attention: T. Reinhardt	1
The Boeing Company Aero Space Division P.O. Box 3707 Seattle, Washington 98124 Attention: Ruth E. Peerenboom (1190) C. W. Tiffany D. T. Lovell, MS 88-03	1 3 1
Carnegie Institute of Technology Department of Civil Engineering Pittsburgh, Pennsylvania Attention: Robert B. Anderson	1
Chemical Propulsion Information Agency Applied Physics Laboratory 8621 Georgia Avenue Silver Spring, Maryland 20910	1
Chrysler Corporation Missile Division Warren, Michigan Attention: John Gates	1

Chrysler Corporation
Space Division
New Orleans, Louisiana
Attention: Librarian 1

Curtiss-Wright Corporation
Wright Aeronautical Division
Woodridge, New Jersey
Attention: G. Kelley 1

University of Denver
Denver Research Institute
P.O. Box 10127
Denver, Colorado 80210
Attention: Security Office 1

Douglas Aircraft Company, Inc.
Santa Monica Division
3000 Ocean Park Blvd.
Santa Monica, California 90405
Attention: B. Whiteson 1
D. A. Eitman 1
R. A. Rawe 1

Fairchild Stratos Corporation
Aircraft Missiles Division
Hagerstown, Maryland
Attention: J. S. Kerr 1

Convair division of General Dynamics
P.O. Box 1128
San Diego, California 92112
Attention: Library & Information Services (524-10) 1
W. E. Witzell, Mat's. Res. Group 1
J. E. Christian, MS 572-10 1

General Electric Company
Flight Propulsion Lab. Department
Cincinnati 15, Ohio
Attention: D. Suichu 1

Grumman Aircraft Engineering Corporation
Bethpage, Long Island,
New York

Attention: Library

1

Hercules Powder Company
Allegheny Ballistics Laboratory
P.O. Box 210
Cumberland, Maryland 21501

Attention: Library

1

IIT Research Institute
Technology Center
Chicago, Illinois 60616

Attention: K. E. Hafer

1

Kidde Aero-Space Division
Walter Kidde & Company, Inc.
675 Main Street
Belleville 9, New Jersey

Attention: R. J. Hanville,
Director of Research Engineering

1

Lockheed Missiles & Space Company
P.O. Box 504
Sunnyvale, California

Attention: Richard E. Lewis, Bldg. 204
W. Sterbentz, Bldg. 537
Technical Information Center

1

1

1

Lockheed-California Company
Burbank, California

Attention: R. O. Enearl

1

Lockheed Propulsion Company
P.O. Box 111
Redlands, California 92374

Attention: Miss Belle Berlad, Librarian

1

Lockheed Missiles & Space Company
Propulsion Engineering Division (D.55-11)
1111 Lockheed Way
Sunnyvale, California 94087 1

Marquardt Corporation
16555 Saticoy Street
Box 2013 - South Annex
Van Nuys, California 91404
Attention: Librarian 1

Martin-Marietta Corporation
Denver Division
Denver, Colorado 80201
Attention: F. R. Schwartzberg 1

McDonnell Aircraft Corporation
P.O. Box 6101
Lambert Field, Missouri
Attention: R. A. Herzmark 1

North American Aviation, Inc.
Space & Information Systems Division
12214 Lakewood Boulevard
Downey, California 90242
Attention: Technical Information Center, D/096-722 (AJ01) 1

Northrop Space Laboratories
1001 East Broadway
Hawthorne, California
Attention: Dr. William Howard 1

Purdue University
Lafayette, Indiana 47907
Attention: Technical Librarian 1

Republic Aviation Corporation
Farmingdale, Long Island
New York
Attention: Dr. William O'Donnell 1

Rocket Research Corporation 520 South Portland Street Seattle, Washington 98108	1
Rocketdyne, Division of North American Aviation, Inc. 6633 Canoga Avenue Canoga Park, California 91304	
Attention: Library, Department 596-306	1
Rohn and Haas Company Redstone Arsenal Research Division Huntsville, Alabama 35808	
Attention: Librarian	1
Space-General Corporation 777 Flower Street Glendale, California	
Attention: C. E. Roth	1
Thiokol Chemical Corporation Redstone Division Huntsville, Alabama	
Attention: John Goodloe	1
United Aircraft Corporation Corporation Library 400 Main Street East Hartford, Connecticut 06118	1
United Aircraft Corporation United Technology Center P.O. Box 358 Sunnyvale, California 94088	
Attention: Library	1
Vought Astronautics Box 5907 Dallas 22, Texas	
Attention: Warren C. Trent	1

Frankford Arsenal Philadelphia, Pennsylvania	
Attention: D. F. Armiento, SMOFA-1324	1
Franklin Research Institute Benjamin Franklin Parkway Philadelphia, Pennsylvania 19103	
Attention: C. Hays	1
Harvey Engineering Laboratories 19200 South Western Avenue Torrance, California	
Attention: Paul Anderson, R&D Division	1
Southwest Research Institute 8500 Calebra Road San Antonio, Texas 78206	
Attention: E. B. Norris	1
Syracuse University Research Institute Department of Metallurgy Syracuse, New York	
Attention: H. W. Liu	1
Volker Weiss	1
U.S. Steel Corporation Applied Research Laboratory Monroeville, Pennsylvania 15146	
Attention: T. L. Boblenz, MS 62	1
Sciaky Brothers's, Inc. 4915 West 67th Street Chicago, Illinois 60638	
Attention: Eugene P. Vilkos, Fusion Welding Lab.	1
A. O. Smith Corporation Milwaukee, Wisconsin 53201	
Attention: Paul W. Ramsey, Welding Research and Development	1

Applied Mechanics Research Laboratory
U.S. Army Materials Research Agency
Watertown, Massachusetts 02172

Attention: Robert J. Morrissey

1